Final technical report

Optical hole burning studies in glasses doped with dyes and rare-earth ions

Grant No.: F49620-97-1-0258

Submitted to

Air Force Office of Scientific Research
Directorate of Physics and Electronics
801 N. Randolph Street, Room 732
Arlington, VA 22203-1977
Program Manager: Dr. Kent L. Miller
Tel: 703-696-8573, E-mail: kent.miller@afosr.af.mil

By

Alabama A& M University
Department of Physics
P.O. Box 1268
Normal, AL 35762
Principal investigator: B. R. Reddy
Tel: 256-858-8101, E-mail: brreddy@aamu.edu

November 28, 2000

REPORT DOCUMENTATION PAGE

AFRL-SR-BL-TR-01-

0067

1. AGENCY USE ONLY (Leave blank)	2. REPORT DATE	3. REPORT TYPE AND DATES COVERED: Final technical report
	November 28, 2000	May 1, 1997 to August 31, 2000

4. TITLE AND SUBTITLE
Optical hole burning studies in glasses doped with dyes and rare-earth ions

5. FUNDING NUMBERS
F49620-97-1-0258

6. AUTHOR(S)
B. R. Reddy, PI, Alabama A&M University
Anshel Gorokhovsky (subcontractor), CUNY/CSI

7. PERFORMING ORGANIZATION NAME(S) AND ADDRESS(ES)

Alabama A&M University
Department of Physics
P.O. Box 1268
Normal, AL 35762

The College of Staten Island, CUNY
Department of Engineering Science and Physics
2800 Victory Boulevard
Staten Island, NY 10314

8. PERFORMING ORGANIZATION REPORT NUMBER

Final Technical Report

9. SPONSORING / MONITORING AGENCY NAME(S) AND ADDRESS(ES)

Air Force of Scientific Research
Dr. Kent Miller, Program Manager
Directorate of Physics and Electronics
801 N. Randolph Street, Room 732
Arlington, VA 22203-1977

10. SPONSORING / MONITORING AGENCY REPORT NUMBER

11. SUPPLEMENTARY NOTES

12a. DISTRIBUTION / AVAILABILITY STATEMENT

Unlimited access to all

DISTRIBUTION STATEMENT A
Approved for Public Release
Distribution Unlimited

12b. DISTRIBUTION CODE

13. ABSTRACT *(Maximum 200 Words)*

Rare-earth ion doped glasses and dye doped sol-gel glasses and spin-coated polymers were prepared and investigated by optical methods at room and liquid helium temperatures. Eu3+ glasses revealed large inhomogeneous broadenings (3-6 nm) and these samples also exhibited transient spectral hole burning at cryogenic temperatures. Hole burning studies in Eu3+ doped YSO and CaF2 revealed more than 40 sites for the dopants. These were due to clustering of the dopants and dopant induced microscopic defects. Infrared quantum counter studies were also performed on Eu3+ doped materials. Our studies revealed that Eu3+ doped materials are suitable for the development of room temperature photon detectors for infrared radiation using the two-photon absorption scheme.

Spectroscopy of thulium doped chelates was performed. Broad spectral holes (180-360 MHz)were burned in the 3H6→3H4 transition, which lasted for 10 hours at 1.4K. Suitability of this material for frequency and time domain information storage is under investigation. The effect of mechanical vibrations of the closed cycle refrigeration system was also investigated by optical means. A rigidly held device was found to vibrate with an amplitude of 50 microns.

14. SUBJECT TERMS: Optical hole burning, optical memory, high-resolution spectroscopy, glasses, chelates, infrared quantum counter, europium, thulium, dyes, polymers, sol-gels, two-photon excitation studies	15. NUMBER OF PAGES: 88
	16. PRICE CODE

17. SECURITY CLASSIFICATION OF REPORT	18. SECURITY CLASSIFICATION OF THIS PAGE	19. SECURITY CLASSIFICATION OF ABSTRACT	20. LIMITATION OF ABSTRACT
unclassified	unclassified	unclassified	unlimited

2. Work done at Alabama A&M University

Optical hole burning studies in glasses doped with dyes and rare-earth ions

3. Project objectives at Alabama A&M University

- Establish facilities for optical hole burning studies
- Train minority students in the fields of interest to DoD
- Preparation of high temperature glasses doped with rare-earth ions and pursue optical hole burning studies
- Prepare sol-gel glasses doped with dyes and pursue optical hole burning studies
- Prepare polymer films doped with dyes and pursue optical hole burning studies

Accomplishments at Alabama A&M University

- Two students Angela Davis and Andre Jackson completed their M.S. thesis. The performed their thesis work on optical hole burning studies. They published their thesis work in scientific journals (Journal of Applied Physics and Applied Optics).
- Pursued hole burning in Eu^{3+} doped Y_2SiO_5
- Pursued hole burning in Eu^{3+} doped CaF_2
- Prepared high temperature oxide glasses doped with europium and observed transient hole burning
- Prepared sol-gel glasses doped with dyes and rare-earth ions. Upconversion signals were detected on exposure to a dye laser
- Prepared dye doped polymer films and performed spectroscopic studies
- Pursued infrared quantum counter studies in europium doped calcium fluoride (another important phenomenon observed during the course of study)
- Published two papers in refereed journals and a third paper was published in conference proceedings. Two papers were presented in conferences

Future plans

- Prepare europium and samarium doped moisture ridden glasses for high temperature hole burning studies
- Pursue hole burning in dye doped sol-gel and polymer films
- Continue the work on compositional dependence of hole burning

Work done at CUNY (see page 54)

4. Personnel and students graduated

The following people participated in this work at Alabama A&M University.

Angela Davis (graduate student)- completed her M.S. degree with thesis option.

Thesis title: Spectral hole burning studies and optical investigations of Rare-earth ion and dye doped materials

Andre Jackson (graduate student)- completed his M.S. degree with thesis option.
Thesis title: An investigation of spectral hole burning studies in Eu^{3+} doped materials

Wenyan Tian (graduate student)- pursuing his Ph. D. degree

Ranjit Pandher (Research Associate)

B. R. Reddy (Principal Investigator)

City University of New York (subcontractor)

Anshel Gorokhovsky- Co-investigator

Alexey Turukhin (graduate student)- completed his Ph.D. degree.

Dissertation title: Persistent spectral hole burning in organic and inorganic Materials

Alexander Vaysman (undergraduate student)

5. Equipment purchased at Alabama A&M University

Hole burning work has been started at Alabama A&M University (AAMU) with the funding from Air Force Office of Scientific Research. The following equipment has been purchased at AAMU with this funding.

A closed cycle cryostat (Janis Research company, Model CCS-150)
A vacuum pumping station (Varian, Model TP70)
Temperature controller (Lakeshore, Model)
Electro-Optic Modulator (Quantum Technology, TWAP-10) and Driver, Model 3500
Electro-optic modulator (Conoptics, Model 350-80)
Frequency generator (Rhode & Schwarz Model SMT 02)
Frequency generator (SRS Model DS 345)
r.F. Amplifier (Amplifier Research, Model 25A250A)
Oscilloscope (Tektronix Model 210)
Optical table (Newport, Model RT-48-8 with NN4-28)
Partial payment for an Ar+ laser (Lexel laser Model 95)
Spectrum analyzer and controller (Coherent-Ealing, Models 33-6305 and 33-2635)
Wavemeter (Coherent-Ealing Model 33-2684)
Spin-coater (Chemat Technology, Model KW-4A)
Muffle furnace (Thermolyne) Fischer catalog No. 10-554-2B
A pocket lock-in amplifier (Electro-solutions, Model VK-90)
Current and voltage amplifiers (ORIEL Models 70710 and 70721)
F/# matcher (spectrometer to fiber) Model 77529 (ORIEL)
Five-axis aligner (New focus) Model 9082
Tunable diode laser (Polytec PI Models: DL100/792, DL100/1527, DC100/HV)
Polarization modulator (Thorlabs)
Laser power controller (Cambridge Research and instrumentation) Model LPC-VIS
External cavity tunable laser Newport Model 2010)
Acousto optic modulator (NEOS technology, Model N23080 and N21080)
Laser powermeter (Coherent Model 330241/33-0324)

6. Method of Approach: Sample preparation

(a) Preparation of high temperature oxide glasses

We have used several different compositions to make oxide glasses. One such composition is given below. La_2O_3 (11.6wt%), PbO (11.6wt%), SiO_2 (11.6wt%), B_2O_3 (11.6wt%), $MgTiO_3$ (5.8 wt%), TeO_2 (34.9wt%), $Ba_3Y_3WO_9$(11.6wt%) and R_2O_3 (1.3wt%). All the chemicals were mixed together thoroughly for about half an hour and then melted in an alumina crucible at 800C for two hours and then at 1350C for another two hours. The resulting melt was poured into an aluminum mold, which was kept in ambient atmosphere and allowed to cool to room temperature naturally. The resulting glass was polished on a spinning metallic disc, using different grades of polishing paper and polishing powders. The resulting glass was found to be transparent. Absorption spectral recordings verified the presence of europium dopant. Hole burning studies revealed transient hole burning in these glasses whose details are given later on.

(b) Preparation of Eu^{3+} doped sol-gel glasses

We made two different solutions. (1) **Solution 1**: 0.001 g europium nitrate was dissolved into 6 mL ethanol and stirred until dissolved completely. Then 6 ml of silica (Silbond H-5) was added and stirred (2 minutes). (2) **Solution 2**: 6 ml of ethanol (200 proof), 9 ml distilled water and 0.03 ml 30% NH_3/H_2O was mixed and stirred for a few minutes (1 to 2 minutes). Solution 1 was added to solution 2 and stirred briefly (1 to 2 minutes). The resulting solution was poured into a petridish and then sealed. After gelling the solution was allowed to remain in the sealed dishes until it was dried completely (about a week). A good sol-gel glass was obtained. We made such glasses doped with erbium also.

© Preparation of dye doped sol-gel glasses

The first step is to dissolve the dye into appropriate solvent. For this purpose about 0.19 mg of Alizarin Yellow R / disperse red 13 was dissolved into 6mL of ethanol and then stirred with 6mL of silica (Silbond H-5). Afterwards the dye solution was added to another solution that has the following composition: 6mL of (200 proof) ethanol, 9mL of distilled water and 0.03mL (30% NH_3/H_2O). Then the mixture was poured into a petri dish and the top was sealed and allowed to stay for 5 days. Later on the top was covered with an aluminum foil. The foil was punctured with holes and the solution was allowed to dry for couple of weeks. Using this procedure we made good samples of sol-gel glasses doped with disperse red and alizarin yellow.

Disperse red doped sol-gel glass showed absorption in the region 200 - 620 nm with peaks at 220, 290 and 440 nm. Under dye laser excitation it showed upconversion emission signals at 300-400 nm due to sequential two-photon excitation process. So far there is no evidence for hole burning effect if any.

Alizarin yellow doped sol-gel glass showed upconversion emission at 250 - 450 nm (with a sharp peak at 434 nm) under 514.5 nm laser excitation.

(d) Preparation of spin-coated polymer films with dye dopants

(d1) Polyvinyl alcohol films

About 20 mg of PVA, 30 mL of ethanol and 5 mL of H_2O were mixed in glass cup and heated at 90C for three hours. A saturated solution was obtained, by adding more PVA whenever it was necessary. About 10mg of DODCI was added to this solution and mixed uniformly. Then it was poured on a glass slide spun it for 20 seconds at 400 rpm and at

1200rpm for 1 minute. Then the films were heated for 30 minutes at 50C. Its absorption spectrum revealed a peak at 593 nm as expected.

(d2) Polystyrene sulfonic acid films

About 30mg of polystyrene sulfonic acid, 30 mL of H_2O were mixed and a saturated solution was formed if necessary by adding either sulfonic acid or H_2O About 10mg Styryl 7 dye was added and mixed uniformly. It was used to spin coat glass slides at 400rpm for 20 seconds and 1500 rpm for 1.5 minutes. The film was heated in an oven at 40C for 30 minutes. Its absorption spectrum revealed a strong peak at 550nm.

(d3) PMMA films

About 20mg of PMMA and 30mL of toluene were mixed and heated at 70C for 30 minutes followed by another 30 minutes at 50C. About 10mg of Rhodamine 590 chloride was added and heated at 50C for 20 minutes and at 90C for 10 minutes. It was poured on a glass slide and spun at 450rpm for 20 s and at 1600rpm for 20 s. The film was heated at 70C for 20 minutes. Its absorption spectrum revealed peaks at 509 and 537.5nm.

We made several other guest-host combinations (dye doped polymers). Other types of dyes used to make polymer films are Quinzarin, Alizarin, Ethyl orange, methyl orange, and pthalocyanine based dyes.

7. Hole burning studies

We performed hole burning studies using a Spectra-Physics ring dye laser whose instantaneous linewidth ~3MHz in stablok mode and 15MHz in free running mode. We obtained some significant results in the following systems. The laser used for this study was procured by another faculty member a longtime ago. For this work we proposed to

use the existing laser. We started the hole burning work at Alabama A&M University for the first time. We also bought several other instruments including a cryostat. So we wanted to check the performance of the laser and other equipment by performing hole burning studies in a material that was already investigated. Europium doped YSO was investigated in the past by the Japanese and American scientists. We obtained this material from Scientific Materials Corp.

(a) YSO: Eu^{3+}

We made some significant contributions to the understanding of hole burning effect in this material. The past investigations revealed that Eu^{3+} ions enter this host only in two different types of sites. However our measurements revealed that Eu^{3+} ions enter in 42 distinct sites in this material, though two of them are predominant. This effect occurs due to clustering of the dopant ions and the presence of dopant induced microscopic defects. We have published two papers (Applied Optics 38, 5662 (1999) and SPIE 3802, 238 (1999)). Copies of the publications are attached at the end of the report.

(b) CaF_2: Eu^{3+}

We wanted to verify whether the phenomenon observed by us is universal or a unique characteristic of YSO:Eu^{3+}. So we decided to investigate hole burning in CaF_2: Eu^{3+}. According to the work done by J. C. Wright's group (J.Chem. Phys. 77, 683 (1982)), Eu^{3+} was known to occupy predominantly five different sites in CaF_2 host. Manson's group (Australia), (Phys.Rev.B34, 4854 (1986)) performed hole burning studies of oxygen compensated trigonal sites. Macfarlane's group performed hole-burning studies of the tetragonal sites. Macfarlane and J.C. Wright investigated materials with

low concentrations of Eu^{3+}(0.1%). However, we investigated a material that has 0.5% Eu^{3+} concentration. Our low resolution work of the $^7F_0$--$^5D_0$ transition revealed about 22 different peaks (corresponding to different sites) within the wavelength interval of 3nm and the high resolution work revealed about 40 different peaks within 1 nm interval centered at 580nm. A material with higher concentration exhibited more number of sites. This clearly demonstrates that clustering of the ions is mainly responsible for the multisite behavior; though dopant induced microscopic defects also contribute to this effect. We also performed hole burning efficiency measurements. These results were published in the Journal of Applied Physics 87, 3570 (2000). A copy of this publication is attached at the end of this report.

Our studies also indicate that this is a common phenomenon in all the crystals. However these are clearly revealed in Eu^{3+} doped systems because the $^5D_0$--$^7F_0$ transition exhibits a single peak and there are no near by Stark components to create spectral overlap, as in the $^1D_2$--$^3H_4$ transition of Pr^{3+} doped crystals.

© Characterization of oxide glasses

We made Eu^{3+} and Pr^{3+} doped glasses. However we are not able to investigate Pr^{3+} doped materials due to the broad laser linewidth. We concentrated mainly on Eu^{3+} doped materials. Emission spectra were recorded by pumping the samples (9K), with a ring-dye laser wavelength tuned to resonantly excite the $^7F_0 \rightarrow {}^5D_0$ transition (578nm) of Eu^{3+}. Excited ions showed characteristic emission by relaxing to different lower multiplets. In Eu^{3+} -doped glasses the strongest emission was at 612nm. We also recorded their zero-phonon linewidths. Glasses are amorphous and hence their inhomogeneous linewidths are very large. To get some idea about the inhomogeneous

broadenings we also recorded the excitation spectrum of 612nm-emission peak of Eu^{3+} by scanning the dye laser wavelength. The inhomogeneous profile of the transition, $^5D_0 \rightarrow {}^7F_0$ centered at 579.4 nm is shown in Fig. 1. Its inhomogeneous width is about 3nm (2673 GHz) FWHM and it is about 6nm, at 10% of the peak height. The inhomogeneous broadening ~GHz in Eu^{3+} doped single crystals. Inhomogeneous broadening is at least 1000x higher in these glasses when compared to crystals. We made some more glasses by slightly varying the glass composition as well as the dopant concentration. It appears that, for recording the hole burning spectrum one has to record the absorption spectrum before and after exposure to the laser radiation, and subtract the latter from the first, because the efficiency is very weak.

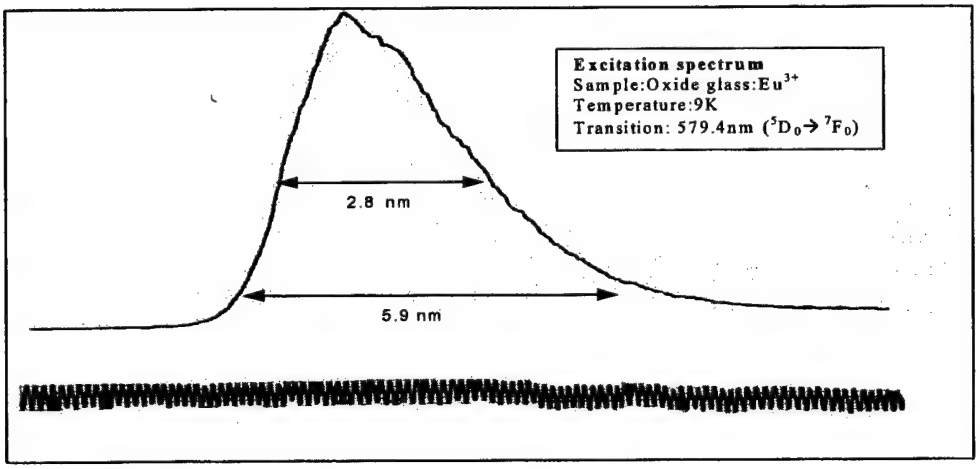

Fig.1: Excitation spectrum of 612nm emission signal of Eu^{3+} doped oxide glass at 9K. The Excitation spectrum reveals the inhomogeneous profile of the transition ($^5D_0 \rightarrow {}^7F_0$) centered around 579.4nm.

Because these glasses were made at 1350 C the water concentration is minimized. As a result these materials did not exhibit persistent spectral hole burning. However we did detect transient hole burning in glasses. This was revealed by the sideband spectroscopy measurements (Fig.2).

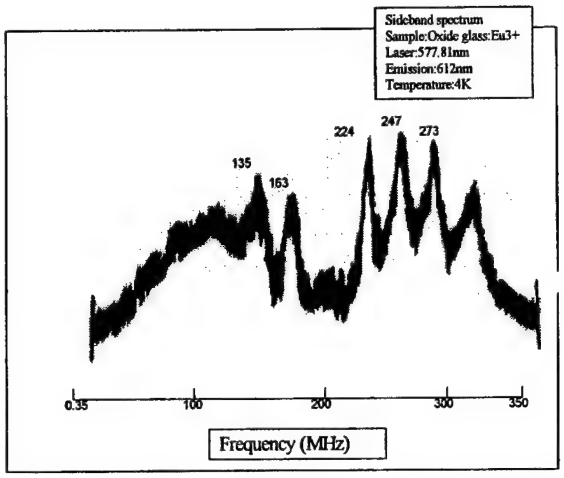

Fig.2: Side-band frequency spectrum of Eu^{3+} doped oxide glass. Numbers listed on the peaks are their frequencies in MHz.

8. Resonance enhanced population gratings in LaF_3: Pr^{3+}

When the $^1D_2$ level of LaF_3: Pr^{3+}, that is at 16 872cm^{-1} was resonantly excited with a single frequency dye laser (linewidth ~3MHz) we have observed fringes in the transmitted beam direction. This particular effect was observed only in irradiated uniaxial materials, and that too when the laser frequency is tuned to the absorption maximum (to within a GHz) and at low sample temperatures. If the laser frequency is changed by a couple of GHz from the resonance the fringes disappeared.

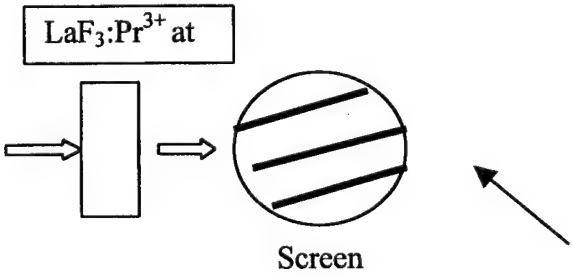

Fig. 3: Experimental configuration used to detect fringes

We spent more time to investigate this unusual behavior. Our cryostat is equipped with one pair of Sapphire windows (slightly birefringent) and one pair of fused silica windows

(isotropic). Our continued investigation reveled that the fringes are seen only when the beam is passed through the sapphire windows. However the sapphire windows are randomly polarized. It appears that the fringes may be due to strain induced, population dependent birefringence produced in the material, though further investigations are needed to confirm it.

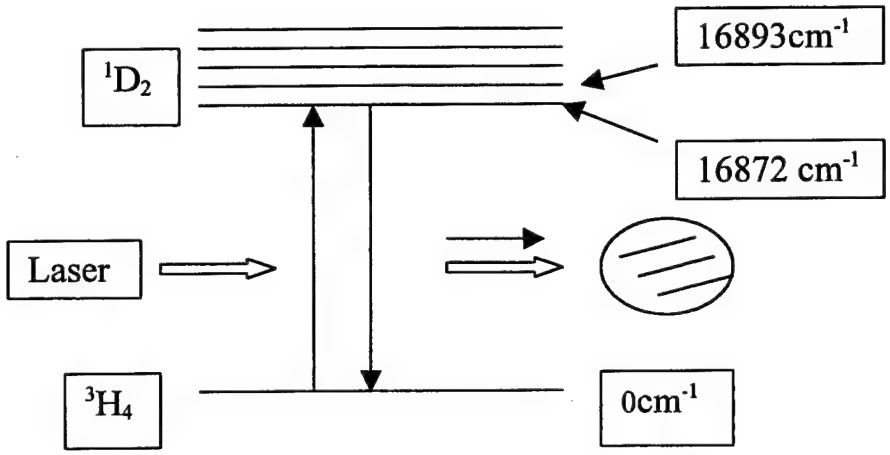

Fig. 4: Detailed excitation schemes

9. Computer interfacing

We bought an A/D converter and other accessories from the National Instruments and designed interface circuits in the Labview environment for data acquisition. These circuits are designed suitable to our experimentation. Some preliminary experiments were performed with this setup.

10. Optical investigation of dye doped systems

Absorption spectra of the dye-doped samples are shown in Fig. 5 for a few samples. The absorption spectra clearly revealed the expected features of the dopants. Styryl 7 and DODCI samples exhibited absorption bands centered at 600 as well as

300nm. These samples when exposed to 580nm are expected to absorb two photons in a stepwise mechanism. In some media, when these molecules are in a highly excited state, undergo photochemical change. So we will pursue these studies in the near future.

For example ethyl orange and methyl orange dyes were known to change from one isomer to another isomer when they are in a highly excited state (cis-trans isomerization). The absorption spectrum revealed two peaks in Fig.5 (first and second excited states). If the molecules undergo cis-trans-isomerization the absorption features will change. When such a change occurs they are expected to show persistent hole burning. These studies will be pursued in near future.

11. Infrared quantum counter (IRQC) studies in europium doped crystals

When we were pursuing hole burning studies we accidentally detected upconversion signals. So we pursued energy upconversion studies under dye laser excitation in LaF_3: Eu^{3+} and CaF_2: Eu^{3+}. We also performed infrared quantum counter studies (IRQC) in these materials by irradiating the samples with visible and infrared beams. We performed IRQC studies for the first time on Eu^{3+} doped materials. We also estimated the excited state absorption cross sections by performing pump-probe experiments. IRQC studies are useful for the development of room temperature infrared detectors. This is one of the interests of DoD. We have published a paper on this subject in the Journal of Applied Physics 88, 2191 (2000) and another paper was communicated to Journal of the Optical society of America B.

12. Suggestions for further work

We will prepare rare-earth ion doped inorganic glasses which retain some moisture and pursue persistent hole burning studies. We will also pursue hole burning studies in dye doped polymers. For this purpose different guest-host combinations will be investigated.

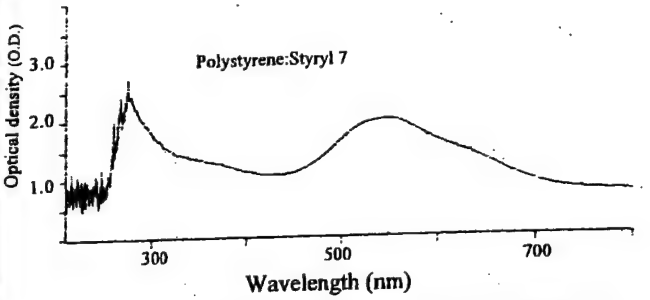

Fig. Absorption spectrum of Polystyrene doped with Styryl 7 dye

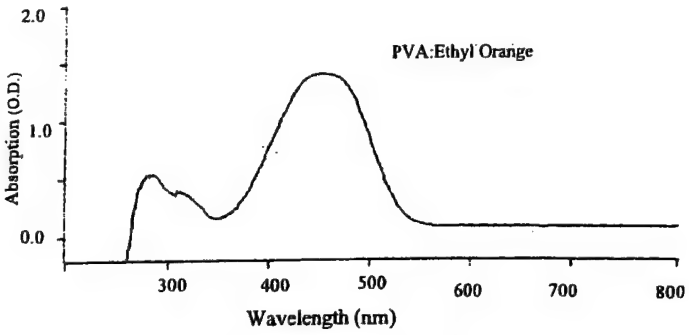

Fig. Absorption spectrum of PVA doped with ethyl orange dye

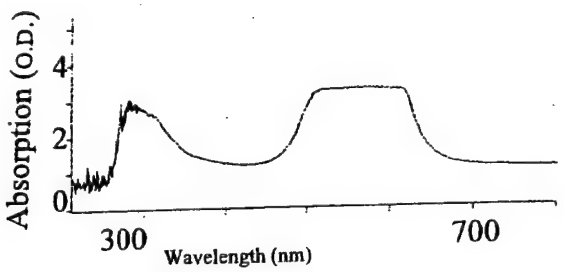

Fig. Absorption spectrum of Polystyrene doped with DODCI

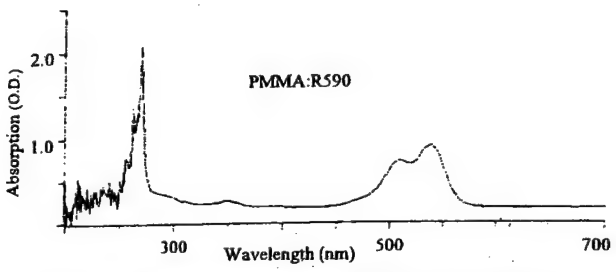

Fig: Absorption spectrum of PMMA doped with Rhodamine 590

High-resolution spectroscopy and optical hole burning studies of the $^7F_0 \rightarrow {}^5D_0$ transition of europium-doped calcium fluoride

Ranjit S. Pandher, Angela Davis, Andre Jackson, and B. Rami Reddy[a)]
Alabama A&M University, Department of Physics, P.O. Box 1268, Normal, Alabama 35762

(Received 5 November 1999; accepted for publication 30 December 1999)

High-resolution spectroscopic study of the $^7F_0 \rightarrow {}^5D_0$ transition revealed more than 40 different sites for the rare-earth ion. The multisite behavior was found to be due to clustering of the dopants and dopant induced microscopic defects. Hole-burning efficiencies were measured for some sites.
 [S0021-8979(00)02607-4]

Calcium fluoride is a cubic material. Rare-earth ions were known to occupy different sites due to charge compensation. Hamers *et al.*[1] identified five different sites in CaF_2:Eu^{3+} (0.1%) whose $^7F_0 \rightarrow {}^5D_0$ absorption wavelengths fall at 579±0.6 nm. High-resolution spectral studies were also performed on these materials by the hole-burning technique. Hole-burning studies of the tetragonal site[2] and oxygen-compensated trigonal site were performed in the past.[3–5] Hole burning was also pursued in several other europium-doped crystals and glasses.[6–10] The $^5D_0$ and $^7F_0$ states of Eu^{3+} are singlets in the crystal field. A transition between these two states is expected to reveal a single peak either in absorption or emission, in defect free perfect crystals. A recent investigation[11] on the $^7F_0 \rightarrow {}^5D_0$ transition of Eu^{3+} doped Y_2SiO_5 revealed more than 40 different satellite lines for the dopant though the prior studies revealed only two sites.[12] Similar observations were made in $EuVO_4$[13] and $YAlO_3$:Eu^{3+}[14] also. The satellite lines were ascribed to ions that were on the sites differently perturbed, by defects or clustering of Eu^{3+} ions. It is not clear yet whether this multisite behavior is universal or dependent on the host material. So, we reinvestigated the high-resolution spectroscopy and hole-burning phenomena in CaF_2:Eu^{3+}. Our studies revealed more than 40 different sites for the Eu^{3+} ion whose transition wavelengths ($^7F_0 \rightarrow {}^5D_0$) fall within 1 nm centered around 579.5 nm.

The sample is of size $0.8 \times 0.6 \times 0.4$ cm^3 and was obtained from Optovac, Inc. The concentration of the dopant is 0.5 mol %. Absorption spectrum was recorded by a Varian-CARY3E spectrophotometer. A high-resolution ring-dye laser of linewidth ~3 MHz and a low-resolution dye laser of linewidth ~60 GHz were used to excite the samples. The sample was cooled to 9 K in a closed cycle cryostat for all the emission and excitation measurements. The emission was processed by a medium resolution spectrometer that has a dispersion of 1.7 nm/mm. In some high-resolution excitation measurements the slitwidth limited bandpass of the instrument was about 5 nm. The light was detected by a Hamamatsu Model R928 photomultiplier tube. Its output was amplified and plotted on a chart recorder. In high-resolution excitation spectral measurements the amplified signal was given to a storage oscilloscope whose output was plotted on an $X-Y$ recorder. The use of a spectrometer simplifies the analysis of different sites. The ring dye laser was operated in the free running mode for recording the high-resolution excitation spectra and in the stablock mode for burning and recording spectral holes. The laser wavelengths were measured by a Coherent–Ealing wavemeter, Model 33-2684.

Absorption spectrum revealed two strong peaks centered at 230 and 360 nm, which are very broad when compared to the Eu^{3+} transitions. These wavelengths are in close agreement with the Eu^{2+} transitions.[1] Fluorescence spectrum was recorded by resonantly exciting the $^5D_0$ level. Emission occurred at 579, 590, 617, 650, and 701 nm to different ^7F_J levels ($J=0-4$). Strong emission occurred at 590 and very weak emission occurred at 650 nm. The emission intensity and the number of peaks in any group varied dramatically depending on the laser wavelength used (or site that was excited). Emission from all the sites overlapped at 593.7 nm. A low resolution excitation spectrum of 593.7 nm revealed about 21 peaks, in the wavelength interval 577–581 nm, suggesting that there are at least 21 different sites for the rare-earth ion. There are marked differences in the emission spectral characteristics whenever the laser excitation wavelength was tuned slightly within the wavelength interval 579.6–580.2 nm. This indicates that all the excitation peaks represent different sites of the dopant. However, a high-resolution excitation spectrum revealed about 42 peaks in the wavelength interval 579–580 nm (Fig. 1). The low-resolution excitation spectrum was recorded with a laser whose linewidth is ~60 GHz. So, some of the closely spaced peaks were not separated. The high-resolution spectrum was recorded by operating the ring dye laser in the free running mode whose linewidth is ~15 MHz. As a result, we were able to detect more than 40 peaks in the high-resolution excitation spectrum whose wavelengths fall within 1 nm of the central wavelength. High-resolution excitation spectra were recorded in several overlapping segments with each segment covering ~40 GHz. The strongest peaks were peak No. 5, at 579.9 (579.412 nm) and peak No. 31, at 579.0 nm (578.446 nm) and the numbers given in the parentheses are those reported by Hamers *et al.*[1] The intensity of any other peak is ~10× less than that of the strongest peak. There is some

a)Electronic mail: brreddy@aamu.edu

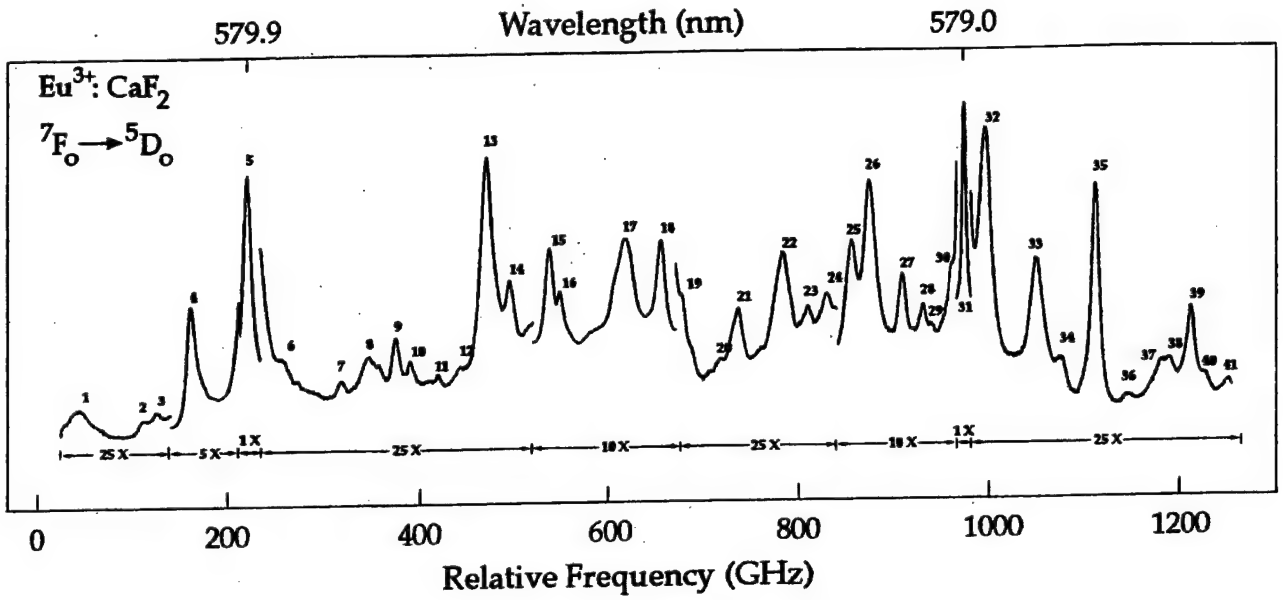

FIG. 1. High-resolution spectrum of the $^7F_0 \rightarrow {}^5D_0$ transition of CaF_2:Eu^{3+}. The excitation spectrum was recorded by monitoring emission at 593.7 nm.

discrepancy between the wavelengths measured by the wavemeter (in the present case) and those reported by Hamers *et al.*[1] However the wavelength interval between the strong peaks is comparable.

All the peaks shown in Fig. 1 represent electronic levels of different sites and not phonon-coupled levels. This was confirmed by recording the hole-burning spectra for all the peaks (or sites). Hole formation was also verified by recording the temporal evolution of the emission intensity for all the peaks. Holes were burnt in the absorption spectrum by exposing the sample to about 20 mW of laser radiation for about 20 s. Excitation spectrum was recorded by sweeping the same laser frequency at reduced power. A 1 GHz scan was completed in less than 2 s. For some peaks, a recording of the hole spectrum revealed side holes and antiholes also (Fig. 2). Analysis of the hole-burning spectra revealed that each satellite peak has its own hyperfine splittings indicating that they all represent electronic levels. Some of the holes are long lived at 9 K. The hole lifetime varied from 3 min (longest for peak No. 5) to 10 s (least for peak No. 27), for all the other peaks the hole lifetimes are in between. The ionic concentration is 1.225×10^{20} cm^{-3}. Integrated absorption measurements revealed that about half of the ions contributed to the formation of the two strong peaks Nos. 5 and 31. Hole-burning efficiency was estimated by using the procedure given elsewhere.[15] Based on relative estimates, it was found that peak No. 31 exhibited the highest hole burning efficiency and peak No. 39 the lowest, and the efficiency was in between for all the other peaks. The efficiency of peak No. 5 is about 27% less than that of peak No. 31. The total inhomogeneous broadening of all the sites was estimated as ~410 GHz (full width at half maximum).

In a 0.1% sample Hamers *et al.*[1] observed only about five dominant sites. However, in a 0.5% sample the number of sites were found to be 20 under low-resolution measurements and 42 under high-resolution measurements. This indicates that the multisite behavior is predominantly due to clustering of the dopant ions and the presence of microscopic defects induced by the dopants in the crystal. Our results indicate that this effect is universal and should be observable in all the materials. However, this effect was not detected in the $^3H_4 \rightarrow {}^1D_2$ transitions of Pr^{3+} doped materials[16] because of the occurrence of a strong absorption to the neighboring Stark levels.

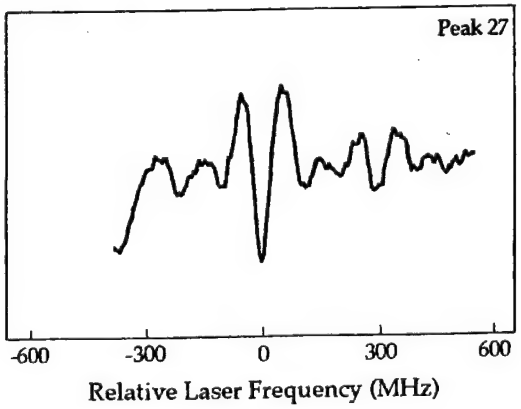

FIG. 2. Hole-burning spectrum for peak No. 27 of Fig. 1. The transition is $^7F_0 \rightarrow {}^5D_0$.

This work was supported by Air Force Office of Scientific Research Grant No. F49620-97-1-0258.

[1] R. J. Hamers, J. R. Wietfeldt, and J. C. Wright, J. Chem. Phys. **77**, 683 (1982).
[2] A. J. Silversmith and R. M. Macfarlane, Phys. Rev. B **45**, 5811 (1992).
[3] A. P. Radlinski and A. J. Silversmith, Phys. Rev. B **34**, 86 (1986).
[4] A. J. Silversmith and N. B. Manson, Phys. Rev. B **34**, 4854 (1986).
[5] A. J. Silversmith, A. P. Radlinski, and N. B. Manson, Phys. Rev. B **34**, 7554 (1986).
[6] K. Fujita, K. Tanaka, K. Hirao, and N. Soga, Opt. Lett. **23**, 543 (1998).
[7] Y. Mao, P. Gavrilovic, S. Singh, A. Bruce, and W. H. Grodkiewicz, Appl. Phys. Lett. **68**, 3677 (1996).
[8] D. M. Boye, Y. Sun, and R. S. Meltzer, J. Lumin. **66&67**, 184 (1996).
[9] K. Koyama and T. Suemoto, J. Lumin. **66&67**, 164 (1996).

[10]L. E. Erickson and K. K. Sharma, Phys. Rev. B **24**, 3697 (1981).
[11]R. S. Pandher, A. Jackson, A. Davis, and B. R. Reddy, Appl. Opt. **38**, 5662 (1999).
[12]R. Yano, M. Mitsunaga, and N. Uesugi, J. Opt. Soc. Am. B **9**, 992 (1992).
[13]M. Yamaguchi, K. Koyama, T. Suemoto, and M. Mitsunaga, J. Lumin. **76&77**, 681 (1998).
[14]R. L. Cone, P. C. Hansen, and M. J. M. Leask, J. Opt. Soc. Am. B **9**, 779 (1992).
[15]W. E. Moerner, M. Gerhtz, and A. L. Huston, J. Phys. Chem. **88**, 6459 (1984).
[16]R. M. Macfarlane, in *Persistent Spectral Hole Burning: Science and Applications*, Topics in Current Physics, Vol. 44, edited by W. E. Moerner (Springer, New York, 1988).

Site-selective hole burning in Eu^{3+}:Y_2SiO_5

Ranjit S. Pandher, Andre Jackson, Angela Davis, and B. Rami Reddy

We found that the Eu^{3+} ion occupies several distinct sites in Y_2SiO_5. We were also able to perform hole-burning studies in more than 40 different transitions. © 1999 Optical Society of America

OCIS codes: 160.5690, 300.6320, 210.4680, 210.4810, 250.5230, 300.6460.

The optical hole-burning phenomenon is known to facilitate large amounts of information storage within a small piece of optical material. For this purpose several types of material are under investigation, and, in particular, Pr^{3+}- and Eu^{3+}-doped samples were investigated thoroughly.[1] In rare-earth ion-doped materials a hole's lifetime depends on the spin-lattice relaxation time. Of all the materials investigated, Eu^{3+}-doped samples were known to retain the hole for a long period of time.[2,3] Eu^{3+} was known to occupy different sites in CaF_2, owing to charge compensation.[4] However, in Y_2SiO_5 material, Eu^{3+} was known to occupy the Y^{3+} location at two different types of site[5] with the site symmetry C_1. Hole-burning studies were performed for these two sites by resonant excitation of the $^5D_0$ and the $^5D_1$ levels.[5–7] Hyperfine-interaction studies of Eu^{3+} were also performed, by recording of the hole-burning spectra.[8] Hole-burning studies were also investigated in several other materials doped with europium.[9–12] The advantage of Eu^{3+} is that its $^5D_0$ level remains a singlet even in the presence of a crystal field. The $^5D_0$ energy level is then well separated from other levels and gives rise to isolated spectral lines when compared with other multiplets and other rare-earth ions. This characteristic makes spectral analysis much simpler. In this study we capitalized on this feature of Eu^{3+} centers in europium-doped Y_2SiO_5. We found evidence, for the first time to our knowledge, that Eu^{3+} occupies numerous distinct sites in this material, which is in contrast to what has been reported previously.[5] Our findings suggest that this material's information storage capacity is greater than that predicted previously.[5–8]

We performed high-resolution spectroscopic studies in Y_2SiO_5 doped with Eu^{3+} (0.1 mol. %). This concentration is the same as that used by Yano *et al.*[5,8] The sample used in this study was obtained from Scientific Materials Corporation. It is of size 1.0 cm × 0.6 cm × 0.4 cm. The sample temperature was ~9 K in all these measurements. The temperature sensor was mounted on a cold finger. The emission was processed by a low-resolution monochromator (Acton Research Corporation, SpectraPro-150), which is fitted with a Hamamatsu Model R928 photomultiplier tube. The photomultiplier tube output was given to a picoammeter and then plotted on a strip-chart recorder. The low-resolution excitation spectrum of the 612-nm signal was recorded by tuning of the wavelength of a broadband dye laser beam (linewidth, ~60 GHz). These excitation wavelengths were measured with a Coherent-Ealing wavemate (Model 33-2684), whose calibration was verified prior to the usage. We recorded the high-resolution excitation spectrum by giving the photomultiplier tube output, to a storage oscilloscope, and the weak signals were amplified in advance when necessary. The use of a spectrometer in the recordings of the excitation or hole-burning spectra minimizes the background that is due to stray light.

As expected, emission was seen from $^5D_0 \rightarrow {}^7F_j$ (j = 0–2), in the wavelength region 570–640 nm. A low-resolution excitation spectrum of 612 nm reveals two strong peaks at 580.5 (B) and 580.7 nm (C) and three weak peaks at 580.4 (A), 580.9 (D), and 581 nm (E) (Fig. 1). All the excitation wavelengths to the $^5D_0$ state are within 0.6 nm. The strong peaks correspond to those reported by Yano *et al.*,[5] whereas the other peaks, 2 orders of magnitude weaker in intensity, have not been reported previously. The presence of these five peaks indicates that there are at least five different Eu^{3+} centers in this crystal of

The authors are with the Department of Physics, Alabama A&M University, P.O. Box 1268, Normal, Alabama 35762. B. R. Reddy's e-mail address is brreddy@aamu.edu.

Received 20 November 1998; revised manuscript received 20 April 1999.

0003-6935/99/05662-04$15.00/0

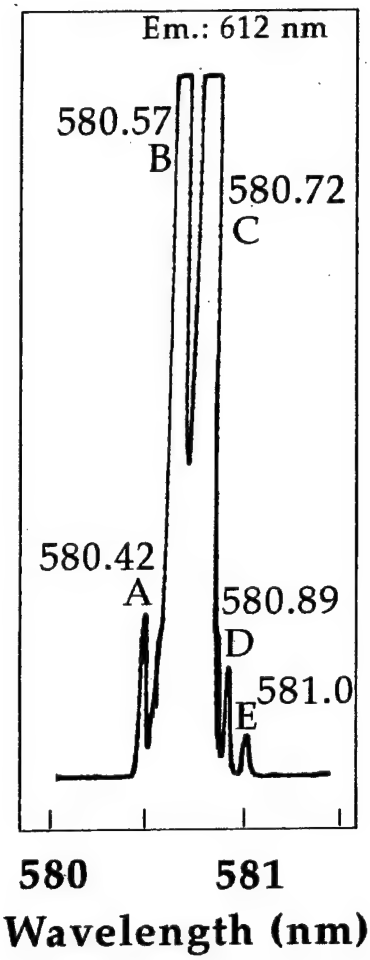

Fig. 1. Excitation spectrum of the 612-nm peak revealing the absorption transition, $^7F_0 \rightarrow {}^5D_0$.

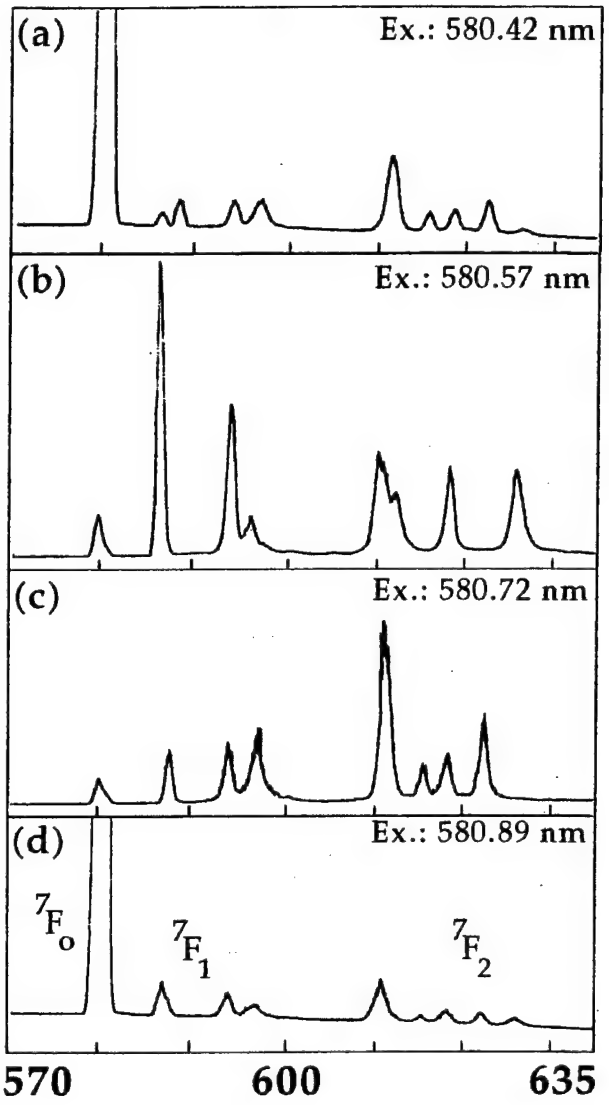

Fig. 2. $^5D_0 \rightarrow {}^7F_j$ (j = 0–2) emission spectra observed on excitation of different sites: (a) λ_{ex} = 580.42 nm, (b) λ_{ex} = 580.57 nm, (c) λ_{ex} = 580.72 nm, (d) λ_{ex} = 580.89 nm. The 612- and the 613-nm peaks are not resolved in this figure. (a) and (d) are expanded 100× when compared with the other two.

Y_2SiO_5. The $^5D_0$ level remains a singlet even in the crystal field. The fact that the excitation spectrum revealed five peaks indicates that there are at least five sites for the europium ion in this material. We also recorded the emission spectrum associated with the different excitation wavelengths (Fig. 2). The emission spectra revealed differences in structure and relative intensities. For example, under 580.57-nm laser excitation, the emission spectrum revealed only eight peaks in the 570–635-nm region [Fig. 2(b)]. However, under 580.89-nm laser excitation, the emission spectra revealed nine peaks [Fig. 2(d)]. These differences in the emission spectra also confirm the prediction that the weak excitation peaks correspond to different Eu^{3+} sites and not to the phonon-coupled levels. The emission intensity of the peaks in Figs. 2(a) and 2(d) is much weaker. To facilitate recording, the scale was expanded 100×. As a result the intensity of the $^5D_0 \rightarrow {}^7F_0$ transition exceeded the chart. Emission is predominantly from the sites that were excited by the laser beam.

High-resolution excitation spectral measurements revealed inhomogeneous linewidths (full-width at half-maximum) of approximately 4.2 and 2.9 GHz, respectively, for the B and the C sites and less for the other sites (~1 GHz). The emission peak at 612 nm (Fig. 2) and others are due to the superposition of several distinct peaks. When the laser is tuned within the absorption profile, peak B (or C) (Fig. 1), we found evidence for a large number of distinct sites. That is, excitation spectra revealed differences in structure whenever the laser is tuned to a slightly different frequency within the absorption peak. One such excitation spectrum is shown in Fig. 3. It has two peaks instead of one. The difference in the two peaks is ~2.9 GHz, and each has a linewidth of ~1.2 GHz. This prompted us to scan the whole excitation region of width ~0.7 nm (580.3–581 nm). To our surprise we found a total of 42 excitation

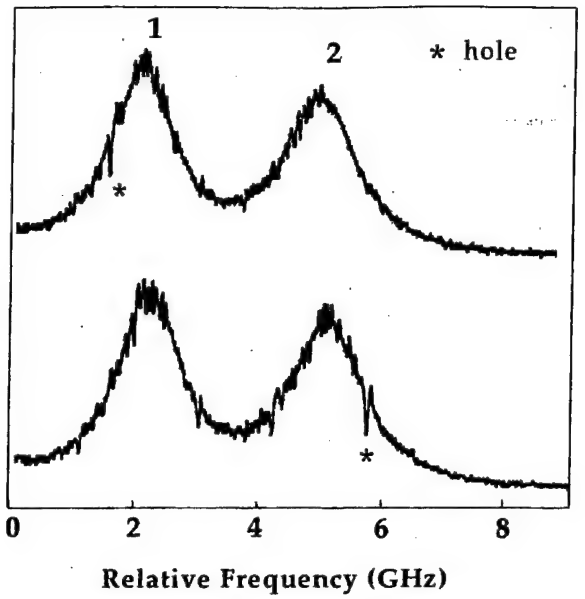

Fig. 3. Excitation spectrum ($^7F_0 \rightarrow {}^5D_0$) reveals holes in both peaks 1 and 2, indicating that they are electronic levels of different sites.

peaks (Fig. 4), indicating that there are 42 distinct sites. The intensities of the new peaks are ~2 orders of magnitude weaker than that of the strongest peaks, numbered 12 and 34, which were studied by Yano *et al.*[8] The other peaks were not known in the past. The weaker peaks are sufficiently strong, and their distinct nature could be seen with unaided eye. To our knowledge, this was the first observation of its kind. The spectrum shown in Fig. 4 was reproduced even for a different spatial location of the laser beam and orientation of the material. Figure 4 was recorded in several overlapping segments with each segment covering ~40 GHz, whereas the laser was operated in the free-running mode, whose effective linewidth is ~35 MHz.

The peaks numbered 3–38 (Fig. 4) are very closely

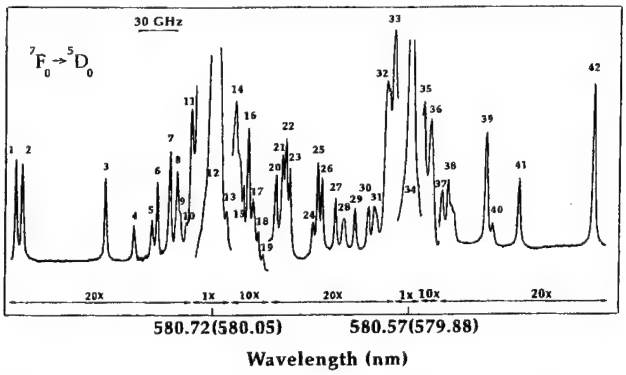

Fig. 4. Excitation spectrum of the 612-nm emission peak reveals 42 distinct peaks. Each peak represents the $^5D_0$ level of a particular site. Peaks 12 and 34 are the strongest and were reported by Mitsunaga *et al.*, and the wavelengths they measured are given in parentheses (Refs. 5 and 8). The numbers along the bottom are multiplication factors used to record the spectrum.

separated. That is, the spacing between any two successive peaks is less than 30 GHz. Since the low-resolution excitation spectrum was recorded with a dye laser whose linewidth is ~60 GHz, the satellite lines are not resolved, and they contributed to the broadening of the strong peaks numbered 12 and 34, and thus the low-resolution spectrum revealed only five peaks (Fig. 1). However, the high-resolution excitation spectrum was recorded with a laser whose linewidth is ~3 MHz, which is much narrower than the frequency spacing between the successive satellite lines. Hence the high-resolution excitation spectrum (Fig. 4) revealed 42 peaks. Such satellite lines in the excitation spectra have also been observed in other materials.[13,14] The satellite lines are narrower when compared with the strong peaks 12 and 34, for the following reasons. The number of ions contributing to the satellite lines is less when compared with that of strong peaks. It may be possible that the strong peaks resulted from the superposition of several closely spaced narrower peaks.[15]

To verify that these satellite peaks do not represent phonon-coupled levels, we performed hole-burning studies by tuning the laser to resonantly excite the $^5D_0$ level of each site. A hole was burned in the absorption spectrum by irradiation of the sample for a few seconds by the laser beam. Then the same laser frequency at reduced power was swept within 10 s to record the hole. When the laser is tuned to peaks 12 and 34 (580.72 and 580.57 nm), the holes last for >10 s and ~1 s, respectively. These two sites were found to have long lifetimes at 6 K in the earlier studies.[5,8] However, the hole-burning measurements in the current investigation were performed at 9 K, because the lowest limit is set by the closed-cycle cryostat used in this study. The emission intensity of the strong peaks decreased to 20% of their peak values in ~200 msec after the laser (whose power was 30 mW) was turned on. For the other peaks similar measurements revealed longer times. This indicates that the hole-burning efficiency of the strong peaks is very high when compared with that of other peaks. In general, hole lifetimes of the peaks numbered 1–27 (>10 s) are longer than those of the others (~1 s). The hole-burning spectra obtained with a computer for peaks 3 (weak peak) and 12 (strong peak) are shown in Fig. 5. The high-frequency noise of the spectrum was removed by use of fast-Fourier-transform filtering and then displayed in Fig. 5. The figure reveals side holes, which correspond to the hyperfine splittings in the $^5D_0$ state. It is also evident from the figure that the side-hole frequencies are different for those two peaks. In other words, each satellite line has its own hyperfine splittings. This confirms our findings that the satellite lines do not represent phonon-coupled levels.

This is a clear indication that there are different sites for Eu^{3+} ion in Y_2SiO_5. Our studies indicate that the information storage capacity of this material is much greater than was thought in the past. The multiple sites arise because of microscopic defects in the material, clustering of the dopant ions, differ-

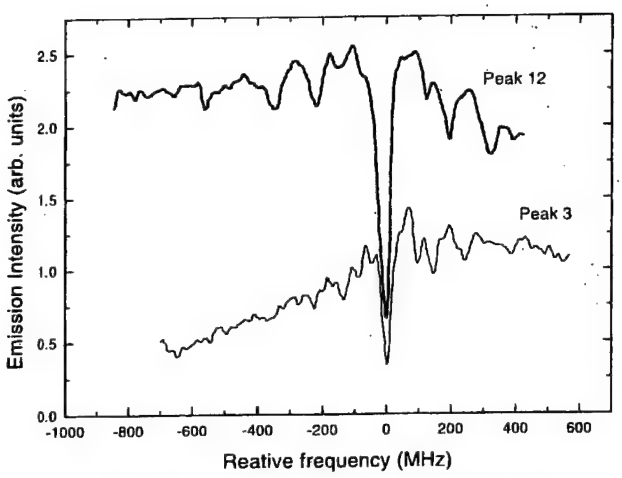

Fig. 5. Hole-burning spectra of the $^7F_0 \rightarrow {}^5D_0$ transition in Y_2SiO_5:Eu^{3+} observed at 9 K for peaks 3 and 12. The data were acquired with a computer, and the high-frequency noise was removed by use of fast-Fourier-transform filtering.

ences in the mass and the size of Eu^{3+} and Y^{3+} ions, and differences in the force constants with the surrounding ligands.[15,16]

This research was supported by U.S. Air Force Office of Scientific Research grant F49620-97-1-0258.

References

1. W. E. Moerner, ed., *Persistent Spectral Hole-Burning: Science and Applications*, Vol. 44 of Topics in Current Physics (Springer-Verlag, New York, 1988).
2. Y. Mao, P. Gavrilovic, S. Singh, A. Bruce, and W. H. Grodkiewicz, "Persistent spectral hole burning at liquid nitrogen temperature in Eu^{3+}-doped aluminosilicate glass," Appl. Phys. Letts. **68,** 3677–3679 (1996).
3. K. Fujita, K. Hirao, K. Tanaka, N. Soga, and H. Sasaki, "Persistent spectral hole burning of Eu^{3+} ions in sodium aluminosilicate glasses," J. Appl. Phys. **82,** 5114–5120 (1997).
4. R. J. Hamers, J. R. Weitfeldt, and J. C. Wright, "Defect chemistry in CaF_2:Eu^{3+}," J. Chem. Phys. **77,** 683–692 (1982).
5. R. Yano, M. Mitsunaga, and N. Uesugi, "Ultralong optical dephasing time in Eu^{3+}:Y_2SiO_5," Opt. Lett. **16,** 1884–1886 (1991).
6. M. Mitsunaga, R. Yano, and N. Uesugi, "Time- and frequency-domain hybrid optical memory: 1.6-kbit data storage in Eu^{3+}:Y_2SiO_5," Opt. Lett. **16,** 1890–1893 (1991).
7. X. A. Shen and R. Kachru, "$^7F_0$–$^5D_1$ Transition in Eu^{3+}:Y_2SiO_5," J. Opt. Soc. Am. B **11,** 591–596 (1994).
8. R. Yano, M. Mitsunaga, and N. Uesugi, "Nonlinear laser spectroscopy of Eu^{3+}:Y_2SiO_5 and its applications to time domain optical memory," J. Opt. Soc. Am. B **9,** 992–997 (1992).
9. L. E. Erickson and K. K. Sharma, "Nuclear quadrupole resonance measurement of the anisotropic magnetic shielding and quadrupole coupling constants of $^{151}Eu^{3+}$ and $^{153}Eu^{3+}$ dilute in $YAlO_3$ single crystal," Phys. Rev. B **24,** 3697–3700 (1981).
10. R. M. Macfarlane and R. M. Shelby, "Measurement of optical dephasing of Eu^{3+} and Pr^{3+} doped silicate glasses by spectral holeburning," Opt. Commun. **45,** 46–51 (1983).
11. A. J. Silversmith, A. P. Radlinski, and N. B. Manson, "Optical study of hyperfine coupling in the $^7F_0$ and $^5D_0$ states of two Eu^{3+} centers in CaF_2 and CdF_2," Phys. Rev. B **34,** 7554–7563 (1986).
12. N. B. Manson, M. J. Sellers, P. T. H. Fisk, and R. S. Meltzer, "Hole burning of rare-earth ions with kHz resolution," J. Lumin. **64,** 19–23 (1995).
13. M. Yamaguchi, K. Koyama, T. Suemoto, and M. Mitsunaga, "Mapping of site distribution in Eu^{3+}:$YAlO_3$ on RF-optical frequency axes by using double resonance spectroscopy," J. Lumin. **76/77,** 681–684 (1998).
14. R. L. Cone, M. J. M. Leask, M. G. Robinson, and B. E. Watts, "Nuclear quadrupole optical hole burning in stochiometric $EuAsO_4$," J. Phys. C **21,** 3361–3380 (1988).
15. A. M. Stoneham, "Shapes of inhomogeneously broadened resonance lines in solids," Rev. Mod. Phys. **41,** 82–108 (1969).
16. A. L. Schawlow, "Width and positions of sharp optical lines," in *Advances in Quantum Electronics III*, P. Grivet and N. Bloembergen, eds. (Columbia U. Press, New York, 1963) pp. 645–653.

PROCEEDINGS OF SPIE

SPIE—The International Society for Optical Engineering

Advanced Optical Data Storage: Materials, Systems, and Interfaces to Computers

Pericles A. Mitkas
Zameer U. Hasan
Hans J. Coufal
Glenn T. Sincerbox
Chairs/Editors

20–22 July 1999
Denver, Colorado

Sponsored and Published by
SPIE—The International Society for Optical Engineering

Volume 3802

Insight into optical hole-burning studies in europium doped YSO

B. Rami Reddy, Ranjit S. Pandher, Andre Jackson and Angela Davis

Alabama A&M University, Department of Physics, P.O. Box 1268, Normal, AL 35762

ABSTRACT

High-resolution spectroscopic studies of Eu^{3+} doped Y_2SiO_5 revealed certain new aspects, which were not known in the past. Our studies indicate that europium occupies several distinct sites in this host material. Temporal evolution revealed unusual behavior.

Keywords: Optical hole-burning, high-resolution spectra, excitation spectra, $Y_2SiO_5:Eu^{3+}$, site-selective hole-burning, inhomogeneous broadening, spectral diffusion, hyperfine splittings.

1. INTRODUCTION

Optical hole-burning is a high resolution spectroscopic technique which has applications in data storage. These studies also reveal fundamental interactions at the atomic level. For this purpose several types of inorganic and organic materials are under investigation[1]. Praseodymium and europium doped materials were investigated thoroughly for this purpose because, the $^1D_2$ level of Praseodymium and the $^5D_0$ level of europium can be resonantly excited with a Rhodamine 6G dye laser[2,3]. However, the hole is short lived in Pr^{3+} doped materials, due to fast spin-lattice relaxation times. If the material has to be used as a device the hole has to last for a long time, for certain applications. It is possible to store vast amounts of information in a material if the ratio of inhomogeneous linewidth to homogeneous line width is large[4]. At low temperatures, the homogeneous linewidth is dependent on the lifetime of the excited state, guest-host interactions and interactions among the guest ions. The inhomogeneous linewidth depends on the strain in the material. In general europium and samarium doped materials were known to retain the hole for long periods of time[5-8]. The hole lifetime in $LaF_3:Pr^{3+}$ is about 0.5 s where as that in $CaF_2:Eu^{3+}$ is ~s. CaF_2 is a divalent material and rare-earth ions are trivalent. Rare-earth ions were known to occupy several different sites in CaF_2 due to charge compensation[9]. It was also possible to produce holes at several of these sites. The guest host interactions are minimized in Y_2SiO_5 host because the magnetic moments of the host atoms are very small. Of all the materials investigated so far europium doped YSO was known to retain the hole for a long period of time permitting the storage of vast amounts of information[10]. The europium was known to occupy two different sites with coordination numbers 6 and 7 respectively. Both the sites have C_1 symmetry[11,12] with inhomogeneous linewidths of about 8.6 and 5.6 GHz respectively for the two sites. The lifetime of the $^5D_0$ excited state is also very long ~2 ms. These characteristics facilitate the storage of vast amounts of data in this material. Different groups performed hole-burning experiments in the $^7F_0 \rightarrow {}^5D_0$ and $^7F_0 \rightarrow {}^5D_1$ transitions. All the past investigations revealed only two types of sites. However our investigations revealed 42 different sites for the europium ion in this host.

2. EXPERIMENTAL DETAILS

The YSO: Eu^{3+} (0.1%) sample used in the study is of the size 8x6x4 mm^3 and was obtained from Scientific Materials Corporation. The room temperature absorption spectrum was recorded with a CARY3E spectrophotometer. The emission spectra were recorded by cooling the sample to 9K in a closed cycle cryostat. A cw dye laser (linewidth ~60 GHz) was used to record the low-resolution excitatation spectra. A Spectra-Physics ring dye laser (linewidth~3 MHz) was used for hole burning and high-resolution excitation spectral recording. The emission intensity was processed by a low-resolution monochromator (dispersion~5 nm/mm) which is equipped with a Hamamatsu, R928 photomultiplier tube (PMT). The PMT signal was measured by a picoammeter and then plotted on a strip-chart recorder (Fig. 1). The ring dye

25 Part of the SPIE Conference on Advanced Optical Data Storage: Materials, Systems, and Interfaces to Computers • Denver, Colorado • July 1999
SPIE Vol. 3802 • 0277-786X/99/$10.00

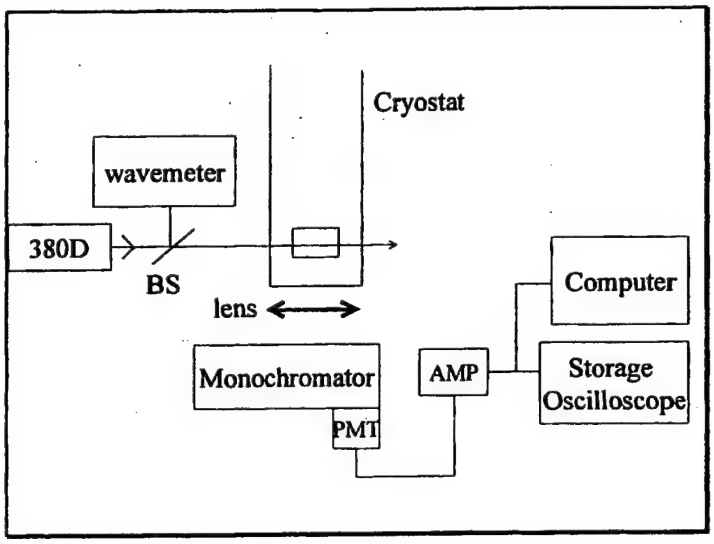

Fig. 1 Experimental configuration

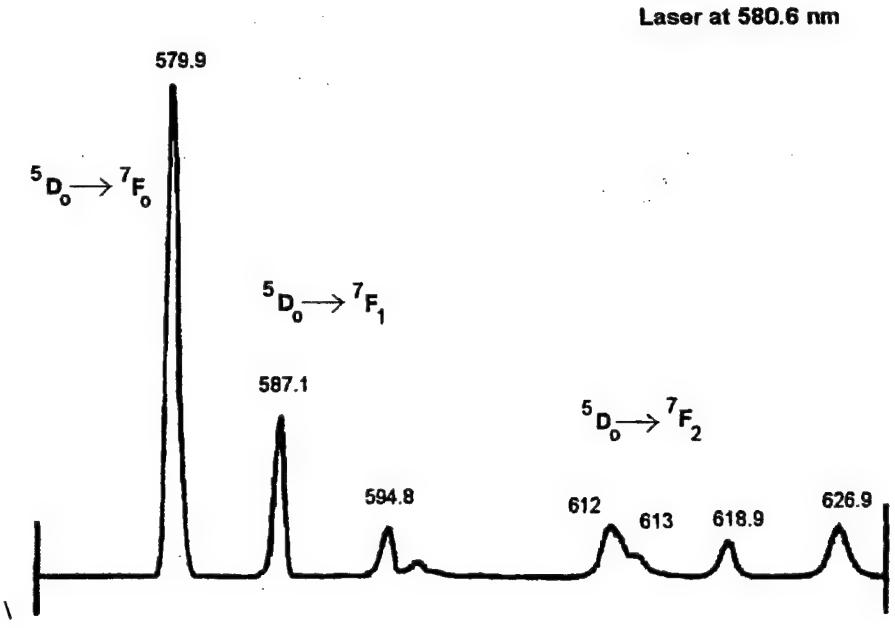

Fig.2 Emission spectrum observed under dye laser excitation

laser wavelength was measured by a Coheren-Ealing Wavemate (Model No. 33-2684). The high-resolution excitation spectra were recorded by giving the PMT output to a storage oscilloscope. In case of weak signals they were amplified before giving to the storage oscilloscope. For excitation and hole burning recordings the emission at 612 nm was monitored.

3. RESULTS AND DISCUSSION

3.1 Absorption, emission and low-resolution excitation spectral measurements

At room temperature a recording of the absorption spectrum revealed peaks at 579.8, 533, 464.3, 401.9, 397.8, 394.4, 381, 363.2, 322.1, 319.3 and 299.1 nm. The peak at 579.8 nm is identified to be due to $^7F_0 \rightarrow {}^5D_0$ transition. The angular momentum of the $^5D_0$ and $^7F_0$ states is 0. So, even in crystal field the corresponding energy levels are expected to be singlets. A dye laser is used to resonantly excite the $^7F_0 \rightarrow {}^5D_0$ transition. Emission occurred from $^5D_0$ to $^7F_0$ (580 nm), $^7F_1$ (585-600 nm), $^7F_2$ (608-630 nm) and to the other ^7F_J levels (J=3 to 6) in the wavelength region 630-670 nm. A typical spectrum is shown in Fig. 2. The transitions are also identified in the same figure. Excitation spectra were recorded for all the emission wavelengths. A typical spectrum is shown in Fig. 3, which reveals only two sharp peaks in the

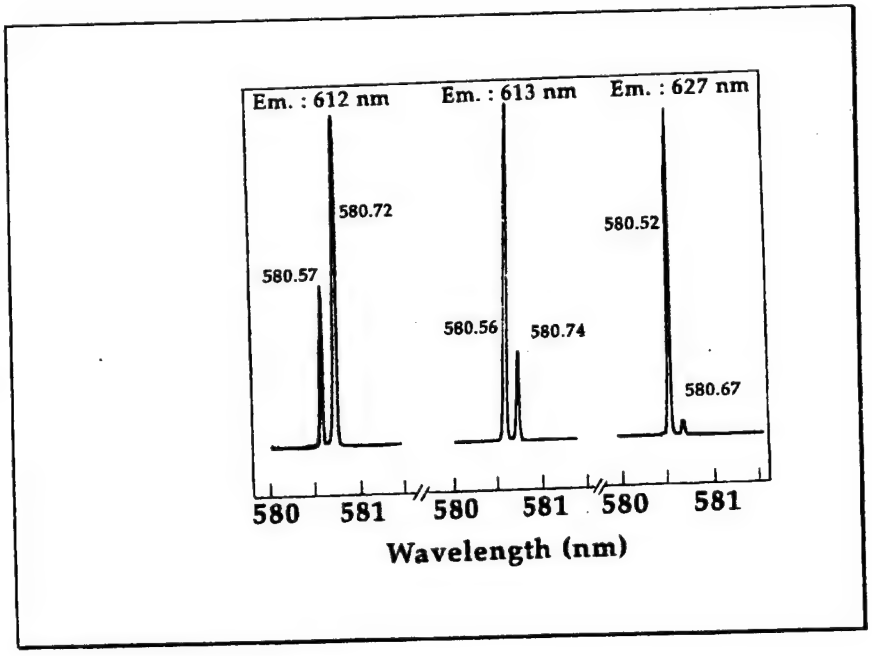

Fig. 3 Low-resolution excitation spectrum of three different emission wavelengths.

wavelength interval 580-581 nm. Since the ground and excited states coupled by the laser are singlets only a single peak is expected in the excitation spectrum. The fact that the excitation spectrum revealed two peaks indicates that there are two different sites for the rare-earth ion in this host material. However, there are dramatic changes in relative intensities of the peaks. This indicates that there may be more than two sites for the dopant. So the excitataion spectrum of 612 nm was recorded on an expanded scale (100x). Such an excitation spectrum revealed two strong peaks and three weak peaks, that is a total of five peaks. The next point is to find out whether the weak peaks represent electronic levels or phonon levels. So, we

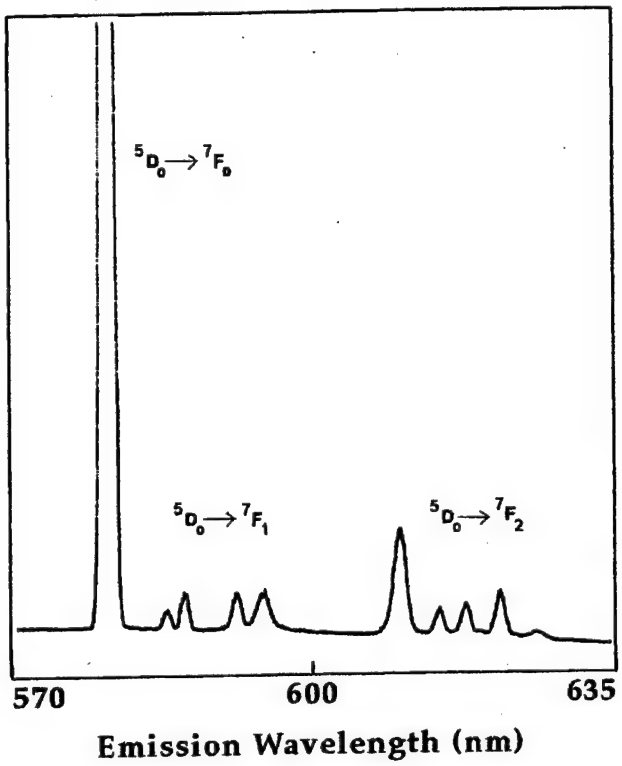

Fig.4 Emission spectrum observed under 580.42 nm laser excitation. The emission peaks are very weak. So the spectrum is recorded with a gain of 100 when compared to Fig.5.

recorded the emission spectra for different laser excitation wavelengths. The emission spectra exhibited differences in relative intensities and the number of peaks (Figs. 4 and 5). This clearly suggests that the peaks of the excitation spectrum represent electronic levels and not phonon levels. Thus the low-resolution studies indicate that there are at least five different sites for the Eu^{3+} ion in the YSO host.

3.2 Hole-burning and high-resolution excitation spectral measurements

The $^5D_0$ level has a long lifetime ~2 ms. Europium has a nuclear spin of 5/2. As a result each crystal field level is split further due to hyperfine interactions (Fig. 6). There are two isotopes, which are naturally abundant. When the pump laser linewidth is smaller than the hyperfine splittings excitation gets saturated easily because the nuclear spin does not change during the time of excitation. An excitation spectrum is recorded by monitoring the emission at 612 nm. One such spectrum is shown in Fig. 7, which reveals a hole. The hole lasts for several seconds when the laser is tuned to 580.57 (579.88) and 580.72 (580.05) nm, these are the dominant sites and the numbers given in parentheses were reported by Mitsunaga et al[11] for the same sites. The inhomogeneous linewidth of the peak in Fig. 8 is about 1.2 GHz and is 5x smaller than the value reported earlier[10]. When the laser wavelength was tuned to a slightly different value the excitation spectrum revealed two peaks separated by about 5 GHz (Fig.8). A thorough and systematic investigation revealed about 42 different sites for the rare-earth ion. A detailed discussion will appear in

Applied Optics (in press). Such satellite peaks were also observed in other europium doped materials[13,14]. A good description of the inhomogeneous linewidths and their origin is given elsewhre[15].

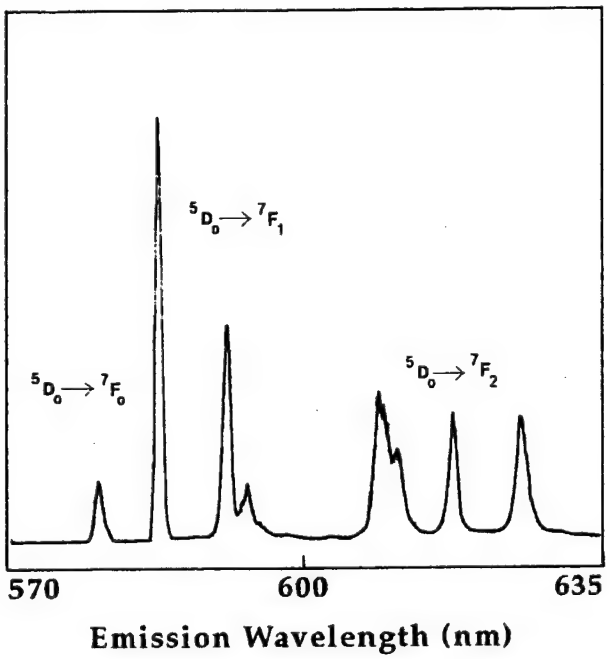

Fig.5 Emission spectrum observed under 580.57 nm laser excitation. The peaks are 100x more intense than those in Fig.4.

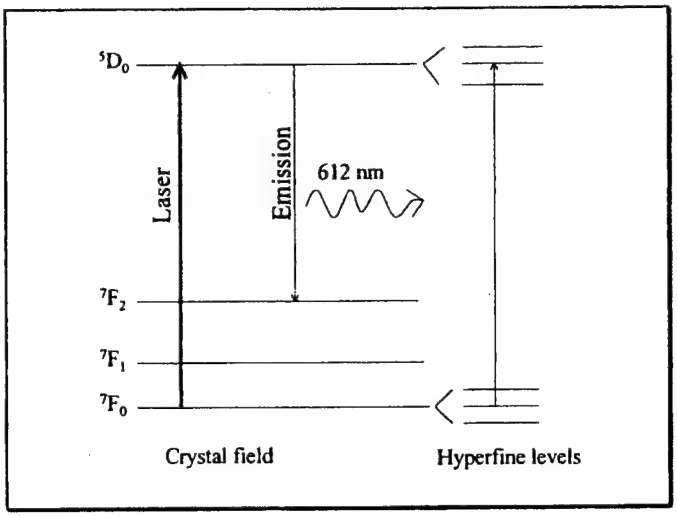

Fig. 6 Energy level diagram of Eu^{3+} in YSO. Laser excites the $^7F_0 \rightarrow {}^5D_0$ transition. 612 nm emission is monitored.

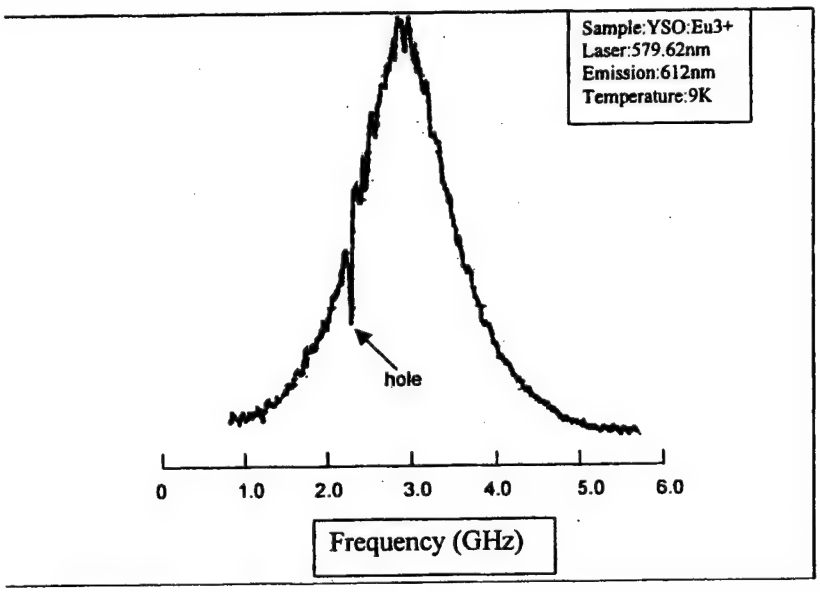

Fig.7: Excitation spectrum of 612 nm emission signal after burning a hole in the $^5D_0 \leftarrow ^7F_0$ transition. The inhomogeneous linewidth is ~1.2 GHz and the laser linewidth is ~3 MHz. Scale in the bottom is for relative estimation only. The line-width is much different from the published value.

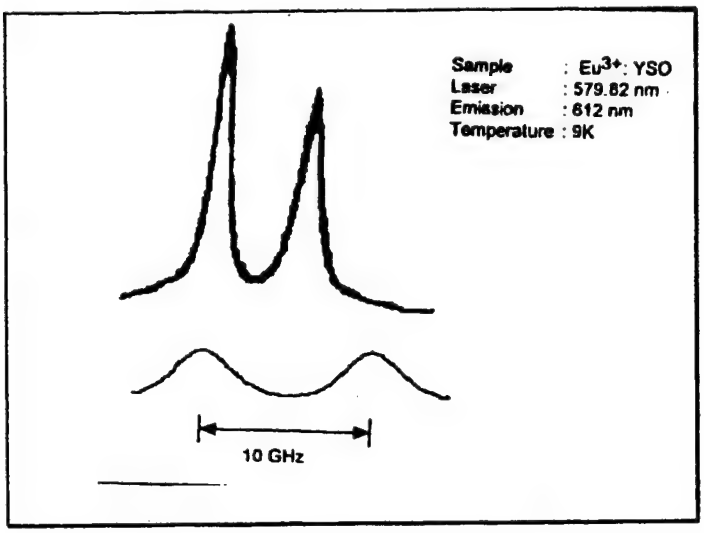

Fig.8 High-resolution excitation spectrum

3.3 Time dependence of the emission intensity

As soon as the laser was turned on the emission intensity had grown to the maximum value and then decreased eventually reaching the lowest value. The recording also revealed spikes occurring periodically at equal intervals of time. These spikes are not due to energy transfer among different europium ions because the excited state has a lifetime of only ~2 ms. Similar spikes were not observed in CaF_2: Eu^{3+} hole burning studies. So this indicates that the laser frequency was stable and there was no spurious scattering. These peaks were observed all the time, after the crystal was exposed to the laser beam. One such time dependent plot is shown in Fig.9. The spikes in Fig. 9 are separated by ~62 ms. This behavior was seen even at very low laser powers also and temperatures up to 15K. Such a behavior is noticed whenever the laser was tuned to any of the absorption peaks (sites). That is, whenever the laser is turned on emission increases and reaches the maximum value as expected due to excitation of more ions. Later on the emission intensity decreases due to saturation of the excitation and hole burning effect. If nothing else happens we expect the emission intensity to decrease continuously to reach the lowest level. On the contrary the intensity rises again and then decreases alternately at equal intervals of time (Fig. 9). A possible explanation is the following. It appears that some of the ions, which were non-resonant to the laser frequency, are coming into resonance. How the other ions are coming into resonance with the laser frequency is a puzzling question? When several ions are in the excited state the macroscopic polarization changes which might slightly shift the position of other ionic levels into resonance with the laser frequency.

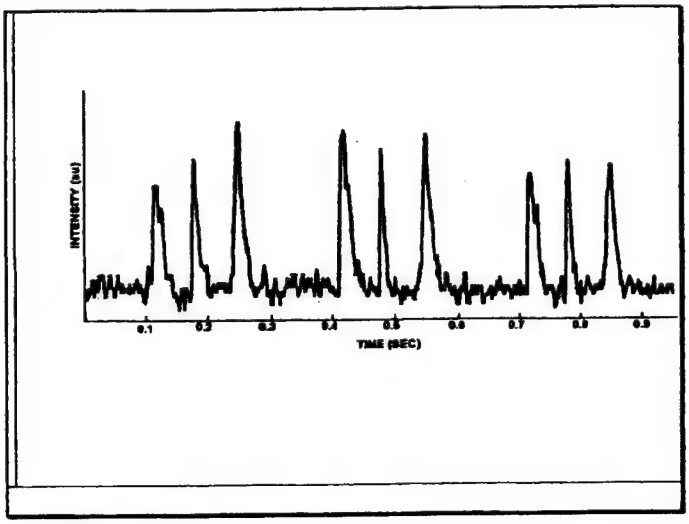

Fig.9: Time dependence of the emission intensity after a spectral hole was burned. Emission at 612 nm was monitored.

So, the emission intensity increases again, reaching the maximum value, and then decreasing again due to saturation and subsequent hole burning. This process continues for a long period of time. Similar results were observed in time domain measurements also[16-18]. If it were the case (that is, excited state population induced level shifting) then at higher laser powers the time interval between the spikes should decrease. We did not see any measurable change in the time interval. So, we do not have any strong evidence even to support this hypothesis. .Further studies are in progress.

4. CONCLUSIONS

Our results indicate that europium ion occupies several different sites in Y_2SiO_5. Our measurements also indicate the possibility of energy level shifts/frequency shifts caused by optical excitation.

5. ACKNOWLEDGMENTS

This research was supported by Air Force Office of Scientific Research grant # F 49620-97-1-0258.

6. REFERENCES

1. W.E. Moerner , "Persistent spectral hole-burning: Science and Applications;" Topics in current Physics, Vol 44, (Springer-Verlag, New York) 1988.
2. B. R. Reddy and L. E. Erickson, Nuclear quadrupole resonance study of the ground state of praseodymium in lanthanum trifluoride, Phys. Rev. **B27**, 5217-5222 (1983).
3. L. E. Erickson and K.K. Sharma, "Nuclear quadrupole resonance measurement of the anisotropic magnetic shielding and quadrupole coupling constants of $^{151}Eu^{3+}$ and $^{153}Eu^{3+}$ dilute in $YAlO_3$ single crystal," Phys.Rev. **B24**, 3697-3700 (1981).
4. R. Yano, M. Mitsunaga and N. Uesugi, "Nonlinear laser spectroscopy of Eu^{3+}:Y_2SiO_5 and its applications to time domain optical memory," J.Opt.Soc. Am. **B9**, 992-997 (1992).
5. Room-temperature persistent spectral hole burning of Eu^{3+} in sodium aluminosilicate glasses, K. Fujita, K. Tanaka, K. Hirao, and N. Soga, Opt. Letts. **23**, 543-545 (1998).
6. Room temperature persistent spectral hole burning in Sm^{2+} doped fluoride glasses, A. Kurita, T. Kushida, T. Izumitani and M. Matsukawa, Opt. Letts. **19**, 314-316 (1994).
7. Room temperature persistent spectral hole burning in Sm^{2+} doped silicate glasses prepared by the sol-gel process, M. Nogami, Y. Abe, K. Hirao, and D. H. Cho, Appl. Phys. Letts. **66**, 2952-2954 (1995).
8. K. Fujita, K. Hirao, K. Tanaka , N. Soga and H. Sasaki,"Persistent spectral hole burning of Eu^{3+} ions in sodium aluminosilicate glasses," J. Appl. Phys. **82**, 5114-5120 (1997).
9. J. Silversmith, A.P. Radlinski and N.B. Manson, "Optical study of hyperfine coupling in the $^7F_0$ and $^5D_0$ states of two Eu^{3+} centers in CaF_2 and CdF_2," Phys.Rev.**B34**, 7554-7563 (1986).
10. R. Yano, M. Mitsunaga and N. Uesugi, "Ultralong optical dephasing time in Eu^{3+}:Y_2SiO_5," Opt. Letts. **16**, 1884-1886 (1991).
11. M. Mitsunaga, R. Yano and N. Uesugi, "Time- and frequency-domain hybrid optical memory:16-kbit data storage in Eu^{3+}:Y_2SiO_5," Opt. Letts. **16**, 1890-1893 (1991).
12. X. A. Shen and R. Kachru, "$^7F_0$-$^5D_1$ Transition in Eu^{3+}:Y_2SiO_5," J. Opt. Soc. Am.**B11**, 591-596 (1994).
13. M. Yamaguchi, K. Koyama, T. Suemoto and M. Mitsunaga, "Mapping of site distribution in Eu^{3+}:$YAlO_3$ on RF-Optical frequency axes by using double resonance spectroscopy," J. Luminescence **76&77**, 681-684 (1998).
14. R. L. Cone, M.J.M. Leask, M.G. Robinson and B. E. Watts, "Nuclear quadrupole optical hole burning in stochiometric $EuAsO_4$," J. Phys. C: Solid state Phys. **21**, 3361-3380 (1988).
15. M. Stoneham, "Shapes of inhomogeneously broadened resonance lines in solids," Rev. Mod. Phys. **41**, 82-108 (1969).
16. J. Huang, J. M. Zhang, A. Lezama and T. W. Mossberg, "On the shifting of optical transition frequencies in rare-earth doped insulators by resonant optical excitation," J. Lumines. **45**, 392-396 (1990).
17. S. Kroll, E. Y. Xu, M. K. Kim, M. Mitsunaga and R. Kachru, "Intensity-dependent photon-echo relaxation in rare-earth -doped crystals," Phys. Rev. **B41**, 11 568-11 571 (1990).
18. G. K. Liu, N. F. Joubert, R. L. Cone, and B. Jacquier, "Photon echo relaxation and hole burning in Tb^{3+}: $LiYF_4$ and $LiTbF_4$," J. Lumin **38**, 34-36 (1987).

Further author information:
B.R.R. (correspondence):E-mail:brreddy@aamu.edu; Tel:256-858-8101; Fax: 256-851-5622.

Infrared quantum counter studies in europium doped lanthanum trifluoride

Wenyan Tian, Ranjit S. Pandher, and B. Rami Reddy[a)]
Alabama A&M University, Department of Physics, P.O. Box 1268, Normal, Alabama 35762

(Received 8 May 2000; accepted for publication 26 May 2000)

Violet upconversion signals in the wavelength region 340–420 nm were observed from $LaF_3:Eu^{3+}$ under 583 nm dye laser excitation. The intensities of some upconversion signals enhanced ~8× under double resonance excitation by a 583 nm dye laser and a 790.6 nm Ti: sapphire laser.
 [S0021-8979(00)02417-8]

INTRODUCTION

Several rare-earth ion doped materials were investigated thoroughly to check their suitability for laser development or energy upconversion studies.[1,2] Bloembergen[3] proposed the infrared-optical double resonance technique for the detection of infrared radiation. Such infrared quantum counter (IRQC) studies were observed in few other materials.[4–7] The Eu^{3+} ion does not show ground state absorption at near-infrared (IR) wavelengths.[8–13] Therefore, it was not a popular candidate for energy upconversion studies. However, the $^5D_0$ level has a long lifetime.[13] The energy level structure of an Eu^{3+} ion suggests the possibility that an ion in the $^5D_0$ state can absorb a second photon of infrared or visible wavelength to upconvert energy. Hence, we performed optical-infrared double resonance or infrared quantum counter studies in $LaF_3:Eu^{3+}$. The $LaF_3:Eu^{3+}$ (1%) is of the size: $0.42\times0.42\times0.42\,cm^3$ and was obtained from Optovac, Inc. Tunable dye and Ti: sapphire lasers were used to pump the crystal. Emission spectra were processed by a medium resolution monochromator.

ABSORPTION SPECTRUM

Absorption spectrum revealed transitions at 592.4($^7F_0\rightarrow{}^5D_0$), 531.9($^7F_0\rightarrow{}^5D_1$), 487.2($^7F_0\rightarrow{}^5D_2$), 370.2($^7F_0\rightarrow{}^5G_6$), 325.5($^7F_0\rightarrow{}^5H_3$), 316.8($^7F_0\rightarrow{}^5H_6$), 303.5($^7F_0\rightarrow{}^3P_0,{}^5F_2$), and 272.1 nm ($^7F_0\rightarrow{}^5K_5$). The transitions were identified after comparing the absorption wavelengths with the published data.[9–13] The energy gap between $^5H_3$ and its immediate lower level $^5L_{10}$ is ~2400 cm^{-1}, and the gap between $^5D_3$ and its lower level $^5D_2$ is ~3000 cm^{-1}. So the $^5H_3$ and $^5D_3$ levels are expected to emit because the cutoff phonon frequency[14] in LaF_3 is ~350 cm^{-1}. The $^5D_0$ level population easily reaches the saturation limit even at low pump powers because of its long lifetime.[13] So, it is easy to excite the same ion from the $^5D_0$ level to a much higher level if appropriate radiation is used because Eu^{3+} has numerous energy levels[9–11] in the interval 24 000–36 000 cm^{-1}.

ENERGY UPCONVERSION

When the $^5D_0$ level of $LaF_3:Eu^{3+}$ was resonantly excited with a 583 nm dye laser, we detected upconversion signals at 355($^5H_3\rightarrow{}^7F_4$), 382($^5H_3\rightarrow{}^7F_6$), 414($^5D_3\rightarrow{}^7F_1$), 450($^5D_3\rightarrow{}^7F_3$), 479($^5D_2\rightarrow{}^7F_1$), 490($^5D_2\rightarrow{}^7F_2$), and 516 nm ($^5D_2\rightarrow{}^7F_4$) (Fig. 1) in addition to the resonant and long wavelength emissions at 597($^5D_0\rightarrow{}^7F_1$), 690($^5D_0\rightarrow{}^7F_6$), 709($^5D_1\rightarrow{}^7F_6$), 730($^5H_3\rightarrow{}^5D_0$), 763($^5I_5\rightarrow{}^5D_2$), 794($^5F_5\rightarrow{}^5D_2$), 826($^5H_4\rightarrow{}^5D_1$), and 865 nm ($^5H_3\rightarrow{}^5D_1$). The violet emission intensities exhibited quadratic dependence on the laser power indicating a two-photon excitation mechanism. An observation of the energy level diagram reveals that the pump photon energy matches with the transitions $^7F_0\rightarrow{}^5D_0\rightarrow{}^5I_5$,

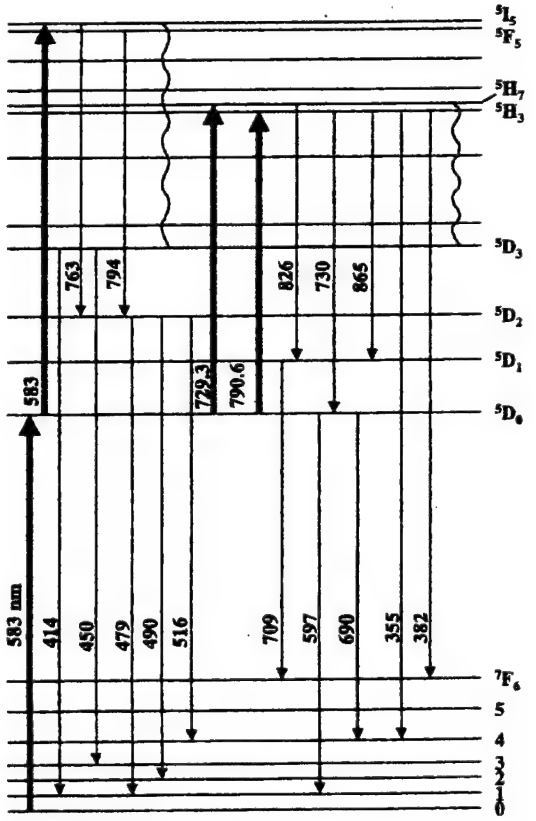

FIG. 1. Partial energy level diagram of $LaF_3:Eu^{3+}$. The upward and downward arrows represent laser excitation and radiative emission. The wavy line represents nonradiative relaxation.

a)Electronic mail: brreddy@aamu.edu

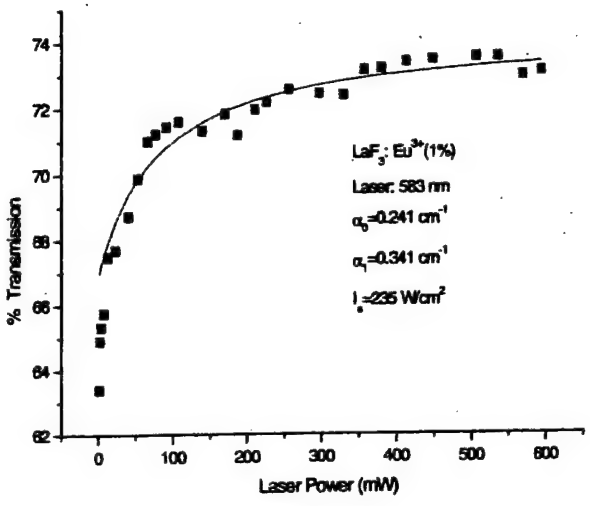

FIG. 2. Transmission of $LaF_3:Eu^{3+}$ as a function of input power at 583 nm. Dots are the experimental points, the solid line is the theoretical obtained fit for $\alpha_{01}=0.241$ and $\alpha_{12}=0.341\ cm^{-1}$, $I_s=235\ W/cm^2$ and the sample length=0.42 cm.

where $\rightarrow$ represents a pump laser photon. The ions in the $^5I_5$ state relax nonradiatively in cascade to the lower levels causing $^5H_3$ and $^5D_3$ levels to emit. Such a stepwise two-photon excitation mechanism was confirmed by performing pump–probe experiments.[15–19] The excited state absorption coefficient is estimated by fitting the transmission data of the sample to[15]

$$dI/dZ=-(\alpha_g+\alpha_{12})I, \tag{1}$$

where α_g and α_{12} are the ground and the excited state absorption coefficients, respectively. Since the $^5D_0$ level has a long lifetime its population tends to saturate at high input power. Hence, the ground state absorption coefficient is given by

$$\alpha_g=\alpha_{01}/(1+I/I_s), \tag{2}$$

where α_{01} is the low power absorption coefficient and I_s the saturation intensity. Figure 2 shows a fitting of the experimental data to Eq. (1) obtained for $\alpha_{01}=0.241$ and $\alpha_{12}=0.341\ cm^{-1}$. A room temperature recording of the excitation spectrum of 382 nm revealed strong absorptions at 579,

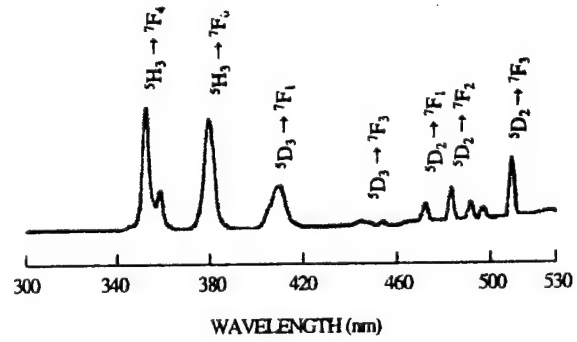

FIG. 3. Energy upconversion spectrum of $LaF_3:Eu^{3+}$ observed under 26 mw of 583 nm dye laser excitation.

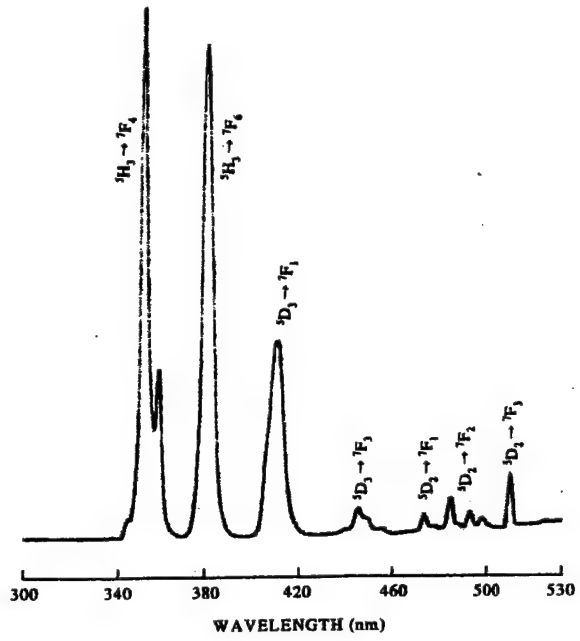

FIG. 4. Energy upconversion spectrum of $LaF_3:Eu^{3+}$ observed under 26 mw of 583 nm dye laser and 370 mw of 790.6 nm Ti: sapphire laser excitation.

580, and 583 nm from the phonon coupled levels above the ground state at 22, 61, and 155 cm^{-1}, ($^7F_0$+phonon $\rightarrow{}^5D_0$) and a weak absorption at 590 nm ($^7F_1\rightarrow{}^5D_0$). This is not a surprise because the zero-phonon transition, $^7F_0\rightarrow{}^5D_0$ is forbidden. In a 1% sample the measured lifetime for the $^5D_0$ state is 0.37 ms, which is much different from the value reported earlier.[13] The lifetime also exhibited some

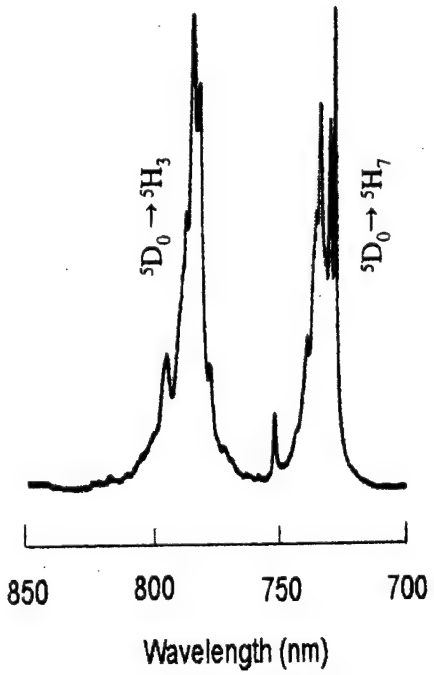

FIG. 5. Excitation spectrum of the 382 nm emission observed by tuning the Ti:Sapphire laser in the wavelength region 740–810 nm. Dye laser wavelength is 583 nm.

dependence on the pump power suggesting the occurrence of an energy transfer process among the excited ions for this sample.

INFRARED QUANTUM COUNTER

Optical-infrared double resonance measurements were also performed by simultaneously exciting the sample with dye and Ti: sapphire lasers. The ions in the ground state were coupled to the $^5D_0$ state by a 583 nm dye laser. A near-infrared laser excites the same ion from the $^5D_0$ state to the $^5H_4$, $^5H_3$ states. The violet emission intensities at 355, 382, 414, and 450 nm enhanced 8× under the double resonance excitation (Figs. 3 and 4). An excitation spectrum of the 382 nm signal was recorded by tuning the Ti: sapphire laser wavelength (Fig. 5). The dye laser wavelength was set to 583 nm. Such an excitation spectrum revealed two groups of transitions at 729.3 nm ($^5D_0 \rightarrow {}^5H_7$) and 790.6 nm ($^5D_0 \rightarrow {}^5H_3$). The Ti: sapphire laser is absorbed by the sample only in the presence of the dye laser excitation. Our experiments also revealed that upconversion signal intensity depended on the powers of both the dye laser and the Ti: Sapphire laser. The maximum increase (eightfold) in the upconversion emission intensity occurred in our experiments for a dye laser power of 1 mW and a Ti: sapphire laser power of 370 mW at 790.6 nm.

CONCLUSIONS

We have demonstrated IRQC detection in the region 710–830 nm because it falls in the optimum lasing region of the Ti: sapphire laser. In principle, this material can be used for detecting IR radiations at 1750, 7060 cm^{-1}, and the interval 8030–11 000 cm^{-1}. Europium doped fibers will be useful in detecting even very weak infrared radiation sources due to the long interaction length encountered in fibers.

ACKNOWLEDGMENTS

This research was supported by NASA and the Air Force Office of Scientific Research.

[1] A. Kaminskii, *Crystalline Lasers* (CRC, Boca Raton, FL, 1996).
[2] R. Scheps, Prog. Quantum Electron. **20**, 271 (1996).
[3] N. Bloembergen, Phys. Rev. Lett. **2**, 84 (1959).
[4] F. Varsanyi, Phys. Rev. Lett. **14**, 786 (1965).
[5] J. C. Wright, D. J. Zalucha, H. V. Lauer, D. E. Cox, and F. K. Fong, J. Appl. Phys. **44**, 781 (1973).
[6] J. S. Chivian, W. E. Case, and D. D. Eden, Appl. Phys. Lett. **35**, 124 (1979).
[7] L. Esterowitz, J. Noonan, and J. Bahler, Appl. Phys. Lett. **10**, 126 (1967).
[8] E. V. Sayre and S. Freed, J. Chem. Phys. **24**, 1213 (1956).
[9] L. G. DeShazer and G. H. Dieke, J. Chem. Phys. **38**, 2190 (1963).
[10] N. C. Chang and J. B. Gruber, J. Chem. Phys. **41**, 3227 (1964).
[11] W. T. Carnall, P. R. Fields, and K. Rajnak, J. Chem. Phys. **49**, 4450 (1968).
[12] W. T. Carnall, P. R. Fields, and K. Rajnak, J. Chem. Phys. **49**, 4412 (1968).
[13] W. T. Carnall, H. M. Crosswhite, and H. Crosswhite, Energy level structure and transition probabilities of the trivalent lanthanides in LaF_3, Special Report No. ANL-78-XX-95 (Chemistry Division, Argonne National Laboratory, Argonne, IL, 1978).
[14] M. J. Weber, Phys. Rev. **157**, 262 (1967).
[15] B. R. Reddy and P. Venkateswarlu, J. Opt. Soc. Am. B **10**, 438 (1994).
[16] J. K. Lawson and S. A. Payne, Opt. Mater. **2**, 225 (1993).
[17] R. Moncorge and T. Benyattou, Phys. Rev. B **37**, 9177 (1988).
[18] H. Manaa and R. Moncorge, Opt. Quantum Electron. **22**, S219 (1990).
[19] L. J. Andrews, S. M. Hitelman, M. Kokta, and D. Gabbe, J. Chem. Phys. **84**, 5229 (1986).

submitted to J. Opt. Soc. Am.B

Efficient infrared quantum counter and excited state absorption cross section measurements in europium doped calcium fluoride

Wenyan Tian, Ranjit. S. Pandher[+], and B. Rami Reddy[*]

Alabama A & M University, Department of Physics, P. O. Box 1268, Normal, Alabama 35672

ABSTRACT

Upconversion signals in the wavelength region 407-550 nm were observed from $CaF_2:Eu^{3+}$ under a 578.7 (or 589.2) nm dye laser excitation. The intensities of the upconversion signals enhanced 25× under double resonance excitation by a 589.2 nm dye laser and 703.6 nm Ti:Sapphire laser. Excited state absorption cross sections were estimated for some of the transitions.

Key words: Infrared quantum counter, optical-infrared double resonance energy upconversion, two-photon excitation, $CaF_2:Eu^{3+}$, excited state absorption cross sections.

OCIS codes: 190.7220, 160.5690, 190.4180, 300.6360, 190.4400.

[*]Electronic mail: brreddy@aamu.edu

[+]Present address: City University of New York, State Island, NY 10314

1. INTRODUCTION

Europium doped materials have been investigated extensively.[1-9] Infrared quantum counter study which was first proposed by Bloembergen,[10] has been applied in few other materials.[7,11-13] The following information is reported for the first time, to our knowledge, on this material. We investigated double resonance measurements in $CaF_2:Eu^{3+}$ by pumping the sample with a 589.2 nm dye laser and 703.6 nm Ti:Sapphire simultaneously. We also estimated the excited state absorption cross sections for some of the transitions. The $CaF_2:Eu^{3+}$ (0.5%) is of size 0.9×0.5×0.5 cm^3 and was supplied by Optovac, Inc. Tunable dye and Ti:Sapphire lasers were used to excite the crystal, and a medium resolution monochromator was used to collect emission spectrum. Lifetimes were measured by pumping the sample with a dye laser, and the signals were processed with an SR430 multichannel scaler. The detector output was amplified and then plotted on a chart recorder. The sample temperature was either 10K or 293K in these measurements.

2. ENERGY UPCONVERSION

Under dye laser excitation room temperature emission spectrum revealed upconversion signals at 407 ($^5D_3 \rightarrow {}^7F_0$), 418 ($^5D_3 \rightarrow {}^7F_1$), 429.9 ($^5D_3 \rightarrow {}^7F_2$), 445 ($^5D_3 \rightarrow {}^7F_3$), 464 ($^5D_2 \rightarrow {}^7F_0$), 472.7 ($^5D_2 \rightarrow {}^7F_1$), 488 ($^5D_2 \rightarrow {}^7F_2$), 509 ($^5D_2 \rightarrow {}^7F_3$), 527 ($^5D_1 \rightarrow {}^7F_0$), 535 ($^5D_1 \rightarrow {}^7F_1$), and 550 nm ($^5D_1 \rightarrow {}^7F_2$) in addition to the resonant and the long wavelength emissions at 591, 613, 648, 690, 751, 807, and 856 nm (Fig. 1). The violet emission intensities exhibited quadratic dependence on the laser power indicating that a two-photon excitation mechanism responsible for their emission. A significant amount of

population exists in the $^7F_1$ state at room temperature due to thermalization. Hence, ions in the $^7F_0$ (or $^7F_1$) state were excited to $^5D_0$ state by the absorption of a dye laser photon of 578.7 (or 589.2) nm, which further absorb a second photon and get excited to $^5I_5$ (or $^5F_5$) state as follows ($^7F_0 \rightarrow {}^5D_0 \rightarrow {}^5I_5$ or $^7F_1 \rightarrow {}^5D_0 \rightarrow {}^5F_5$). Excited ions relax radiatively and non-radiatively. The ions in the $^5I_5$ (or $^5F_5$) state relax nonradiatively in cascade to the lower levels causing $^5H_3$, $^5D_3$, and $^5D_2$ to emit. A room temperature recording of the excitation spectrum of 429.9 nm revealed strong absorption at 578.7 ($^7F_0 \rightarrow {}^5D_0$) and 589.2 ($^7F_1 \rightarrow {}^5D_0$) nm, as well as a weak absorption at 612.7 nm ($^7F_2 \rightarrow {}^5D_0$) (Fig. 2). However, when the sample was at 10K, the excitation spectrum of 429.9 nm fluorescence revealed strong absorption only at 578.7 nm (Fig. 3) because all the population was confined to the ground state, $^7F_0$.

3. INFRARED QUANTUM COUNTER

The experimental lifetime for $^5D_0$ level is 5.6 ms. As a result population easily reaches the saturation limit at a low laser power. So, it is easy to excite the same ion from the $^5D_0$ level to a much higher level if an appropriate radiation is used. That is why we performed infrared quantum counter studies in $CaF_2:Eu^{3+}$. For these measurements, the sample was simultaneously irradiated with dye and Ti:Sapphire lasers. The ions in the ground state were coupled to the $^5D_0$ state by a 578.7 (or 589.2) nm dye laser, and a near-infrared laser beam of wavelength 703.6 nm excites the same ions to the $^5H_5$ state. The intensities of the upconversion signals at 407, 418, 429.9, 445, 464, 472.7, 488, and 509 nm etc. enhanced 25× (the chart recorder voltage setting was 100 mV in Fig. 4 and 500 mV in Fig. 5). The maximum change in the upconversion signal intensity occurred for a dye

laser power of 20 mW and a Ti:Sapphire laser power of 57 mW. Ti:Sapphire laser is absorbed by the $CaF_2:Eu^{3+}$ only in the presence of the dye laser excitation. By fixing the dye laser wavelength at 578.7 (or 589.2) nm, an excitation spectrum of the 429.9 nm signal was recorded by tuning the Ti:Sapphire laser wavelength (Fig. 6). Such a spectrum revealed four groups of transitions at 703-708 ($^5D_0 \rightarrow {}^5H_5$), 715-718 ($^5D_0 \rightarrow {}^5H_4$), 725-728 ($^5D_0 \rightarrow {}^5H_7$), and 739.5 nm ($^5D_0 \rightarrow {}^5H_3$).

4. MEASUREMENT OF EXCITED STATE ABSORPTION CROSS SECTION

Pump-probe experiments were performed to verify the excited state absorption mechanism at a dye laser wavelength, 578.7 nm. A 2 mW probe beam and a 50-300 mW pump beam traveled the same path length of the sample in opposite directions. A photomultiplier tube (PMT) measured the transmitted probe beam intensity during the absence (I_u) and the presence (I_P) of the strong pump beam. The change in absorption coefficient $\Delta\alpha$ is given by[14-18]

$$\Delta\alpha = N_1(\sigma_{12} - \sigma_{01}) = \ln(I_u/ I_P)/L, \quad (1)$$

where σ_{01} and σ_{12} are the ground and excited state absorption cross sections at the dye laser wavelength, L the length of the sample and N_1 the population density in the excited state, $^5D_0$. $\Delta\alpha$ is positive if $\sigma_{12} > \sigma_{01}$, which indicates that $I_u > I_P$. On the other hand, if $\sigma_{12} < \sigma_{01}$, it is the reverse. However, if $\sigma_{12} = \sigma_{01}$, pump-probe experiment does not reveal any evidence for excited state absorption. Excited state absorption coefficient is estimated by fitting the transmission data of the sample to

$$dI/dZ = -(\alpha_g + \alpha_{12})\, I, \quad (2)$$

where α_g and α_{12} are the ground and the excited state absorption coefficients, respectively. And

$$\alpha_g = \alpha_{01}/(1 + I/I_S), \tag{3}$$

where α_{01} is the low power absorption coefficient, I_S is the saturation intensity. Fig. 7 shows a fitting of the experimental data to Eq. (2) obtained for $\alpha_{01} = 0.201$ cm^{-1}, $\alpha_{12} = 0.155$ cm^{-1} and $I_S = 549$ W/cm^2. The ground state absorption cross section is given by

$$\sigma_{01} = \alpha_{01}/N_0, \tag{4}$$

where N_0 represents ground state population. However, $^7F_1$ and $^7F_2$ levels are thermally populated at room temperature, whose population are given by the Boltzmann distribution. After correcting for thermal distribution, the concentration in the ground state is 8.085×10^{19} ions/cm^3, whereas the europium ion concentration is 1.226×10^{20} ions/cm^3 in a 0.5 % doped sample. The ground state absorption cross section σ_{01} is estimated from Eq.(4) as 2.49×10^{-21} cm^2 at 578.7 nm. At low powers, σ_{12} can be estimated by using

$$\sigma_{12} = \alpha_{12}/N_1. \tag{5}$$

N_1 can be estimated from the absorbed power and ground state absorption cross section. N_1 is modified by the relaxation phenomena and energy transfer processes. However, it is possible to estimate the σ_{12} at dye laser wavelengths, without any knowledge of N_1. An observation of Eq. (1) and (5) reveals that

$$\Delta\alpha/(\sigma_{12} - \sigma_{01}) = \alpha_{12}/\sigma_{12}. \tag{6}$$

$\Delta\alpha$ values were obtained from pump-probe experimental data, σ_{01} was obtained from Eq. (4) and the α_{12} was obtained from the fitting shown in Fig. 7. Therefore, σ_{12} is estimated

as $(2.04 \pm 0.21) \times 10^{-21}$ cm^2 at dye laser wavelength. This estimate is in agreement with that predicted by the pump-probe experiment.

We also performed the pump-probe experiments by using a 578.7 nm dye laser that pumps the ions from ground state $^7F_0$ to $^5D_0$ state and a Ti:Spphire laser that excites the same ions from the $^5D_0$ state to a higher state $^5H_5$. So, Eq.(1) can be rewritten as

$$\Delta\alpha = N_1\sigma_{12}', \tag{7}$$

where σ_{01}' and σ_{12}' are the ground state and excited state absorption cross sections at 703.6 nm. There is no ground state absorption at Ti:Sapphire laser wavelengths, hence, $\sigma_{01}' = 0$. N_1 is the ionic concentration in $^5D_0$ state due to dye laser excitation. It is possible that excited state undergoes radiative relaxation and energy transfer at the same time. Hence, all the excited ions are not available for the absorption of a second photon at 703.6 nm. So, one has to apply a correction for the population, N_1, in the $^5D_0$ state. Under steady state excitation conditions and at low pump powers

$$dN_1/dt = N_0\sigma_{01}F - N_1/\tau = 0, \tag{8}$$

where F represents the flux of incident laser photons and τ represents the experimentally measured lifetime (5.6 ms) which accounts for the radiative relaxation and energy transfer phenomena. The effects of two photon absorption at dye laser wavelength and the repopulation of the $^5D_0$ state due to relaxation of the higher levels are assumed to be insignificant in Eq. (8) at the low dye laser power. According to Eq. (8), $N_1 = N_0\sigma_{01}F\tau$ and F is estimated from the focused beam size (radius = 100 μm) and incident laser power. N_1 is estimated for different power levels. A plot of $\Delta\alpha$ versus N_1 gave a straight line whose slope equals σ_{12}' (see Eq.(7)). The excited state absorption cross section for the transition $^5D_0 \rightarrow {}^5H_5$ is estimated as $(1.33 \pm 0.04) \times 10^{-20}$ cm^2 at a Ti:Sapphire laser

wavelength of 703.6 nm (Fig. 8). Since the cross section was derived from the transmission measurements the geometrical effects of the beam shape was assumed to be negligible.

5. CONCLUSIONS

Excited state absorption cross section at 703.6 nm is 7× higher than that at 578.8 nm. That is the reason why have seen an enhancement of 25× in the upconversion signal under near-infrared-optical double resonance excitation conditions. CaF_2:Eu^{3+} is more efficient than LaF_3: Eu^{3+} [7] for these measurements because in the latter upconversion signals enhanced only 8× which is less than that in the former.

6. ACKNOWLEDGMENTS

This work was supported by NASA and the Air Fore Office of Scientific Research.

REFERENCES

1. J. B. Gruber and J. G. Conway, J. Chem. Phys. **34**, 632 (1961).
2. L. G. Deshazer and G. H. Dieke, J. Chem. Phys. **38**, 2190 (1963).
3. W. T. Carnall, P. R. Fields, and K. Rajnak, J. Chem. Phys. **49**, 4450 (1968).
4. J. D. Axe and P. F. Weller, J. Chem. Phys. **40**, 3066 (1964).
5. M .J. Weber, "Relaxation processes for excited states of Eu^{3+} in LaF_3," in optical properties of ions in crystals, H. M. Crosswhite and H. W. Moos, eds., Wiley Interscience, New York, 467.
6. R. J. Hamers, J. R. Wietfeldt, and J. C. Wright, J. Cem. Phys. **77**, 683 (1982).
7. W. Tian, R. S. Pandher, and B. R. Reddy, J. Appl. Phys. **88**, 2191 (2000).
8. R. S. Pandher, A. Davis, A. Jackson, and B. R. Reddy, J. Appl. Phys. **87**, 3570 (2000).
9. W. T. Carnall, H. M. Crosswhite, and H. Crosswhite, Energy level structure and transition probabilities of the trivalent lanthanides in LaF_3, Special report No. ANL-78-XX-95 (Chemistry Division, Argonne National Laboratory, Argonne, IL, 1978).
10. N. Bloembergen, Phys. Rev. Lett. **2**, 84 (1959).
11. J. S. Chivian, W. E. Case, and D. D. Eden, Appl. Phys. Lett. **35**, 124 (1979).
12. L. Esterowitz, J. Noonan, and J. Bahler, Appl. Phys. Lett. **10**, 126 (1967).
13. J. C. Wright, D. J. Zalucha, H. V. Lauer, D. E. Cox, and F. K. Fong, J. Appl. Phys. **44**, 781 (1973).
14. B. R. Reddy and P. Venkateswarlu, J. Opt. Soc. Am. B**10**, 438 (1994).
15. J. K. Lawson and S. A. Payne, Opt. Mater. **2**, 225 (1993).

16. R. Moncorge and T. Benyattou, Phys. Rev. B **37**, 9177 (1988).

17. H. Manaa and R. Moncorge, Opt. Quantum Electron. **22**, S219 (1990).

18. L. J. Andrews, S. M. Hitelman, M. Kokta, and D. Gabbe, J. Chem. Phys. **84**, 5229 (1986).

FIGURE CAPTIONS

Fig. 1. Partial energy level diagram of Eu^{3+} in CaF_2 depicting the excitation scheme and the emission wavelengths. The upward and downward arrows represent laser excitation and radiative emission. The wavy line represents nonradiative relaxation.

Fig. 2. Excitation spectrum of the 429.9 nm emission under dye laser pump at room temperature.

Fig. 3. Excitation spectrum of the 429.9 nm emission under dye laser pump at 10K.

Fig. 4. Energy upconversion spectrum of CaF_2: Eu^{3+} observed under 20 mW of 589.2 nm dye laser excitation. The chart recorder voltage setting was 100 mV.

Fig. 5. Energy upconversion spectrum of CaF_2: Eu^{3+} observed under 20 mW of 589.2 nm dye laser and 57 mW of 703.6 nm Ti:Sapphire laser excitation. The chart recorder voltage setting was 500 mV.

Fig. 6. Excitation spectrum of the 429.9 nm emission observed by tuning the Ti:Sapphire laser in the wavelength region 692-750 nm. Dye laser wavelength was 578.7 nm.

Fig. 7. Transmission of CaF_2: Eu^{3+} as a function of input power at 578.7 nm. Dots are the experimental points, the solid line is the theoretical fit obtained for $\alpha_{01} = 0.201\ cm^{-1}$, $\alpha_{12} = 0.155\ cm^{-1}$, $I_s = 549\ W/cm^2$ and the sample length is 0.9 cm.

Fig. 8. The relationship between absorption coefficient and the excited state ($^5D_0$) ionic concentration. σ_{12}' is the excited state absorption cross section at the Ti:Spphire laser wavelength. The excited state population is corrected to account for the radiative decay energy transfer and other phenomena.

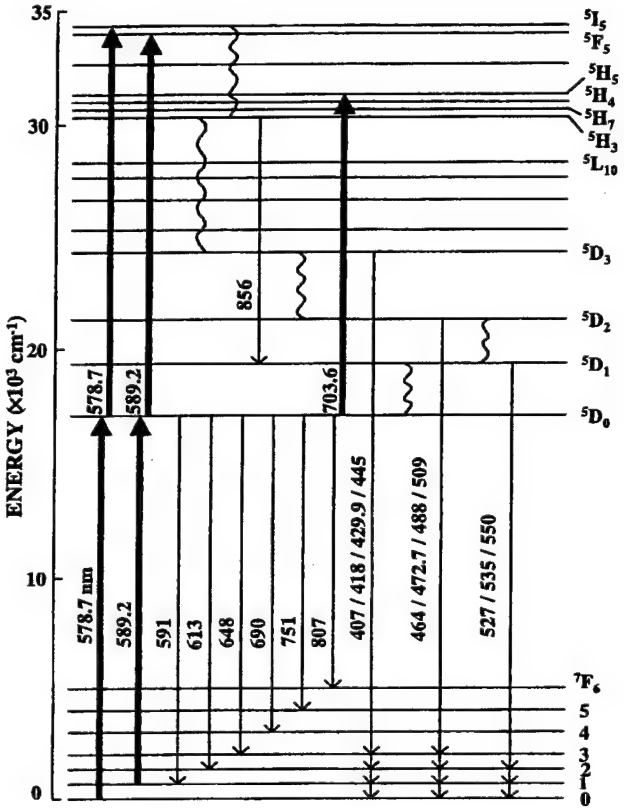
ENERGY (×10³ cm⁻¹)
35
30
20
10
0
$^5I_5$
$^5F_5$
$^5H_5$
$^5H_4$
$^5H_7$
$^5H_3$
$^5L_{10}$
$^5D_3$
$^5D_2$
$^5D_1$
$^5D_0$
$^7F_6$
5
4
3
2
1
0
578.7
589.2
856
703.6
578.7 nm
589.2
591
613
648
690
751
807
407 / 418 / 429.9 / 445
464 / 472.7 / 488 / 509
527 / 535 / 550

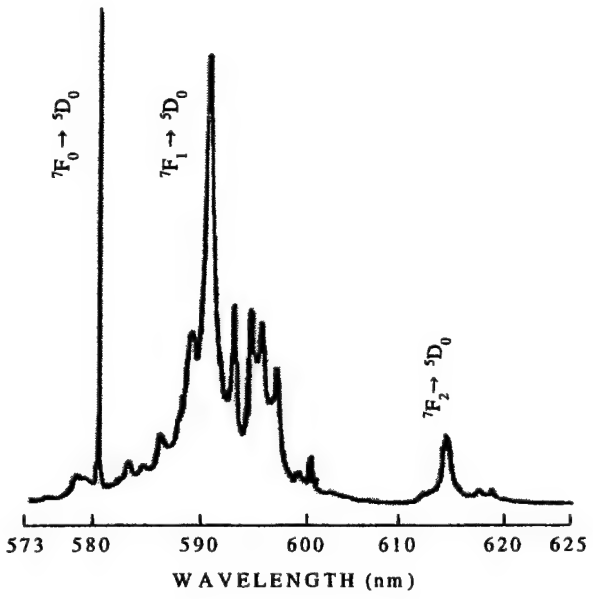
$^7F_0 \rightarrow {}^5D_0$
$^7F_1 \rightarrow {}^5D_0$
$^7F_2 \rightarrow {}^5D_0$
573
580
590
600
610
620
625
WAVELENGTH (nm)

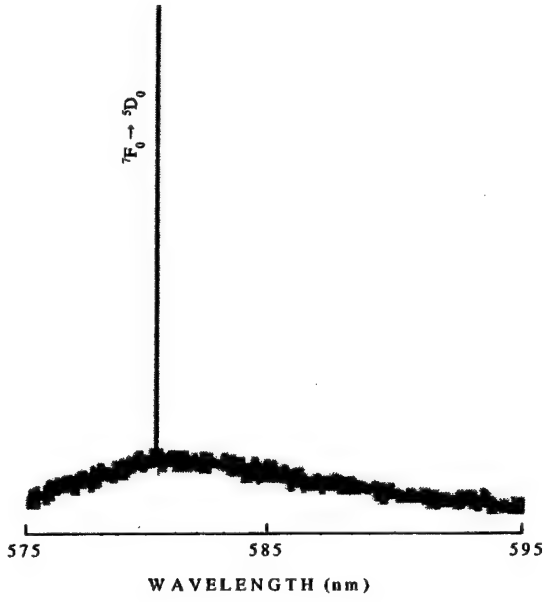
$^7F_0 \rightarrow {}^5D_0$
575
585
595
WAVELENGTH (nm)

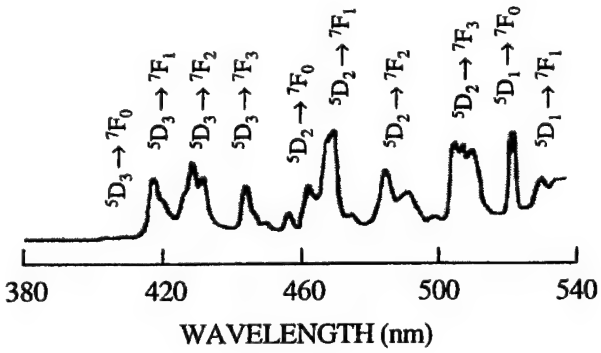
$^5D_3 \rightarrow {}^7F_0$
$^5D_3 \rightarrow {}^7F_1$
$^5D_3 \rightarrow {}^7F_2$
$^5D_3 \rightarrow {}^7F_3$
$^5D_2 \rightarrow {}^7F_0$
$^5D_2 \rightarrow {}^7F_1$
$^5D_2 \rightarrow {}^7F_2$
$^5D_2 \rightarrow {}^7F_3$
$^5D_1 \rightarrow {}^7F_0$
$^5D_1 \rightarrow {}^7F_1$
380
420
460
500
540
WAVELENGTH (nm)

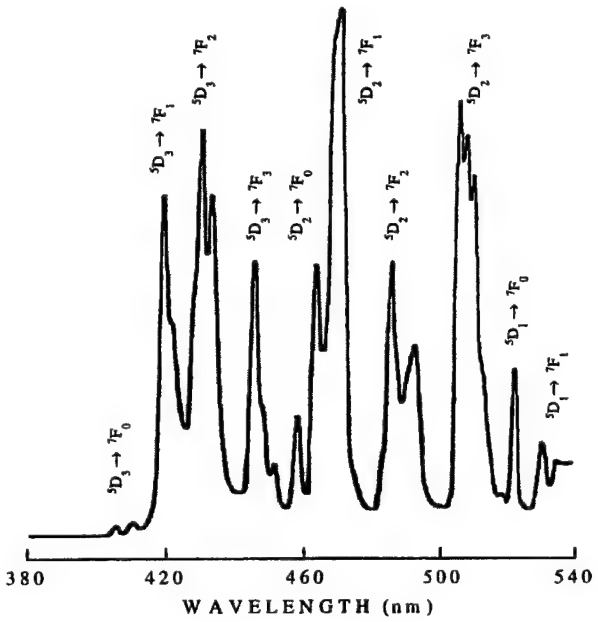
$^5D_3 \rightarrow {}^7F_0$
$^5D_3 \rightarrow {}^7F_1$
$^5D_3 \rightarrow {}^7F_2$
$^5D_3 \rightarrow {}^7F_3$
$^5D_2 \rightarrow {}^7F_0$
$^5D_2 \rightarrow {}^7F_1$
$^5D_2 \rightarrow {}^7F_2$
$^5D_2 \rightarrow {}^7F_3$
$^5D_1 \rightarrow {}^7F_0$
$^5D_1 \rightarrow {}^7F_1$
380
420
460
500
540
WAVELENGTH (nm)

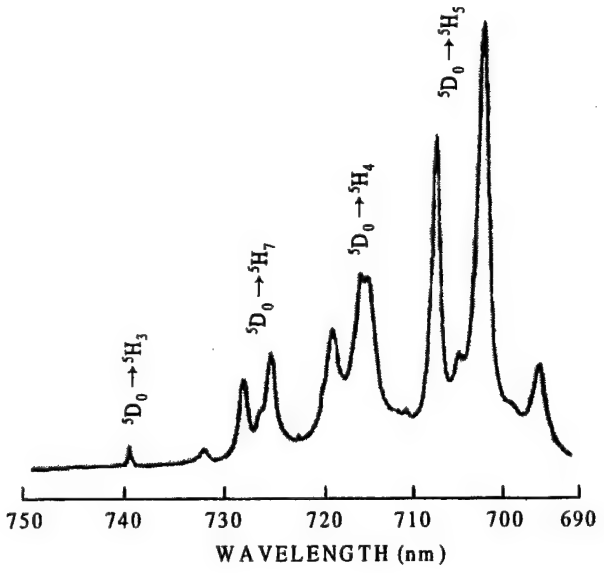
$^5D_0 \rightarrow {}^5H_3$
$^5D_0 \rightarrow {}^5H_7$
$^5D_0 \rightarrow {}^5H_4$
$^5D_0 \rightarrow {}^5H_5$
750
740
730
720
710
700
690
WAVELENGTH (nm)

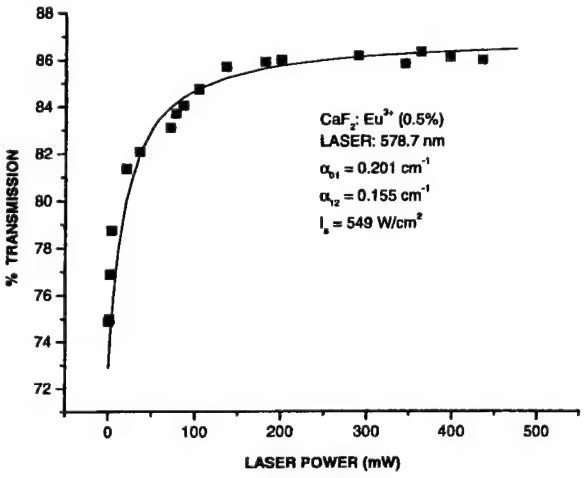
% TRANSMISSION
LASER POWER (mW)
88
86
84
82
80
78
76
74
72
0
100
200
300
400
500
CaF2: Eu3+ (0.5%)
LASER: 578.7 nm
α01 = 0.201 cm-1
α12 = 0.155 cm-1
Is = 549 W/cm2

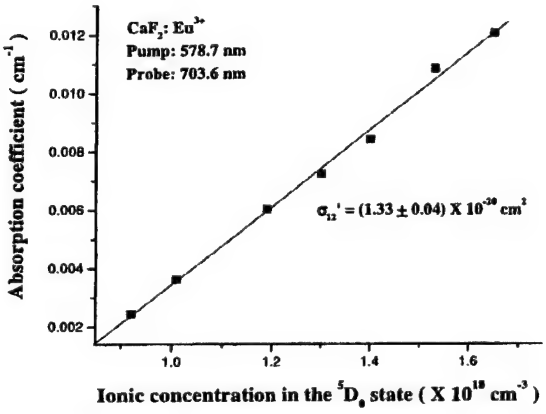
CaF2: Eu3+
Pump: 578.7 nm
Probe: 703.6 nm
σ12' = (1.33 ± 0.04) X 10-20 cm2
Absorption coefficient (cm-1)
0.012
0.010
0.008
0.006
0.004
0.002
1.0
1.2
1.4
1.6
Ionic concentration in the 5D0 state (X 1018 cm-3)

CSI/CUNY

Engineering Science and Physics Department

Final Technical Report

Grant AFOSR F49620-97-1-0258 / RF 770086

Optical Hole-Burning Studies in Glasses Doped with Dyes and Rare- Earth Ions

October 12, 2000

Principal Investigator: Prof. Anshel Gorokhovsky

Ph.D. Graduate Student: Mr. Alex Turukhin

Undergraduate Student: Mr. Alexander Vaysman

Collaborators: Prof. Y. Okamoto, Chemistry Department,

Polytechnic University, Brooklyn, NY

CSI/CUNY

Engineering Science and Physics Department

Final Technical Report

Grant AFOSR F49620-97-1-0258 / RF 770086

Optical Hole-Burning Studies in Glasses Doped with Dyes and Rare- Earth Ions

October 12, 2000

Principal Investigator: Prof. Anshel Gorokhovsky

Ph.D. Graduate Student: Mr. Alex Turukhin

Undergraduate Student: Mr. Alexander Vaysman

Collaborators: Prof. Y. Okamoto, Chemistry Department,

Polytechnic University, Brooklyn, NY

Materials are one of the key elements to advance the spectral hole-burning (SHB) technology for optical storage and processing. Our research is directed to evaluation of some prospective materials for optical hole-burning frequency and time-domain storage applications.

Major focus of our subcontract was on several thulium ions doped polymer materials. Our interest in these metallo-organic materials is motivated by the need to combine unique properties of the rare-earth ion (weak electron-phonon interaction, long coherence time) with the ability of the organic surrounding to change its local structure under laser excitation of the rare-earth ion. The latter may serve as a persistent hole-burning mechanism for multi-frequency optical storage. We performed optical absorption, photoluminescence, and persistent spectral hole burning studies of four Tm^{3+} ion - organic ligand complexes, specifically β-diketons tris chelats of thulium, blended in a poly (methyl methacrylate) matrix. The Tm^{3+} ion is especially of interest because the transition between the $^3H_6(1)$ and the $^3H_4(1)$ crystal field levels occurs in the region of GaAlAs diode lasers near 800 nm, which is clearly advantageous for possible technological applications. To characterize and compare different potential hole burning materials, we determined some material parameters including low-temperature crossection of optical transition, excited state optical lifetime, inhomogeneous linewidth, homogeneous holewidth, hole lifetime, quantum yield of hole burning, persistent hole annealing temperature, and some others.

The progress was achieved in areas of upgrading of laboratory equipment, materials and research.

1. Laboratory

A hole burning laboratory was set up to characterize materials and determine major spectroscopic parameters in broad temperature range 1.4 - 300 K. Major spectroscopic equipment including Perkin Elmer Lambda 900 UV/VIS/NIR Spectrophotometer has been purchased and installed. A simple optical method for studying mechanical vibrations has been developed and applied to investigation of commercial closed cycle refrigeration system CRYO Model 396-022. The method is based on amplitude modulation of laser beam intensity by a knife-edge mounted on the sample holder. A Fourier transform was used to analyze the vibration spectrum. The sensitivity of this optical technique is determined by the diameter of the focused beam, and the

sensitivity of 1 μm is readily achievable. Studies were conducted for different temperatures, orientations, and mechanical holders. The amplitudes of the vibrations were on the order of a 50 μm. The drive motor of the cold head produced strong vibrations at 60 Hz and 120 Hz, while the piston generated major vibrations at 3 Hz. To minimize sample vibrations, a special cold head support was developed. This support allowed us to use this refrigeration system in conjunction with Lambda 900 spectrophotometer for low temperature absorption spectroscopy. However, optical storage applications require additional vibration decoupling interface.

2. Materials

Several Eu^{3+} and Tm^{3+} doped polymers where prepared by Prof. Y. Okamoto' group (Polytechnic University, Brooklyn, NY). After preliminary studies, we focused on four Tm^{3+} ion β-diketone tris chelate complexes. To prepare these complexes, thulium chloride ($TmCl_3 \bullet 6H_2O$) with thenoyltrifluoroacetylacetone (TTFA), 1,1,1-trifluoro-2, 4-pentanedione (TFD), 1-phenyl-1, 3-butanedione (PBD), and 1,3-diphenyl-1, 3-propanedione (DBM) ligands were used. Tris chelats of thulium were blended in a poly (methyl methacrylate) matrix. The concentration of the Tm3+ ion in the samples was determined on the basis of input chemical concentrations and found to be 0.35, 0.14, 0.32, and 0.2 mol % for Tm^{3+} $(TFD)_3$, Tm^{3+} $(TTFA)_3$, Tm^{3+} $(PBD)_3$, and Tm^{3+} $(DBM)_3$ complexes, respectively. Physically, the samples appeared to be transparent slightly yellow colored cylinders, having diameters of 8 -10 mm and lengths of 15-20 mm.

3. Research.

Optical absorption, steady state and time-resolved photoluminescence, and spectral hole burning at the transition between the $^3H_6(1)$ and the $^3H_4(1)$ crystal-field levels, were studied at temperatures between 1.4 and 300 K.

To determine the magnitude of inhomogeneous broadening, an absorption band was numerically fitted by the superposition of a few Gaussians. The width of the Gaussian centered at the transition between the lowest crystal field components, $^3H_4$ (1)← $^3H_6$ (1), gives the inhomogeneous broadening of this transition (the homogeneous broadening can be neglected), and was found to be between 90 and 140 cm^{-1} for different complexes. In addition, the fitting

allowed us to determine the crystal field splitting of the $^3H_4$, as well as $^3H_6$ ground state for each complex.

Luminescence spectra of the Tm3+-ligand complexes were investigated in the region of the $^3H_4 \rightarrow {}^3H_6$ transition in the wavelength range between 750 and 850 nm at temperatures between range 1.4 - 77 K. The $^3H_4 \rightarrow {}^3H_6$ and $^1G_4 \rightarrow {}^3H_5$ luminescence decays, as well as the background emission decays, were also measured in the different materials after $^1G_4 \leftarrow {}^3H_6$ pulsed excitation at 476.5 nm for T = 1.4 K. The luminescence quantum yield was estimated on the bases of relative luminescence intensity, absorption at the laser wavelength, and level lifetime.

Long-lived holes were observed in all materials. No side band structure was observed. Optical spectral hole burning was investigated at different temperatures. Persistent spectral holes were detected at temperatures between 1.4 K and 20 K. The holes show no visible recovery at 1.4 K over the experimental time of 10 hours. The maximum measured hole depth was about 50 %. The hole-burning mechanism appears to be a photoinduced rearrangement of the local structure. The holewidth dependence on burning time at different intensities was used to determine the conditions for the weak burning intensity regime. The "true" holewidths for different materials were found to be Γ_{hole} = 180-360 MHz by using the zero limit of the burning intensity and of the exposure time. Spectral hole widths show weak power law temperature dependence T^n with n = 1 -1.6. To verify the ability of the materials under investigation to store a number of spectral holes, we performed hole burning at different wavelengths over the inhomogeneous broadened absorption band. Holes were observed over the full inhomogeneously broadened band of the $^3H_6(1) \rightarrow {}^3H_4(1)$ transition, i.e. in the bandwidth of 100 cm^{-1}, or 3000 GHz. No visible laser - induced filling or broadening was detected.

To analyze a hole profile, we measured the hole several times at close frequencies and accumulated the spectra. The typical profile observed in all materials was non-Lorentzian. The hole shape was best described by the superposition of two Lorentzians. Attempts to fit the observed shape by combination of Lorentzians with continuous width distributions (either uniform or Gaussian) gave worse results. The dependence of the hole shape upon wavelength position within the inhomogeneous band between 789 nm and 798 nm was studied. An

interesting trend was found: while widths of the constituted Lorentzians remain practically constant across the spectral range studied, the ratio of their amplitudes was changing. The widths of the constituted holes were found to be 230±20 MHz and 1.3±0.2 GHz. The observed results may be explained by the existence of two unresolved overlapping spectral components inside the inhomogeneous absorption band. In this case, the observed spectral hole is a superposition of two independent holes, broad and narrow, with holewidths remaining approximately constant across the inhomogeneous band. Fitting the experimental dependence, the widths of the hidden inhomogeneous components were found to be 5.6 nm and 4.6 nm, respectively and the peak wavelengths close to 793.9 nm for both components. These components most likely originate from two different sites of the Tm^{3+} $(TTFA)_3$ in PMMA having different dephasing rates. These rates are reflected in different widths of the constituted holes. Due to the complex shape of the spectral holes, the holewidth reported above refers to the "effective" holewidth measured at half amplitude.

Kinetics of the spectral hole burning were recorded at time scale of 10^{-2} - 10^{4} s. They showed dispersive behavior associated with random structure of the Tm^{3+} ion surrounding. Analyze of the dispersive kinetics allows to determine the quantum efficiency of SHB. Average quantum efficiency was found to be in range 10^{-6} to 10^{-4} and compared for all samples. Hole burning and refilling mechanisms were analyzed in the frame of ion interaction with two-level low-frequency excitations. The energy barrier between the photoproduct and educt states for the Tm^{3+} $(TTFA)_3$ complex was determined from hole area temperature cycling to be on the order of 700 cm^{-1}. This value corresponds to the maximum annealing temperature T_{Amax} = 20 K for Tm^{3+} $(TTFA)_3$ and about 30% of the initial hole area conservation at our experimental conditions. The maximum annealing temperature was determined for all complexes, and its correlation with the size of the side groups was established. A likely mechanism of the hole filling after temperature cycling is a thermally activated rotational displacement of the ligand side groups. Spectroscopic results indicate glass-like properties for these materials, i.e. a high degree of disorder in the Tm^{3+} coordination surroundings. The materials have large inhomogeneous broadening, and merit further investigation for possible hole burning frequency- and time- domain storage and other applications.

Publications and presentations:

A.V. Turukhin, A.V. Carpenter, A.A. Gorokhovsky, T. Chu and Y. Okamoto, "Hole Burning Spectroscopy of Thulium Chelats", J. of Luminescence **86**, 333 (2000)

A. V. Turukhin, A. V. Carpenter, A. A. Gorokhovsky, R. R. Alfano, T. Chu, and Y. Okamoto, "Optical spectroscopy of Tm^{3+} in organic matrices for hole-burning storage applications", Proc. of the SPIE's 43rd Annual Meeting, San Diego, CA, July 19 - 24, 1998, **Vol. 3468.**

A. V. Turukhin, A. A. Vaysman, and A. A. Gorokhovsky, "Evaluation of vibration generated by closed cycle refrigeration system using optical methods", Proc. of the SPIE's 43rd Annual Meeting, San Diego, CA, July 19 - 24, 1998, **Vol. 3435**.

A.V. Turukhin, A.V. Carpenter, A.A. Gorokhovsky, T. Chu and Y. Okamoto, "Hole Burning Spectroscopy of Thulium Chelats", Presented at the 6th International Meeting on Hole Burning and related Spectroscopies: Science and Applications, Hourtin, France, September 18-23, 1999, p39.

A. A. Gorokhovsky, A. V. Turukhin, A. V. Carpenter, R. R. Alfano, T. Chu, and Y. Okamoto, "Optical spectroscopy of Tm^{3+}: ligand complexes for hole-burning storage applications", Presented at the International Symposium on Optical Science, Engineering, and Instrumentation, SPIE's 43rd Annual Meeting, San Diego, CA, July 19 - 24, 1998, Conference 3468.

A. V. Turukhin, A. A. Vaysman, A. A. Gorokhovsky, "Evaluation of vibrations generated by closed cycle refrigeration system using optical methods", Presented at the International Symposium on Optical Science, Engineering, and Instrumentation, SPIE's 43rd Annual Meeting, San Diego, CA, July 19 - 24, 1998, Conference 3435.

List of persons supported by the project AFOSR F49620-97-1-0258 / RF 770086 in full or partially

1. Prof. A. Gorokhovsky, PI, CUNY
2. Mr. Alexey Turukhin, graduate student, CUNY
3. Mr. Aleksander Vaysman, undergraduate student, CUNY
4. Prof. Aleksander Karasik, visiting scientist, General Physics Institute, Moscow, Russia

List of major equipment purchased using project AFOSR F49620-97-1-0258 / RF 770086

1. Cooled Photomultiplier Housing PC104CE (Products for Research)
2. Multi-channel Spectrometer (Ocean Optics)
3. Partial payment for the LAMBDA-900 Spectrophotometer (Perkin Elmer)
4. Partial payment for the ultrafast laser system (Spectra Physics)

ELSEVIER

Journal of Luminescence 86 (2000) 333–339

JOURNAL OF LUMINESCENCE

www.elsevier.com/locate/jlumin

Hole-burning spectroscopy of thulium chelates

A.V. Turukhin[1], A.V. Carpenter[a], A.A. Gorokhovsky[a,*], T. Chu[b], Y. Okamoto[b]

[a]*The College of Staten Island and Graduate Center of CUNY, 2800 Victory Building, Staten Island, NY 10314, USA*
[b]*New York Polytechnic University, Brooklyn, NY 11201, USA*

Abstract

The spectral hole-burning properties of four Tm^{3+} chelates, specifically β-diketone tris chelates of thulium blended in a poly (methyl methacrylate) matrix are presented. Persistent spectral hole burning was observed at the $^3H_4(1) \leftarrow {}^3H_6(1)$ transition of the Tm^{3+} ion near 795 nm in all of the materials. The holewidth was found to be in the range 180–360 MHz and the hole lifetime is longer than 10 h at 1.4 K. A complex hole profile which was best described by the superposition of two Lorentzians was observed. Temperature cycling experiments were performed. The maximum annealing temperature was determined for all complexes, and its correlation with the size of the side groups was established. The aim of our research was to characterize these novel materials, as well as to evaluate their prospective for optical hole-burning frequency- and time-domain storage applications.

Keywords: Spectral hole burning; Materials; Thulium ion; Chelates and polymers

1. Introduction

Interest in rare-earth ion-doped materials is based on the fact that the optical 4f electrons of the rare-earth ions are shielded by the outer 5s and 5p electrons. As a result, the optical 4f electrons are not strongly affected by the motion of neighboring atoms, and thus the phonon–electron interaction is weak and the optical transition exhibits small homogeneous vibrational broadening. In addition, ions with an even number of 4f electrons have nonmagnetic singlet electronic states, and consequently the homogeneous broadening caused by the magnetic interaction with neighboring spin magnetic moments is small. Many of the rare-earth ions in solids, e.g. Eu^{3+}, exhibit persistent hole burning as a result of the optical pumping of hyperfine levels, with storage lifetimes of a few hours [1]. This mechanism is efficient only at low temperatures, generally less than 10 K, where the hyperfine splitting exceeds the homogeneous line width. It does not operate at elevated temperatures, where the only storage mechanism is the population of electronic levels, and the storage lifetime is limited to 10^{-6}–10^{-2} s. Several other persistent hole-burning mechanisms were observed in Eu^{3+}-doped glasses, including the photoactivated rearrangement of the OH bonds [2] and the photoinduced reduction of the Eu^{3+} ion [3]. Certain rare-earth ions, in particular Tm^{3+}, have no hyperfine splitting and accordingly no hyperfine storage capabilities [4]. Tm^{3+}-doped solids are especially of interest because the transition between the $^3H_6(1)$

[1] Present address: Research Laboratory of Electronics, MIT, Cambridge, MA 02139, USA.

*Corresponding author. Tel.: 718-982-2815; fax: 718-982-2830.

E-mail address: gorokhovsky@postbox.csi.cuny.edu (A.A. Gorokhovsky)

0022-2313/00/$ - see front matter
PII: S0022-2313(00)00193-9

and the $^3H_4(1)$ crystal field levels occurs in the region near 800 nm, matching the wavelength of most diode lasers. This is clearly advantageous for possible technological applications. In addition, a large inhomogeneous-to-homogeneous linewidth ratio, up to 7×10^6, can be obtained [5].

In order to have the combined properties of both small phonon broadening of f–f transitions and long hole lifetime, we chose to investigate hole burning in rare-earth ion-doped polymer matrices as potential materials for frequency selective storage. We expected that these materials would exhibit persistent hole-burning due to a photoinduced rearrangement of the local structure surrounding the ion. This mechanism is probably universal for disordered glass-like solids [6]. Another motivation for the study of the polymer host was to obtain a large inhomogeneous line width. This makes these materials suitable for high-speed applications, e.g. ultrafast communications, femtosecond time-domain holography, and petaflop computing.

In this paper, we present some results on persistent spectral hole burning of four Tm^{3+}- organic ligand complexes in a polymer matrix. Our attention was focused on the $^3H_4(1) \leftrightarrow {}^3H_6(1)$ transition with absorption in the 800 nm region. The absorption and photoluminescence spectra of these materials were discussed in Ref. [7].

2. Experimental

The materials investigated were Tm^{3+} chelates, specifically β-diketone tris chelates of thulium. Samples were prepared by the technique described in Ref. [8] using the reaction of thulium chloride ($TmCl_3 \cdot 6H_2O$) with β-diketonates. The molecular structure of these chelates is shown in Fig. 1, and the symbols assigned to each ligand and substituent side group R_1 and R_2 are listed in Table 1. Six oxygen atoms are available for coordination to the rare-earth ion. There is however evidence [9] that between one and three additional oxygen atoms may be delivered by coordination water molecules. The chelates were subsequently blended in a poly (methyl methacrylate) (PMMA) matrix as a host. The concentration of Tm^{3+} in the samples was

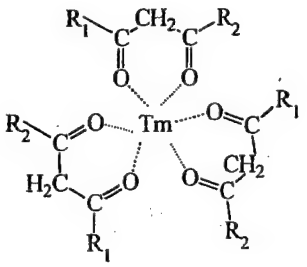

Fig. 1. Chemical structure of β-diketone tris chelates of thulium.

Table 1
Substituent groups

Name of the ligand		Structure of the substituent groups	
Full name	Abbreviation	R1	R2
1,1,1-Trifluoro-2,4-pentanedione	TFD	$-CH_3$	$-CF_3$
1-Phenyl-1,3-butanedione	PBD	$-CH_3$	
Thenoyltrifluoroacetylcetone	TTFA	$-CF_3$	
1,3-Diphenyl-1,3-propanedione	DBM		

determined on the basis of input chemical concentrations and found to be 0.35, 0.14, 0.32, and 0.2 mol% for Tm^{3+} $(TFD)_3$, Tm^{3+} $(TTFA)_3$, Tm^{3+} $(PBD)_3$, and Tm^{3+} $(DBM)_3$ complexes, respectively. Physically, the samples appeared to be transparent slightly yellow colored cylinders, having diameters of 8–10 mm and lengths of 15–20 mm.

Hole-burning measurements were made with a tunable single frequency CW Ti-sapphire laser (Coherent 899-29). The laser intensity was stabilized at the level of 0.1%. Experiments were performed at temperatures 1.4–30 K in a He-bath cryostat (Optistat by Oxford Instruments).

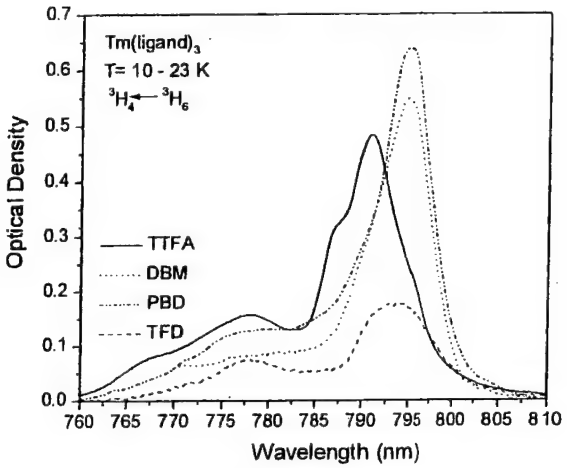

Fig. 2. $^3H_4 \leftarrow {}^3H_6$ absorption bands of Tm^{3+} chelates complexes in PMMA. Temperature range is 10–23 K

3. Results and discussion

The low temperature absorption spectra of the $^3H_4 \leftarrow {}^3H_6$ transition of the four complexes studied are presented in Fig. 2. The absorption band consists of several overlapping elementary bands and has slightly different peak positions and structures for different complexes. These elementary bands represent transitions between separate crystal field components of the involved electronic levels and, in addition, may have some contribution from the different coordination structures (sites). The prominent crystal field splitting of about 250 cm^{-1} is clearly seen for all four of Tm^{3+}–ligand complexes.

To determine the magnitude of inhomogeneous broadening, an absorption band was numerically fitted by the superposition of several Gaussians. The width of the Gaussian centered at the transition between the lowest crystal field components, $^3H_4(1) \leftarrow {}^3H_6(1)$, gives the inhomogeneous broadening of this transition (at low temperature the homogeneous broadening can be neglected). This width was found to be between 90 and 140 cm^{-1} for different complexes (see Table 2). In addition, the fitting permitted the determination of the crystal field splitting of the $^3H_4$ state and the other observed exited states [7].

We studied hole burning in spectra of the $^3H_4(1) \leftarrow {}^3H_6(1)$ transition of Tm^{3+} for all materials listed. Holes were burned at fixed frequencies and recorded subsequently in transmission spectra by scanning the laser frequency at the reduced intensity. Persistent holes were observed in all materials. A hole with depth of about 9% in the spectrum of Tm^{3+} $(TTFA)_3$ is shown in Fig. 3a. The maximum measured hole depth was about 50%. To avoid power saturation, the holewidth dependence on burning time at different intensities was measured (Fig. 3b). This dependence was used to determine the optimum unsaturated burning intensity, which was found to be about 1 mW/mm^2. In addition, for the spectral hole detection, the intensity was reduced by two orders of magnitude to avoid hole profile distortions by the probing light.

To analyze a hole profile, we measured the hole several times at close frequencies and accumulated the spectra. The typical profile observed in all materials was non-Lorentzian. The hole profile for Tm^{3+} $(TTFA)_3$ and a clearly inadequate fit by a single Lorentzian are depicted in Fig. 4a. The hole shape was best described by the superposition of two Lorentzians (Fig. 4b). Attempts to fit the observed shape by the combination of Lorentzians with continuous width distributions (either uniform [10] (Fig. 4c) or Gaussian) gave worse results. The dependence of the hole shape upon wavelength position within the inhomogeneous band between 789 and 798 nm was studied. An interesting trend was found: while widths of the constituted

Table 2
Holewidths and inhomogeneous widths of the $^3H_4(1) \leftarrow {}^3H_6(1)$ transition of Tm^{3+} chelates in PMMA

Parameters	$Tm(TTFA)_3$	$Tm(TFD)_3$	$Tm(PBD)_3$	Tm(DBM)
Γ_{inh} (GHz)	3000	4300	2800	2500
Γ_{hole} (MHz)	220	230	360	180
$\Gamma_{inh}/\Gamma_{hole}$	1.4×10^4	1.9×10^4	0.8×10^4	1.4×10^4
n ($\Gamma_{hole} \sim T^n$)	1.6 ± 0.15	1.3 ± 0.15	1.0 ± 0.15	1.5 ± 0.15

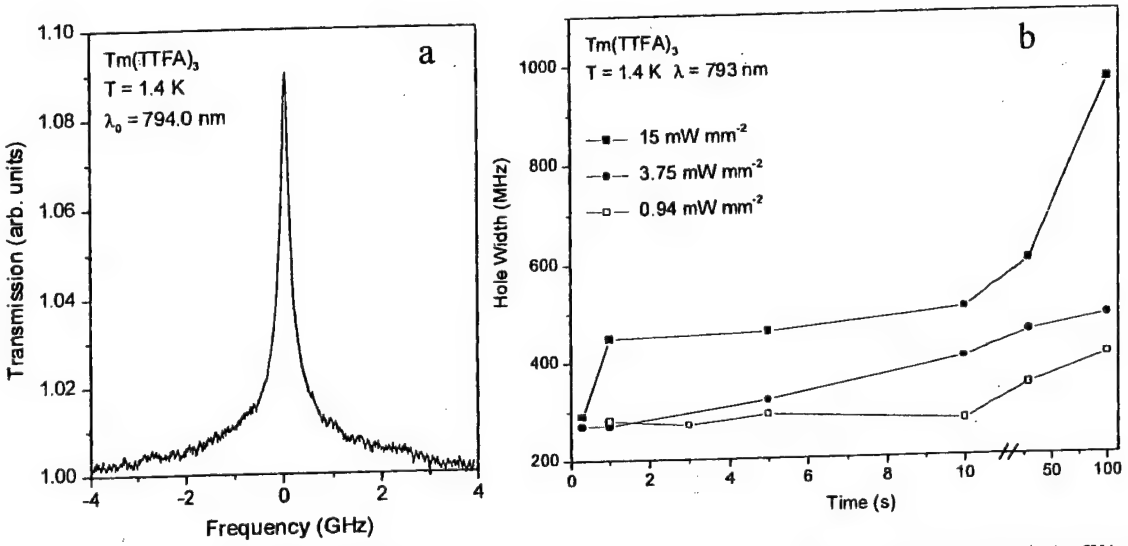

Fig. 3. (a) Representative hole profile. The hole was burnt in Tm $(TTFA)_3$ for 30 s at 1.4 K. Burning intensity was 1 mW/mm (b) Dependence of the holewidth on exposure time at different burning intensities for Tm $(TFFA)_3$ in PMMA.

Lorentzians remain practically constant across the spectral range studied (see Fig. 4d), the ratio of their amplitudes was changing (Fig. 4e). The widths of the constituted holes were found to be 230 ± 20 MHz and 1.3 ± 0.2 GHz. The observed results may be explained by the existence of two unresolved overlapping spectral components inside the inhomogeneous absorption band. In this case, the observed spectral hole is a superposition of two independent holes, broad and narrow, with holewidths remaining approximately constant across the inhomogeneous band. The amplitudes of the constituted holes depend on the intensity of each component at the hole-burning wavelength. Fitting the experimental dependence in Fig. 4e, the widths of the hidden inhomogeneous components 1 and 2 were found to be 5.6 and 4.6 nm, respectively, and the peak wavelengths close to 793.9 nm for both components. These components most likely originate from two different sites of the Tm^3 $(TTFA)_3$ in PMMA having different dephasing rates. These rates are reflected in different widths of the constituted holes. Due to the complex shape of the spectral holes, the holewidth reported elsewhere in the text refers to the "effective" holewidth measured at half amplitude.

The "true" holewidth for different materials was found to be $\Gamma_{hole} = 180$–360 MHz by using the zero limit of the burning intensity and of the exposure time (see Table 2). This "true" holewidth reflects optical dephasing caused by the interaction with phonons, tunneling systems, and surrounding

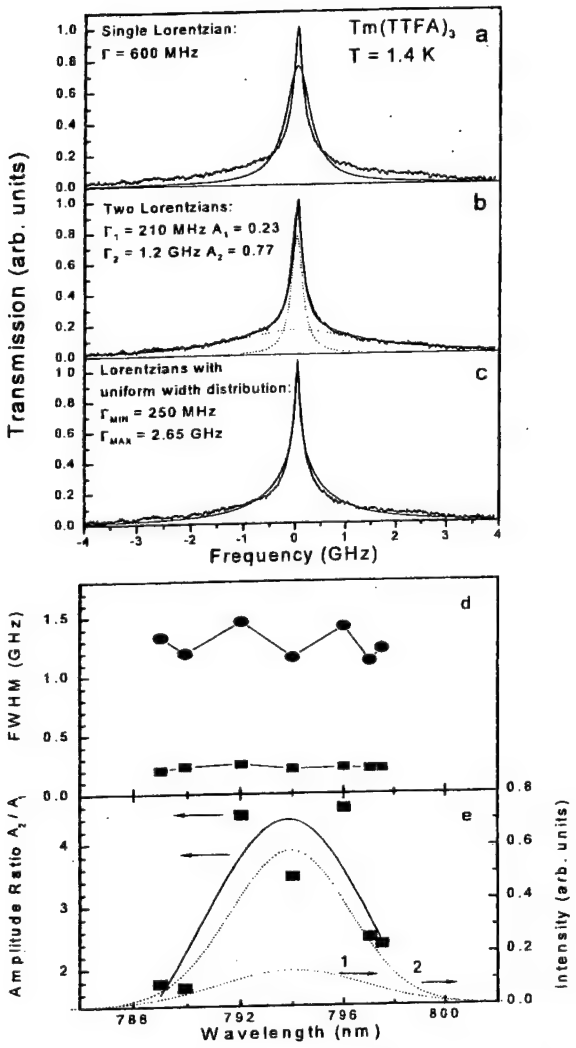

Fig. 4. An experimental spectral hole profile and its fit by: (a) a single Lorentzian, (b) a superposition of two Lorentzians, and (c) superposition of Lorentzians with continuous uniform distribution of widths between Γ_{MIN} and Γ_{MAX}. The spectrum measured in Tm $(TTFA)_3$ at 1.4 K near 794 nm after 30 s of hole burning with intensity 1 mW/mm^2. Results of the fit (c) at different wavelengths are presented in (d) and (e) for the Lorentzian widths and for the amplitude ratio, respectively. The solid line in (e) is a fitted curve of this experimental dependence by the model described in the text. Extracted from the fitting procedure are two hidden components are represented by the dotted lines 1 and 2.

spins (in the time scale of the excited state lifetime), as well as slow spectral diffusion. Separation of these effects requires fast time-resolved measurements [11].

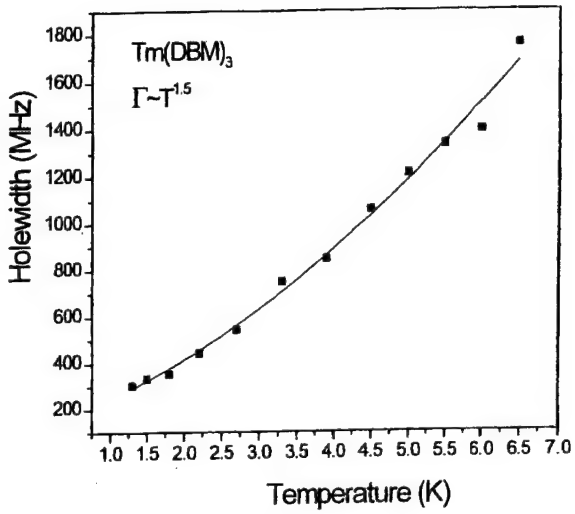

Fig. 5. Experimental temperature dependence of a holewidth for Tm $(DBM)_3$ (squares). The solid line represents a fit by the equation $\Gamma(T) - \Gamma(0) = aT^n$ with $\Gamma(0) = 160$ MHz, $a = 90$, and $n = 1.5$.

The temperature dependence of the holewidth was measured between 1.4 and 16 K. The representative dependence for the Tm $(DBM)_3$ complex is shown in Fig. 5. The holewidth follows a weak power law $\Gamma_{hole} \propto T^{1.5}$. Similarly, a temperature dependence governed by a power law $\Gamma_{hole} \propto T^n$ with $n = 1$–1.6 was observed for other compounds (see Table 2). A similar dependence of the homogeneous line broadening with $n = 1$–2 was observed in many doped glasses and polymers [12]. Interpreting this dependence involves the interaction between the optical transition in the impurity ion and the low-frequency excitations (quasilocal vibrations and tunneling systems) of the amorphous matrix.

The kinetics of the spectral hole-burning were recorded at the time scale 10^{-2}–10^4 s. The kinetics shows dispersive behavior associated with the random structure of the nearby environment of the Tm^{3+} ion and the respective distribution of hole-burning quantum yields. The average quantum yield was estimated to be between 10^{-4} and 10^{-6} for all complexes. The hole burning mechanism appears to be nonphotochemical and due to photoinduced structural rearrangement [6], and will be discussed elsewhere.

The holes show no visible recovery at 1.4 K over the experimental time of 10 h. To investigate the hole stability at elevated temperatures and the nature of the photoproduct state, we performed temperature cycling experiments [13]. During each temperature cycle, a spectral hole was burnt and the hole spectrum was detected at the temperature $T_B = 1.4$ K. Then the temperature was raised to an annealing temperature T_A, maintained at this level for about 600 s, lowered back to T_B, and the hole was detected again. Results for the relative hole area $A(T_A)/A(T_B)$ dependence on T_A are presented in Fig. 6a. The hole area, which is proportional to the number of centers in the photoproduct state, decreases with annealing temperature due to the thermally activated hole-filling reaction. The data was fitted satisfactorily in the framework of a model of distributed barrier heights between photoproduct and educt, and the assumption of a thermally activated barrier crossing [13]. Using a reasonable value for the attempt frequency of 10^{11} s^{-1}, we estimated the maximum barrier height in the ground electronic state of this complex to be on the order of 700 cm^{-1}. This value corresponds to the maximum annealing temperature $T_{A\,max} = 20$ K for Tm^{3+} $(TTFA)_3$ and about 30% of the initial hole area conservation at our experimental conditions. These conditions were the following: the depth of the initial hole was 10%, the minimum depth of the annealed hole of about 1% was determined by our signal/noise ratio, and the broadening of the initial hole due to irreversible spectral diffusion was about threefold. To determine how the maximum annealing temperature related to the ligand, we measured $T_{A\,max}$ for other materials studied as well. Fig. 6b presents the $T_{A\,max}$ corresponding to different side groups. A distinctive monotonic dependence was observed: ligands with heavier and bulkier side groups R_1 and R_2 have higher maximum annealing temperatures. In the case of the thermally activated barrier crossing, we may assume a weak dependence of $T_{A\,max}$ on the side group mass. Therefore, the barrier between educt and photoproduct states is determined mostly by the size of the side groups of the ligand. The interpretation is straightforward: a larger side group is more compressed inside the polymer host than a smaller one and is therefore more stable in its equilibrium configuration. The actual species involved in a reaction could be the side groups themselves or their interacting counterparts of PMMA. The latter is less probable as much higher annealing temperature of about 80 K was reported for the PMMA matrix [14]. Therefore, a likely mechanism for the hole filling after temperature cycling is the thermally activated rotational displacement of the R_1 and/or R_2 side groups, which are attached to the β-diketone ring by a relatively weak single C–C bond, between the equilibrium positions in the PMMA matrix.

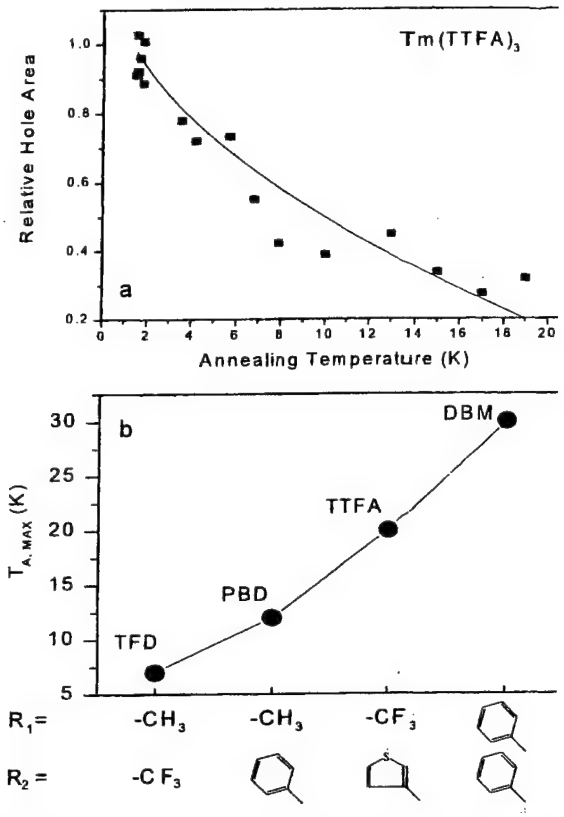

Fig. 6. (a) Dependence of the relative hole area on the annealing temperature in a temperature cycling experiment (squares) for Tm $(TTFA)_3$. The fitted curve (solid line) is calculated from Eq. (8) in Ref. [13]; (b) The maximum annealing temperature for different ligand structures.

It is of interest to compare our results with those previously reported for several Eu^{3+}-doped organic glasses and polymers. In Ref. [15], the observed small inhomogeneous line widths between

1.5 and 16 cm^{-1} and the narrow holes with widths of a few MHz are close to those for inorganic crystalline hosts. These indicate that for Eu^{3+} ions the organic hosts studied provide not glass-like, but more likely crystalline-like structure. In sharp contrast, the Tm^{3+} chelates in PMMA studied in this paper have inhomogeneous broadening of about 100 cm^{-1} and holewidths of about 100 MHz which is typical for most inorganic as well as organic glasses and polymers. This indicates a higher degree of disorder in the coordination of the Tm^{3+} ion in β-diketone chelates. This result is probably connected to the molecular structure of our chelates, which allow a number of different orientational positions of the side groups.

4. Conclusions

Four new Tm^{3+} chelates complexes in PMMA matrix were prepared. Optical spectral hole burning was investigated at different temperatures. Persistent spectral hole burning was observed at the $^3H_4(1) \leftarrow {}^3H_6(1)$ transition of Tm^{3+} ion near 795 nm in all of the materials. The holewidth was found to be in the range 180–360 MHz and the hole lifetime is longer than 10 h at 1.44 K. A two component absorption band structure is proposed to explain the observed non-Lorentzian hole profile. The energy barrier between the photoproduct and educt states for the Tm^{3+} $(TTFA)_3$ complex was determined from hole area temperature cycling. The maximum annealing temperature was determined for all complexes, and its correlation with the size of the side groups was established. A likely mechanism of the hole filling after temperature cycling is a thermally activated rotational displacement of the ligand side groups. Spectroscopic results indicate glass-like properties for these materials, i.e. a high degree of disorder in the Tm^{3+} coordination surroundings. The materials have large inhomogeneous broadening, and merit further investigation for possible hole-burning frequency- and time-domain storage and other applications.

Acknowledgements

This work was supported in part by the US Air Force Office of Scientific Research under contracts F 49620-97-1-0486 and F 49620-97-1-0258.

References

[1] R.M. Macfarlane, R.M. Shelby, in: A.A. Kaplyanskii, R.M. Macfarlane (Eds.), Spectroscopy of Solids Containing Rare Earth Ions, North-Holland, Amsterdam, 1987, p. 51.
[2] M. Nogami, N. Umehara, T. Hayakawa, Phys. Rev. B 58 (1998) 6166.
[3] K. Fujita, K. Tanaka, K. Hirao, N. Soga, J. Opt. Soc. Am. B 15 (1998) 2700.
[4] R.M. Macfarlane, Opt. Lett. 18 (1993) 829.
[5] G.M. Wang, R.W. Equall, R.L. Cone, M.J.M. Leask, K.W. Godfrey, F.R. Wondre, Opt. Lett. 21 (1996) 818.
[6] R. Jankowiak, G.J. Small, Science 237 (1987) 618.
[7] A.V. Turukhin, A.V. Carpenter, A.A. Gorokhovsky, R.R. Alfano, T. Chu, Y. Okamoto, Proc. SPIE 3468 (1998) 165.
[8] Y. Okamoto, Y. Ueba, F.N. Dzhanibekov, E. Banks, Macromolecules 14 (1981) 17.
[9] F. Halverson, J.S. Brinen, J.R. Leto, J. Chem. Phys. 41 (1964) 157.
[10] L.A. Rebane, A.A. Gorokhovskii, J.V. Kikas, Appl. Phys. B 29 (1982) 235.
[11] M. Berg, C.A. Walsh, L.R. Narasimhan, K.A. Littau, M.D. Fayer, Chem. Phys. Lett. 139 (1987) 66.
[12] K.K. Rebane, A.A. Gorokhovskii, J. Lumin. 36 (1987) 237 and references therein.
[13] W. Kohler, J. Meiler, J. Friedrich, Phys. Rev. B 35 (1987) 4031.
[14] W. Kohler, J. Zollfrank, J. Friedrich, J. Appl. Phys. 66 (1989) 3232.
[15] R. Van Den Berg, S. Volker, Chem. Phys. Lett. 150 (1988) 491.

PROCEEDINGS OF SPIE

SPIE—The International Society for Optical Engineering

Advanced Optical Memories and Interfaces to Computer Storage

Pericles A. Mitkas
Zameer U. Hasan
Chairs/Editors

22–24 July 1998
San Diego, California

Sponsored and Published by
SPIE—The International Society for Optical Engineering

SPIE
P
PROCEEDINGS SERIES

Volume 3468

Optical spectroscopy of Tm^{3+} in organic matrices for hole-burning storage applications

Alexey V. Turukhin [a, c], Agnes V. Carpenter [a, c], Anshel A. Gorokhovsky [a, c]
Robert R. Alfano [b, c], Ting-Yi Chu [d], and Yoshiyuki Okamoto [d]

[a] Department of Engineering Science and Physics, The College of Staten Island, CUNY, 2800 Victory Boulevard, Staten Island, NY 10314[1],
[b] Physics Department, The City College of New York, CUNY, New York, NY 10031,
[c] The Graduate School, CUNY
[d] Department of Chemistry and Polymer Research Institute, Polytechnic University, Brooklyn, New York 11201

ABSTRACT

The optical properties of four Tm^{3+} chelates, specifically β-diketone tris chelates of thulium, in a poly(methyl methacrylate) matrix are presented. Samples under investigation were the Tm^{3+} complexes formed using thulium chloride ($TmCl_3 \bullet 6H_2O$) with thenoyltrifluoroacetylacetone (TTFA), 1,1,1-trifluoro-2,4-pentanedione (TFD), 1-phenyl-1,3-butanedione (PBD), and 1,3-diphenyl-1,3-propanedione (DBM) ligands. These materials are interesting from the point of view of potential applications for optical hole-burning frequency and time-domain storage and processing. Optical absorption, steady state and time-resolved photoluminescence, and spectral hole-burning at the transition between $^3H_6(1)$ and $^3H_4(1)$ crystal-field levels were studied at temperatures between 1.4 and 300 K.

Keywords: optical storage, spectral hole burning, materials, lanthanide ions, polymers.

1. INTRODUCTION

Persistent spectral hole burning[1,2] has the potential to advance several state of the art technological applications such as optical storage, coherent signal processors, and ultra-narrow-band optical filters both in the frequency and the time domains. This phenomenon has now became a powerful tool for high-resolution spectroscopy in the fundamental research of solids, particularly for amorphous solids[3,4], and in the study of prospective materials for advanced frequency-selective and ultrafast photonics applications. The material performance is determined, to a large extent, by the homogeneous and inhomogeneous linewidths of the optical transition, their ratio, the hole lifetime, and the hole-burning efficiency. The homogeneous and inhomogeneous linewidths set the minimum width of the frequency channel and the total usable frequency space, respectively, in the frequency domain. Correspondingly, in the time domain, they determine the length of the data stream and the data bandwidth, respectively. The maximum storage density in the frequency space is limited by the inhomogeneous-to-homogeneous linewidth ratio. Despite much research in this field, materials with the unique properties that allow frequency-selective optical storage to compete with existing high volume data-storage systems have not yet been found.

The great potential of frequency-selective optical storage was recently demonstrated for real-time holographic motion pictures[5], high-speed holographic image storage[6], ultrafast single-shot photon echo readout[7], and different aspects of swept-carrier time-domain optical storage and optical data processing[8]. Most of the practical demonstrations of frequency-selective

Further author information -
A.A.G. (correspondence): Email: gorokhovsky@postbox.csi.cuny.edu; Telephone: 718-982-2815; Fax: 718-982-2830
A.V.T.: Email: alexey@scisun.sci.ccny.cuny.edu
A.V.C.: Email: carpenter@postbox.csi.cuny.edu

Part of the SPIE Conference on Advanced Optical Memories and Interfaces to Computer Storage • San Diego, California • July 1998
SPIE Vol. 3468 • 0277-786X/98/$10.00

optical storage have been carried out on inorganic rare-earth ions doped materials, in particular, Tm^{3+} doped crystals. The Tm^{3+} is especially of interest because the transition between the $^3H_6(1)$ and the $^3H_4(1)$ crystal field levels occurs in the region of GaAlAs diode lasers near 800 nm, which is clearly advantageous for possible technological applications. In addition, large inhomogeneous-to-homogeneous linewidth ratio, up to 7×10^6, may be obtain[9].

Interest in rare-earth ion doped materials is based on the fact that the optical 4f electrons of the rare-earth ions are shielded by the outer 5s and 5p electrons. As a result, the optical 4f electrons are not strongly affected by motion of neighboring atoms, and thus the phonon-electron interaction is weak and the optical transition exhibits small homogeneous vibrational broadening. In addition, ions with an even number of 4f electrons have nonmagnetic singlet electronic states, and consequently have small homogeneous broadening caused by the magnetic interaction with neighboring spin magnetic moments. Many of the rare-earth ions in solids, e.g. Eu^{3+}, exhibit persistent hole burning as a result of optical pumping of hyperfine levels with storage lifetimes of a few hours[10]. This mechanisms is efficient only at low temperatures, generally less than 10K, where the hyperfine splitting exceeds the homogeneous linewidth. It does not operate at elevated temperatures, where the only storage mechanism is the population of electronic levels, and the storage lifetime is limited to 10^{-6}- 10^{-2} sec. Certain rare earth ions, in particular Tm^{3+}, have no hyperfine splitting and accordingly no longtime storage capabilities[11].

The lack of a longtime storage mechanism for Tm^{3+} doped systems at low temperature, and for other ions at elevated temperatures, is an obvious disadvantage of rare-earth ion doped crystals. In order to have the combined properties of both small phonon broadening of f-f transitions and long hole lifetime, we chose to investigate hole-burning in rare-earth ion doped polymer matrices as potential materials for frequency selective storage. We expected that these materials would exhibit persistent hole burning due to a photoinduced rearrangement of the local structure surrounding the ion. This mechanism is probably universal for disordered glass-like solids[4]. Another motivation for the study of the polymer host was to obtain large inhomogeneous linewidth. It makes these materials suitable for high-speed applications, e.g. ultrafast communications, femtosecond time-domain holography, and pentaflop computing.

In this paper, we present some preliminary results on the optical properties of four Tm^{3+} - organic ligand complexes in a polymer matrix. The samples that are under investigation are Tm^{3+} chelates, specifically β-diketone tris chelates of thulium, blended in a poly(methyl methacrylate) (PMMA) matrix as a host. Optical absorption, steady state and time-resolved photoluminescence, and spectral hole burning at the transition between the $^3H_6(1)$ and the $^3H_4(1)$ crystal-field levels, were studied at temperatures between 1.4 and 300 K.

2. SAMPLES

Chelates where prepared by the technique described in Ref. 12 using thulium chloride ($TmCl_3 \bullet 6H_2O$) with thenoyltrifluoroacetylacetone (TTFA), 1,1,1-trifluoro-2,4-pentanedione (TFD), 1-phenyl-1,3-butanedione (PBD), and 1,3-diphenyl-1,3-propanedione (DBM) ligands. The molecular structure of these β-diketone tris chelates of thulium is shown in Fig. 1, and the symbols assigned to each ligand are listed in Table 1. Six oxygen atoms are available for coordination to the rare-earth ion. There is however evidence,[13] that between one and three additional oxygen atoms may be delivered by coordination water molecules. The concentration of Tm^{3+} in the samples was determined on the basis of input chemical concentrations and found to be 0.35, 0.14, 0.32, and 0.2 mol % for $Tm^{3+}(TFD)_3$, $Tm^{3+}(TTFA)_3$, $Tm^{3+}(PBD)_3$, and $Tm^{3+}(DBM)_3$ complexes, respectively. Physically, the samples appeared to be transparent slightly yellow colored cylinders, having diameters of 8 -10 mm and lengths of 15-20 mm.

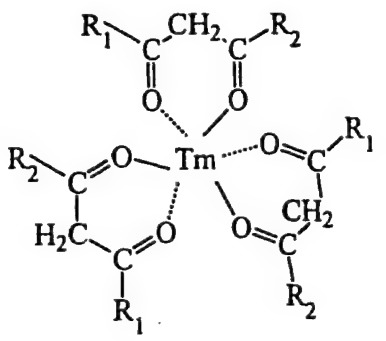

Figure 1. Chemical structure of β-diketone tris chelates of thulium. Substituent groups for the studied ligands are presented in Table 1.

Table 1. Substituent groups.

Name of the ligand		Structure of the substituent groups	
Full name	Abbreviation	R_1	R_2
1,1,1-trifluoro-2,4-pentanedione	TFD	$-CH_3$	$-CF_3$
1-phenyl-1,3-butanedione	PBD	$-CH_3$	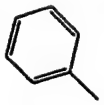
thenoyltrifluoroacetylcetone	TTFA	$-CF_3$	
1,3-diphenyl-1,3-propanedione	DBM	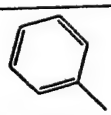	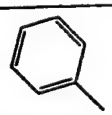

3. EXPERIMENTAL

The optical absorption spectra were recorded by a Perkin Elmer Lambda 9 spectrophotometer with a resolution of 0.2 nm. Samples were installed in Janis He-flow cryostat for measurements between 10 and 300K.

Photoluminescence was excited by Ar laser lines at 457.9, 476.5, and 488 nm. Photoluminescence spectra were recorded using a McPherson Model 2035 0.35 m monochromator with a resolution of 0.1 nm, a cooled GaAs photomultiplier (Hamamatsu R943), and a lock-in amplifier. Experiments at temperatures 1.4 - 30 K were performed in a He-bath cryostat (Optistat by Oxford Instruments). For time-resolved measurements, the laser beam was modulated by the acousto-optic modulator Isomet 1206C with frequency 1000 Hz. The signal of photoluminescence was detected by the photomultiplier and averaged by Tektronix Digital Storage Oscilloscope TDS 724A. The time resolution of 0.7 μs was determined by the response time of the photomultiplier.

Hole burning measurements were made with a tunable single frequency CW Ti-sapphire laser (Coherent 899-29). The laser intensity was stabilized at the level of 0.1 %. Holes were burned at fixed frequencies by irradiating the sample with the intensity level of 1 mW/mm^2. Subsequently, the holes were recorded in transmission spectra by scanning the laser frequency at the reduced intensity of 0.01 mW/mm^2.

4. OPTICAL ABSORPTION

The absorption spectra for Tm^{3+} $(TTFA)_3$ in PMMA measured at 23 K and room temperature are shown in Fig. 2. We can assign individual absorption bands to the transitions in Tm^{3+} ion, ligand, and the host matrix. Absorption bands due to transitions from the $^3H_6$ ground states of Tm^{3+} ion to the exited electronic states $^3H_5$ at 1210 nm, $^3H_4$ at 795 nm, $^3F_{3,2}$ near 690 nm, and $^1G_4$ at 470 nm are clearly visible. Comparison of the absorption spectra of doped and pure PMMA samples shows that the broad complex bands in the near infrared at 1400, 1170, 1000, and 900 nm belong to vibrational transitions of the host PMMA. The steep increase in the absorption at 400 nm is explained by a singlet-singlet transition in the TTFA ligand. The similarity between the low and room temperature spectra indicates that there is only weak interaction of the Tm^{3+} ion with the vibrational excitations of the ligands and of the polymer matrix.

The other three complexes have similar absorption spectra. Still differences can be observed in the structure of particular absorption bands. Low temperature spectra of the $^3H_4 \leftarrow {}^3H_6$ transition for the four complexes are presented in Fig. 3. The absorption bands have different peak positions and consist of several overlapping elementary bands. These elementary

bands represent transitions to separate crystal field components of the $^3H_4$ level and may have some contribution from the different coordination structures of the ligand complexes.

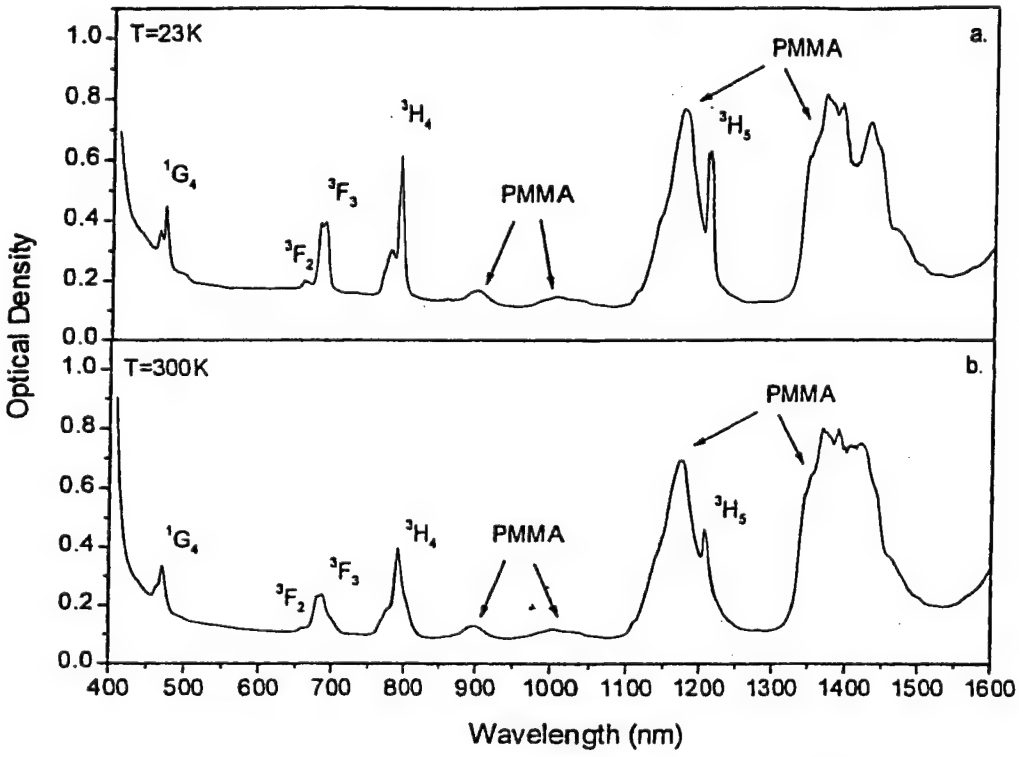

Figure 2. Absorption spectra of $Tm(TTFA)_3$ in PMMA at (a) 23 K and (b) 300 K. The sample thickness was 15 mm.

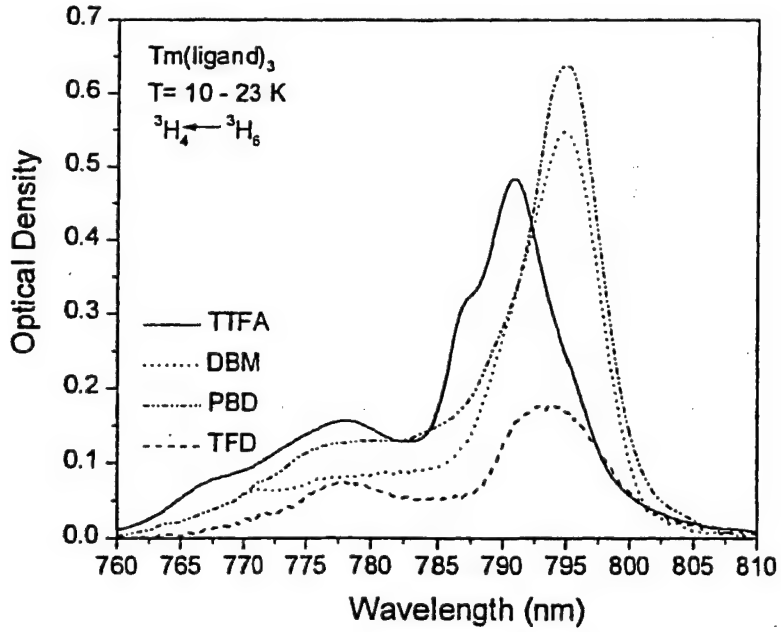

Figure 3. $^3H_4 \leftarrow {}^3H_6$ absorption bands of Tm^{3+} chelates complexes in PMMA. Temperature range is 10 - 23 K

To determine the magnitude of inhomogeneous broadening, an absorption band was numerically fitted by the superposition of a few Gaussians. The width of the Gaussian centered at the transition between the lowest crystal field components, $^3H_4$ (1)← $^3H_6$ (1), gives the inhomogeneous broadening of this transition (the homogeneous broadening can be neglected), and was found to be between 90 and 140 cm^{-1} for different complexes. In addition, the fitting allowed one to determine the crystal field splitting of the $^3H_4$ state and the other observed exited states. The same procedure applied to high temperature spectra allowed one to determine the transitions originating from the thermally populated $^3H_6$ ground state levels. Along with analysis of luminescence spectra, it allows to find the ground state energy splitting for each complex. These results were used to obtain the energy level diagram shown for the Tm^{3+} $(TTFA)_3$ complex in Fig. 4.

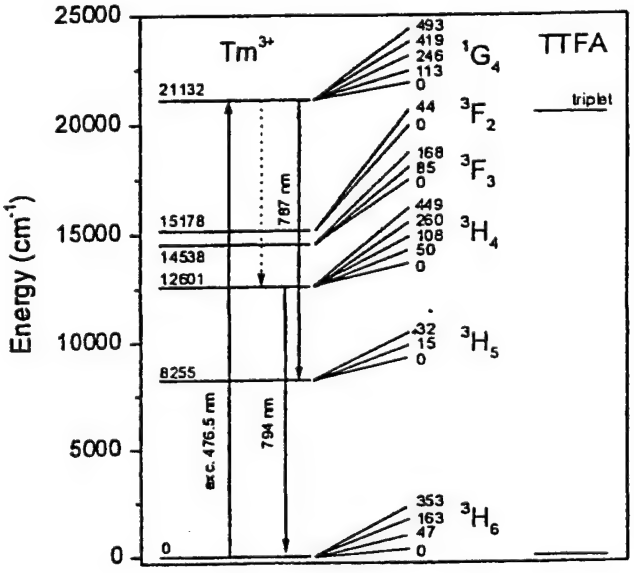

Figure 4. Energy level diagram of the Tm^{3+} $(TTFA)_3$ complex in PMMA

5. PHOTOLUMINESCENCE

Luminescence spectra of the Tm^{3+} chelates were investigated in the region of the $^3H_4 \rightarrow {}^3H_6$ transition near 795 nm. The emission spectra upon excitation by CW Ar laser lines 457.9 nm and 476.5 nm into the $^1G_4$ manifold consist of a few relatively weak narrow bands and a strong broad background. The emission upon 488.0 nm excitation, which is out of resonance with Tm^{3+} ion absorption, shows the background only. Thus, this broadband emission, which is likely related to ligand or unknown impurities, may be separated from the Tm^{3+} luminescence by subtraction. The differential spectra for materials studied are displayed in Fig. 5. Though the intensities are different, the spectrum structure is similar for all materials. It consists of a relatively narrow band with width 2 - 5 nm at 787 nm and a much broader band centered around 798 nm. To find the origin of these bands, we overlapped the absorption and luminescence spectra as shown in Fig. 6 in the case of $Tm^{3+}(PBD)_3$. The broad luminescence band has mirror-like symmetry with the $^3H_4 \leftarrow {}^3H_6$ absorption band. Thus, this luminescence corresponds to the $^3H_4 \rightarrow {}^3H_6$ transition, and originates from the lowest crystal field component of the $^3H_4$ state and terminates in the $^3H_6$ state manifold. The shoulder in each spectrum corresponds to the crystal field splitting of about 250 cm^{-1}, for both the ground $^3H_6$ and the excited $^3H_4$ states. After careful analysis, based on level positions and the temperature dependence of the spectra, the narrow peak at 787 nm was assigned to the luminescence corresponding the $^1G_4 \rightarrow {}^3H_5$ transition (see Fig. 4). The smaller width of the peak at 787 nm in comparison with the width of the peak at 798 nm is a result of laser-induced line narrowing of the $^1G_4 \rightarrow {}^3H_5$ luminescence at the laser excitation at $^1G_4 \leftarrow {}^3H_6$ transition, i.e. only a given subset of sites absorbing at excitation wavelength radiates within the inhomogeneously broadened $^1G_4 \leftarrow {}^3H_6$ absorption band. This effect is absent for the $^3H_4 \rightarrow {}^3H_6$ luminescence, apparently due to the loss of correlation with site distribution of the $^1G_4 \leftarrow {}^3H_6$ transition after nonradiative relaxation from $^1G_4$ to $^3H_4$ state.

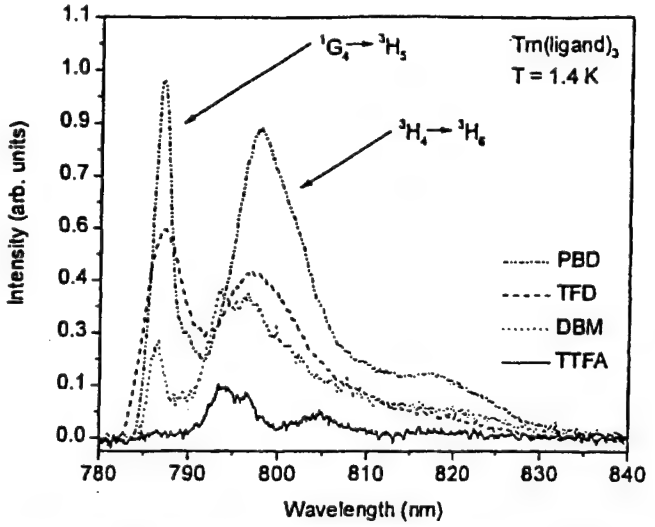

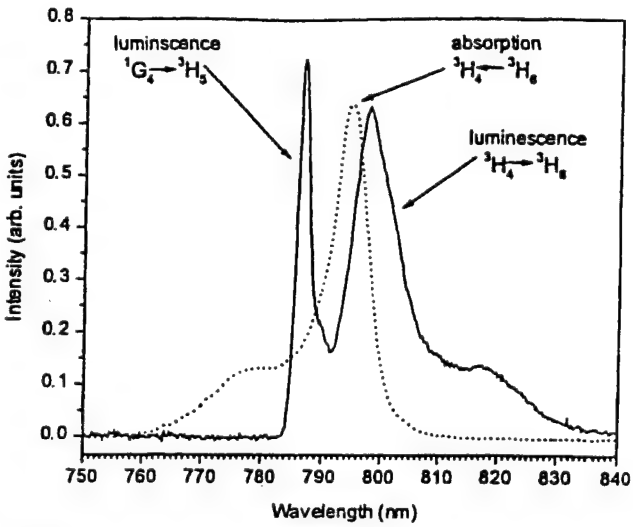

Figure 5. (left) Photoluminescence spectra of Tm^{3+} chelates in PMMA at 1.4 K upon 476.5 nm excitation by Argon laser.
Figure 6. (right) Absorption (dotted line) and photoluminescence (solid line) of the Tm(PBD)$_3$ in PMMA. The absorption spectrum was measured at 12 K. The photoluminescence spectrum was measured using the conditions indicated in Fig. 5.

The $^3H_4 \rightarrow {}^3H_6$ and $^1G_4 \rightarrow {}^3H_5$ luminescence decays, as well as the background emission decays, were also measured in the different materials after $^1G_4 \leftarrow {}^3H_6$ pulsed excitation at 476.5 nm for T = 1.4 K. The decay curves were fitted by single exponentials. The results are reported in Table 2 together with the relative quantum yields of luminescence. The quantum yields were estimated on the basis of relative luminescence intensity, absorption at the laser wavelength, and level lifetime. The decay time of each luminescence band is different, in agreement with our assignment of their respective origins. The decay times are about two orders of magnitude shorter than reported for the same transitions in inorganic indium based fluoride glasses[14] with comparable Tm^{3+} concentration. This is most likely related to specific features governing nonradiative relaxation in the organic matrix, e.g. additional vibrational frequencies of the polymer matrix, presence of O-H vibrations of coordinated water[15], and an additional deexcitation path through the triplet states of ligand due to its close proximity to the $^1G_4$ level[16] of Tm^{3+} (see Fig. 4).

Table 2. Photoluminescence lifetimes and relative quantum yields.

Transition	Tm(ligand)$_3$ complexes	Lifetime (μs) ±15%	Relative Quantum Yield
$^1G_4 \rightarrow {}^3H_5$	TFD	13.9	0.88
	PBD	9.2	0.17
	TTFA	25.4*	0.015
	DBM	3.1	0.013
$^3H_4 \rightarrow {}^3H_6$	TFD	19.5	1.0
	PBD	13.7	0.20
	TTFA	25.4*	0.16
	DBM	5.1	0.034

* Luminescence components for Tm(TTFA)$_3$ were not resolved due to low level of signal.

6. SPECTRAL HOLE BURNING

So far only transient holes with a population storage mechanism have been reported for Tm^{3+} doped crystals[11]. Several conference talks were presented on persistent hole burning for Tm^{3+} doped organic materials[17]. We studied spectral hole-burning at the $^3H_4$ (1) ← $^3H_6$ (1) transition of Tm^{3+} in the samples listed in Table 1. Long lived holes were observed in all materials. The example of the spectral hole profile for the case of $Tm^{3+}(TTFA)_3$ is shown in Fig. 7. No side band structure was observed. The holes show no visible recovery at 1.4 K over the experimental time of 10 hours The maximum measured hole depth was about 50 %. The hole-burning mechanism appears to be a photoinduced rearrangement of the local structure and will be discussed elsewhere.

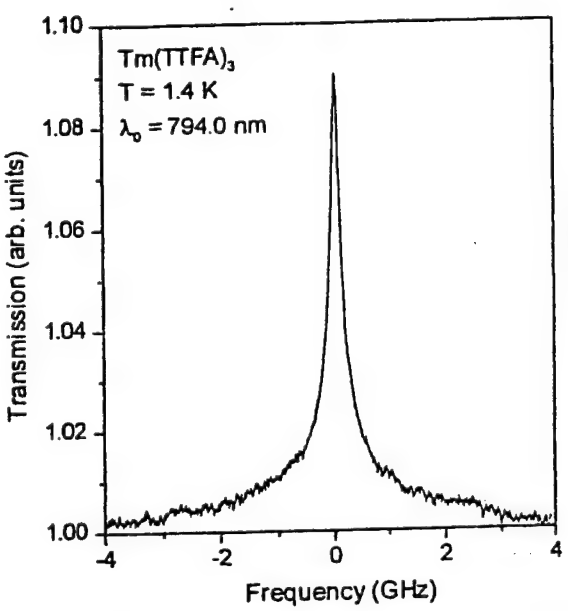

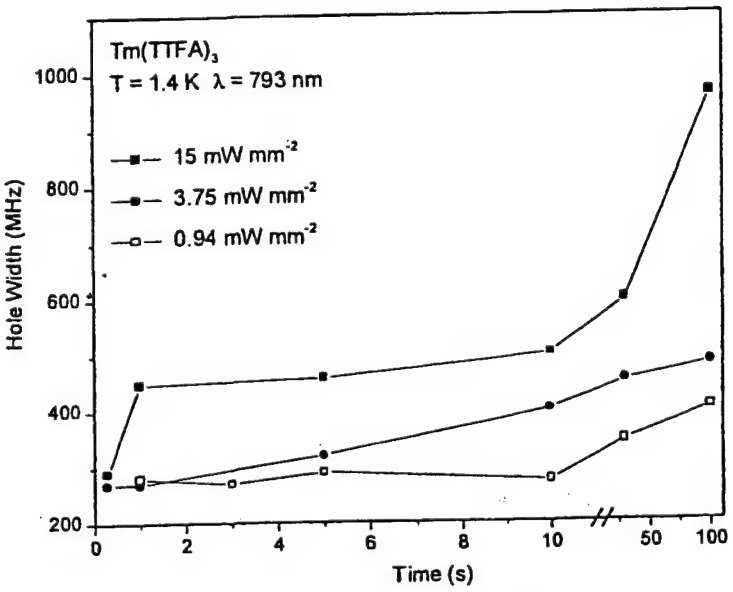

Figure 7. (left) Representative hole profile. The hole burnt in $Tm(TTFA)_3$ for 30 s at 1.4 K. Burning intensity was 1 mW/mm^2.

Figure 8. (right) Dependence of the holewidth on exposure time at different burning intensities for $Tm(TFFA)_3$ in PMMA.

The holewidth dependence on burning time at different intensities (Fig. 8) was used to determine the conditions for the weak burning intensity regime. The "true" holewidths for different materials were found to be Γ_{hole} = 180-360 MHz by using the zero limit of the burning intensity and of the exposure time (see Table 3). These "true" holewidths reflect optical dephasing caused by the interaction with phonons, tunneling systems, and surrounding spins (in the time scale of the excited state lifetime), as well as the slower spectral diffusion. Separation of these effects requires fast time-resolved measurements[18]. The temperature dependence of the holewidths was measured at temperatures between 1.4 and 16 K. A weak power law temperature dependence $\Gamma_{hole} \propto T^n$ with n = 1 - 1.6 was observed. A similar dependence of the homogeneous line broadening with n = 1 - 2 were observed in many doped glasses and polymers[19], and explained as to be due to the interaction between the optical transition in the impurity ion and the low frequency excitations (quasilocal vibrations and tunneling systems) of the amorphous matrix.

It is of interest to compare our results with previously reported hole-burning in several Eu^{3+} ion doped organic glasses and polymers. In Ref. 20, the observed small inhomogeneous linewidths between 1.5 and 16 cm^{-1} and the narrow holes with width of a few MHz are close to those for inorganic crystalline hosts. These indicate that for Eu^{3+} ions the organic hosts studied provide not glass-like, but more likely crystalline-like structure. In sharp contrast, the Tm^{3+} chelates in PMMA studied in this paper have inhomogeneous broadening of about 100 cm^{-1} and holewidths of about 100 MHz which is typical for most inorganic as well as organic glasses and polymers. This indicates a high degree of disorder in the coordination of the Tm^{3+} ion in β-diketone chelates. This result is probably related to the molecular structure our chelates (Fig. 1), which

allow a number of different orientational positions of the substituents R_1 and R_2 attached to the β-diketone ring by a relatively weak single C-C bond.

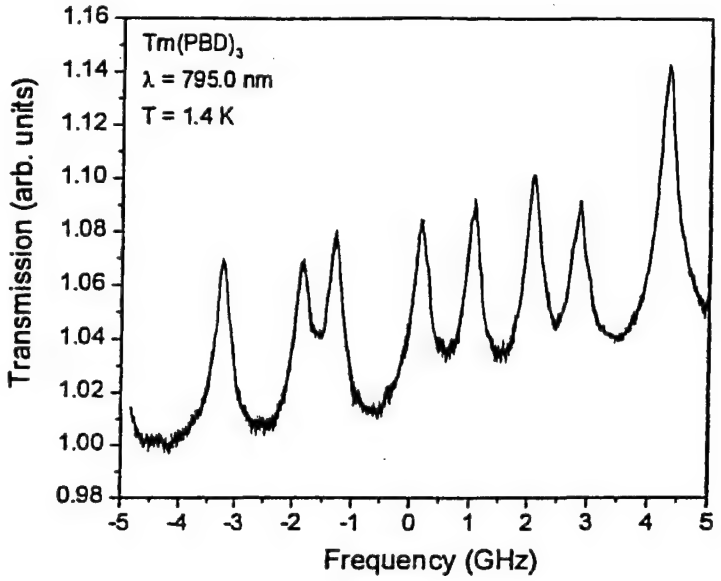

Figure 9. Spectra of eight spectral holes burnt in $Tm(PBD)_3$ complex in PMMA at 1.4 K near 794.0 nm. Burning intensity was 1 mW/mm^2 with 30 s exposure for each hole.

To verify the ability of the materials under investigation to store a number of spectral holes, we performed hole-burning at different wavelengths over the inhomogeneous broadened absorption band. Holes were observed over the full inhomogeneously broadened band of the $^3H_4$ (1) ← $^3H_6$ (1) transition, i.e. in the bandwidth of 100 cm^{-1}, or 3000 GHz. Fig. 9 displays a set of eight consecutive holes burned over a region of 8 GHz. No visible laser - induced filling or broadening was detected on test hole # 1 at - 3.2 GHz over the time of burning of the other seven holes. We expect the same behavior over the full inhomogeneously broadened absorption band. Data on the inhomogeneous broadening and the holewidth for all of the materials studied are presented in Table 3.

Table 3. Holewidths and inhomogeneous widths of the $^3H_4$ (1) ← $^3H_6$ (1) transition of Tm^{3+} chelates in PMMA.

Parameters	$Tm(TTFA)_3$	$Tm(TFD)_3$	$Tm(PBD)_3$	$Tm(DBM)_3$
Γ_{inh} (GHz)	3000	4300	2800	2500
Γ_{hole} (MHz)	220	230	360	180
$\Gamma_{inh} / \Gamma_{hole}$	1.4×10^4	1.9×10^4	0.8×10^4	1.4×10^4

7. CONCLUSIONS

Four new Tm^{3+} - organic ligand complexes in PMMA matrix were prepared. Optical absorption, photoluminescence, and spectral hole burning were investigated at different temperatures. Persistent spectral hole-burning was observed in the $^3H_4(1) \leftarrow {}^3H_6(1)$ transition of Tm^{3+} ion near 795 nm in all of the materials. The hole lifetime is longer than 10 hours at 1.4 K. Spectroscopic results indicate glass-like properties for these materials, i.e. a high degree of disorder in the Tm^{3+} coordination surroundings. The materials have large inhomogeneous broadening, and are suitable for research in low temperature hole-burning frequency and time-domain storage and processing applications.

8. ACKNOWLEDGEMENTS

This work was supported in part by the U.S. Air Force Office of Scientific Research.

9. REFERENCES

1. A. A. Gorokhovskii, R. K. Kaarli, L. A. Rebane, *JETP Lett.* **20,** 216 (1974).
2. B. M. Kharlamov, R. I. Personov, L. A. Bykovskaya, *Opt. Commun.* **12,** 191 (1974).
3. J. Friedrich and D. Haarer, in *Optical Spectroscopy of Glasses,* edited by I. Zschokke (Reidel, Dordrecht, Netherlands, 1986), p. 149.
4. R. Jankowiak and G. J. Small, *Science,* **237,** 618 (1987).
5. M. Mitsunaga, N. Uesugi, H. Sasaki, and K. Karaki, *Opt. Lett.* **19,** 752 (1994).
6. X. A. Shen, E. Chiang, and R. Kachru, *Opt. Lett.* **19,** 1246 (1994).
7. I. Zeylikovich, G. Bai, A. Gorokhovsky, and R. R. Alfano, *Opt. Lett.* **20,** 749 (1995).
8. H. Lin, T. Wang, G. A. Wilson, and T. W. Mossberg, *Opt. Lett.* **20,** 91 (1995); H. Lin, T. Wang, and T. W. Mossberg, *Opt. Lett.* **20,** 1658 (1995); H. Lin, T. Wang, and T. W. Mossberg, Opt. Lett. **21,** 1866 (1996).
9. G. M. Wang, R. W. Equall, R. L. Cone, M. J. M. Leask, K. W. Godfrey, and F. R. Wondre, *Opt. Lett.* **21,** 818 (1996)
10. R. M. Macfarlane and R. M. Shelby, in *Spectroscopy of Solids Containing Rare Earth Ions*, edited by A. A. Kaplyanskii and R. M. Macfarlane (North-Holland, Amsterdam, 1987) p. 51.
11. R. M. Macfarlane, *Opt. Lett.* **18,** 829 (1993).
12. Y. Okamoto, Y. Ueba, F. N. Dzhanibekov, and E. Banks, *Macromolecules*, **14,** 17 (1981).
13. F. Halverson, J. S. Brinen, and J. R. Leto, *J. Chem. Phys.* **41,**157 (1964).
14. C. Guery, J. L. Adam, and J. Lucas, *J. Lumin.* **42,** 181 (1988).
15. W. DeW. Horrocks, Jr., and D. R. Sudnick, *J. Am. Chem. Soc.* **101,** 334 (1979).
16. P.K. Sharma, A.R. van Doorn, and A.G.J. Staring, *J. Lumin.* **62,** 219 (1994).
17. A. V. Carpenter, A. V. Turukhin, A. A. Gorokhovsky, R. R. Alfano, T. Chu, and Y. Okamoto, *Proceedings of the 5th International Meeting on Hole Burning and Related Spectroscopies: Science and Applications,* Brainerd, Minnesota, September 13 - 17, 1996, p. 89; *Abstracts of the MRS 1996 Fall Meeting,* Boston, MA, December 2 - 6, 1996.
18. M. Berg, C. A. Walsh, L. R. Narasimhan, K A. Littau, and M. D. Fayer, *Chem. Phys. Lett.*, **139,** 66 (1987).
19. K. K. Rebane and A. A. Gorokhovskii, *J. Lumin.* **36,** 237 (1987) and references therein.
20. R. Van Den Berg, and S. Volker, *Chem. Phys. Lett.* **150,** 491 (1988).

PROCEEDINGS OF SPIE

SPIE—The International Society for Optical Engineering

Cryogenic Optical Systems and Instruments VIII

James B. Heaney
Lawrence G. Burriesci
Chairs/Editors

20–21 July 1998
San Diego, California

Sponsored and Published by
SPIE—The International Society for Optical Engineering

Volume 3435

Evaluation of vibration generated by closed cycle refrigeration system using optical methods

Alexander A. Vaysman, Alexey V. Turukhin and Anshel A. Gorokhovsky

Laser and Photonics Laboratory, Department of Engineering Science and Physics, The College of Staten Island and Graduate School of The City University of New York, 2800 Victory Boulevard, Staten Island, NY 10314

ABSTRACT

A simple optical method for studying vibration has been developed and applied to the investigation of a commercial closed cycle refrigeration (CCR) system. This method utilizes an amplitude modulation of a laser beam by the knife-edge attached to the cold finger of the CCR system. The sensitivity of the proposed optical technique is determined by the diameter of the focused laser beam and a displacement of 1 μm is readily detectable. For the system CRYO Model 396-022 based on CTI CRYODYNE Model 22 refrigerator, experimental studies were conducted for different cold finger temperatures, cold head orientations, and mechanical holders. The total amplitude of the displacement was on the order of 50 μm for a cold head fixed into rigid mechanical holder placed on the optical table and 30 μm for the same holder placed on a special stand decoupled from the optical table. Three main frequency components at 3 Hz, 60 Hz, and 120 Hz have been observed.

Keywords: closed cycle refrigeration system, cold head, mechanical vibration, optical method.

1. INTRODUCTION

Low temperatures are required for optical research, in particular for spectroscopic investigation of solids, including laser spectroscopic experiments such as Raman scattering, luminescence line narrowing, spectral hole burning and spectral holography. Recent research directed to new materials for high-density frequency domain optical data storage demonstrated the necessity to have simple, dependable low-cost refrigeration systems that provide cryogenic temperatures for a long continuous period of time[1]. Two well-developed low temperature techniques are employed: helium-bath cryostats and closed cycle refrigeration systems. The helium-bath cryostats provide temperatures near 4.2 K, however require expensive liquid helium and extensive preparation time. Alternative modern closed cycle refrigeration (CCR) systems are very attractive for temperatures above 8 K due to their immediate advantages of a compact size, operation in any orientation, lack of liquid helium and ability to achieve low temperatures in relatively short time. The main disadvantage of low priced commercial CCR systems is vibration, which might substantially effect experimental results if not taken into consideration. Only a limited number of experimental data on vibration of commercial CCR systems are available in the literature[2].

In this paper, we present a simple optical technique for studying mechanical vibration and the application of this technique for investigating the vibration of a commercial CCR system. By analyzing the spectra of vibration of the cold finger, frequencies of the major Fourier components were determined. Reported results can be useful in optical technology that utilizes CCRs.

Further author information -
A.A.G. (correspondence): Email: gorokhovsky@postbox.csi.cuny.edu; Telephone: 718-982-2815. Fax: 718-982-2830
A.V.T.: Email: alexey@scisun.sci.ccny.cuny.edu
A.A.V.: Email: 09097f97@student.csi.cuny.edu

Part of the SPIE Conference on Cryogenic Optical Systems and Instruments VIII
San Diego, California • July 1998
SPIE Vol. 3435 • 0277-786X/98/$10.00

2. EXPERIMENTAL TECHNIQUE

A few sensitive vibrometric methods have been developed in the past. The most common method is based on accelerometry. A regular accelerometer consists of a small mass supported on a force transducer. The force required to accelerate the mass is proportional to the acceleration for nonresonance frequencies. The force is measured by a piezoelectric system: a crystal of quartz or a material such as barium titanate, when stressed, will produce a charge proportional to stress. The crystal may be used in direct compression or in shear. Accelerometry is the dominate method for measuring vibration, however it requires tedious mounting and wiring of sensors[3]. Consequently, it hardly can be applied for evaluation of vibration at places with limited access such as compact vacuumed chamber at cryogenic temperatures. An alternative method is Laser Doppler Vibrometry (LDV), which is used for the detection of vibration without surface contact. LDV measures velocity using the frequency shift of a laser wave caused by motion of a reflecting target. Due to high sensitivity of the LDV, the measured surface does not need to be specially modified or prepared in advance. At the present time, commercially available LDV systems remain too expensive to be cost-effective for occasional measurements. Other methods based on laser interferometry use the principle of the standard Michelson interferometer[4]. Interferometric methods provide high sensitivity, however require time-consuming alignment. Also, they become particularly complex when instabilities make the measurement object move more than the vibration to be measured.

We propose an optical technique for direct measurement of the displacement based on amplitude modulation of the probe laser beam by the vibrating element. To implement our technique, a sharp knife-edge has to be attached to the vibrating element perpendicular to the axis of a laser beam in such a manner that the laser beam is partially blocked by a knife-edge (see Figure 1). Hence, the intensity of the transmitted laser beam depends on the displacement of the knife-edge along Y-axis. The transmitted intensity is measured and analyzed to obtain the amplitude and spectrum of the vibrational motion in the Y-direction.

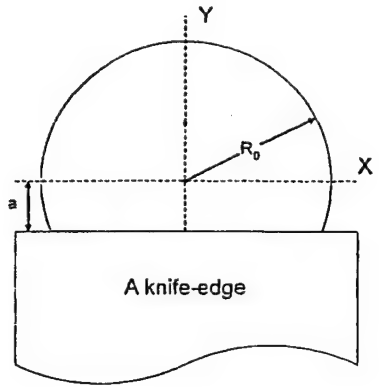

Figure 1. A cross section of the laser beam in the knife-edge plane is shown. The detected intensity is proportional to the transmitted part of the beam cross section (see text below). a is the linear displacement of the knife-edge; R_0 is a radius for the Gaussian laser beam in the knife-edge plane on the level of intensity $1/e^2$.

Due to negligible diffraction of the laser beam on the knife-edge, the intensity modulation of the transmitted beam is considered in terms of geometrical optics. Taking into account Gaussian distribution of intensity across radius of the laser beam, the variable part of the photosignal is linked to the displacement of the edge by the integral:

$$\Delta I(a) = I_0 \int_0^a \int_0^{\sqrt{R_0^2 - y^2}} \exp\left(-\frac{2(x^2+y^2)}{R_0^2}\right) dx dy \qquad (1)$$

where ΔI is a variable part of the photosignal, a stands for a linear displacement of the knife-edge, R_0 is a radius for the Gaussian laser beam in the knife-edge plane on the level of intensity $1/e^2$ and I_0 is a normalization constant (see Figure 1).

Analytical solution for the displacement as a function of photosignal is not possible. For small displacement amplitudes, $a < R_0/4$, linear approximation can be used:

$$\frac{a}{R_0} \approx 0.58 \cdot \frac{\Delta I}{I_0} \qquad \left(a < \frac{R_0}{4}\right) \qquad (2)$$

A calibration curve based on the numerical integration of (1) has been used to convert the detected photosignal to the amplitude of displacement. Using the displacement amplitude normalized to the beam radius in the edge plane, the calibration curve and linear approximation (2) are shown in Figure 2. Absolute values of amplitude can be easily obtained if the beam diameter in the edge plane is known.

The minimal amplitude of vibration detectable by the proposed method is proportional to the diameter of the laser beam in the edge plane. Using focusing optics, a laser spot diameter of 10 μm could be easily achieved. Assuming a simple detection system with capability to analyze signals with depth of modulation of 1%, we may estimate measurable displacement as low as 0.1 μm.

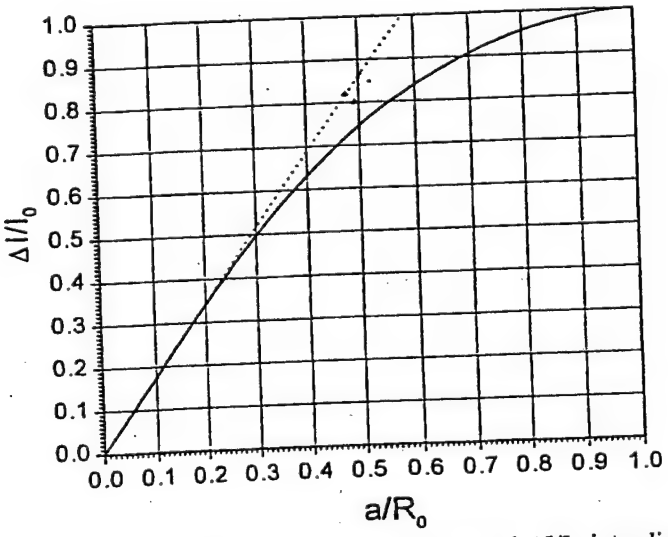

Figure 2. The calibration curve used to convert the normalized photosignal $\Delta I/I_0$ into displacement amplitude. Solid line represents the numerical calculation of integral (1). Dotted line is the linear approximation for the small displacements with $a < R_0/4$ (see text above).

3. EXPERIMENTAL SETUP

A standard green He-Ne laser (output power 4 mW, wavelength of irradiation 543.5 nm) was focused onto a lightweight knife-edge mounted on the sample holder inside the cold head. Initially, without vibration, the position of the edge was adjusted to block half of the input beam. The intensity of the transmitted laser beam was modulated by the vibration of the knife-edge in the perpendicular direction to the beam axis. The transmitted light was collected by an output lens and focused onto photodiode PD (see Figure 3). An amplified silicon photodiode PD150 (THORLABS) allowed us to measure frequency of vibration up to 50 MHz. All elements were assembled on the optical top supported by six I-2000 vibration isolators. (Newport RS 3000).

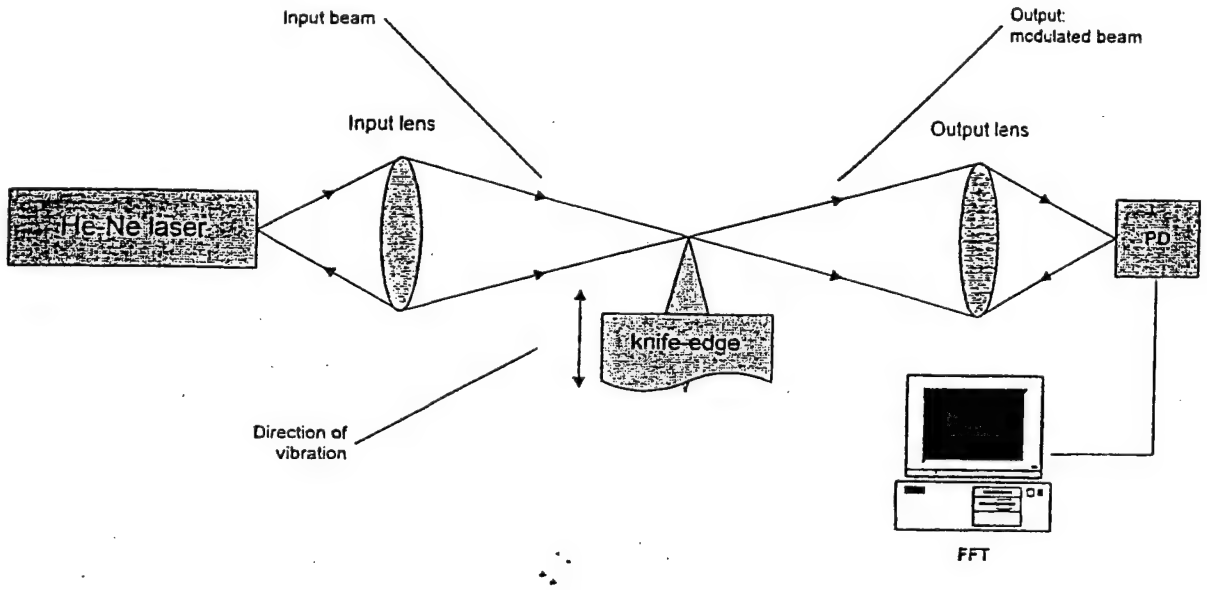

Figure 3. Optical setup for evaluation of vibration based on the beam modulation by the knife-edge (see text).

To calibrate the photosignal in the units of displacement, we measured the diameter of the laser spot by moving the knife-edge attached to a micrometric table perpendicular to the beam axis and recording the photosignal as a function of displacement. Analyzing obtained curve on the basis of integral (1), a spot diameter of 200 μm has been found. Displacements of 1 μm were easily detectable. Since the measured amplitude of vibration of our CCR system was on the order of 30 μm (see results section below), no attempts to reduce spot diameter and increase sensitivity of detection were made.

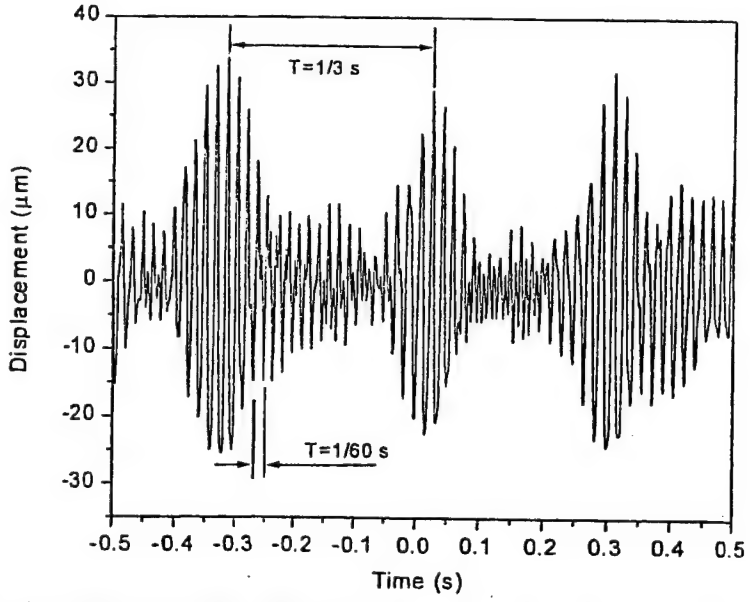

Figure 4. Representative detected waveform with the cold head fixed into rigid holder attached to the optical table. The Z-axis was directed vertically (see Figure 5). The waveform has been taken at 8 K for vibration in the X-direction and averaged 500 times. The 3 Hz and 60 Hz spectral components can be clearly seen.

The detected photosignal was averaged and analyzed by Tektronix 7248 Digital Storage Oscilloscope. A typical observed signal pattern is presented in Figure 4. Using the oscilloscope's built-in Fast Fourier Transform (FFT) option, the power spectrum of vibration was generated. Analysis of spectral components of the vibration was extremely useful for identifying sources of vibration and designing a custom made holder for reducing the level of vibration.

4. DESCRIPTION OF THE CCR SYSTEM

Our study has been conducted for the commercial system CRYO Model 396-022 based on CTI CRYODYNE Model 22 refrigerator. This CRYODYNE system is comprised of a water cooled compressor unit with oil separation system and refrigerator unit (cold head) remotely located from the compressor. Temperature is controlled by digital cryogenic temperature controller CONDUCTUS Model LTC-10. Helium gas is used as a refrigerant.

The cold head includes vacuumed chamber with four quartz windows and a sample holder attached to the cold finger. This allows the CCR system to be used for various optical and spectroscopic measurements. In the present paper, our attention has been concentrated on vibration of the cold finger as the most critical element for optical measurements.

Cool-down and warm-up procedures were performed. The minimal temperature was found to be 8 K. The system was able to reach this temperature in approximately 1.5 hour. Reverse process (with the compressor and the cold head turned off) takes approximately 20 minutes to warm up to 50 K, and about 4 hours to reach the initial room temperature.

5. EXPERIMENTAL RESULTS AND DISCUSSION

Different sets of experiments were performed to measure vibration along the three axes of rectangular coordinates. A schematic representation of the cold head and the system of coordinates are shown in Figure 5. Vibration was analyzed for different temperatures of the cold finger, different orientations of the cold head and two methods for mounting of the cold head's holder.

Table 1. Representative total amplitudes of vibration in different directions and with different mounting apparatus. Temperature at the cold finger was 8 K.

Mounting	Maximum Displacement (microns)		
	X-direction	Y-direction	Z-direction
Holder on the optical table	50	50	22
Holder on the stand	--	30	12

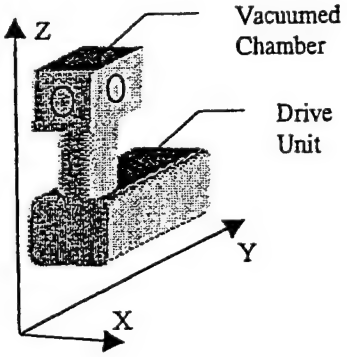

Figure 5. A schematic picture of the cold head with coordinate system used in Table 1 and elsewhere in the text.

To check vibration dependence on the orientation of the cold head, the measurements were taken with the cold head held with its Z-axis directed horizontally and vertically. All vibration characteristics measured are independent on the orientation of the cold head. This proves that the investigated CCR system is suitable for mounting in different orientations.

The temperature range during the course of experiments was 300 - 8 K. The total magnitude of vibration in all three directions appear to be slightly lower with decreasing temperature, i.e. with increasing the operating time. This effect can be attributed to warming up of the equipment.

Two different methods of mounting the cold head have been used. First, the cold head was secured into rigid mechanical holder attached directly to the optical table. However, vibration of the optical table generated by the cold head disrupted operation of the other optical equipment located on the same optical table. To avoid this problem, a second method of mounting of the cold head was tested. The cold head in the same mechanical holder was attached to a special stand placed on the floor in the laboratory. In this case, the cold head was decoupled from the optical top through room floor and vibration isolators of the optical top. Data for both mounting methods in the case of vertical orientation of the Z-axis and temperature at the cold finger 8 K are presented in Table 1. As we can see, the second mounting method provides, in addition to decoupling of the cold head from the optical table, substantial decrease of magnitude of vibration due to damping in the rigid frame of the stand.

Results of spectral analysis of the vibration are shown in Figure 6. The spectra consist of a combination of three main components of 3 Hz, 60 Hz and 120 Hz for the holder placed on optical table. For the holder placed on the stand, some additional components are clearly visible.

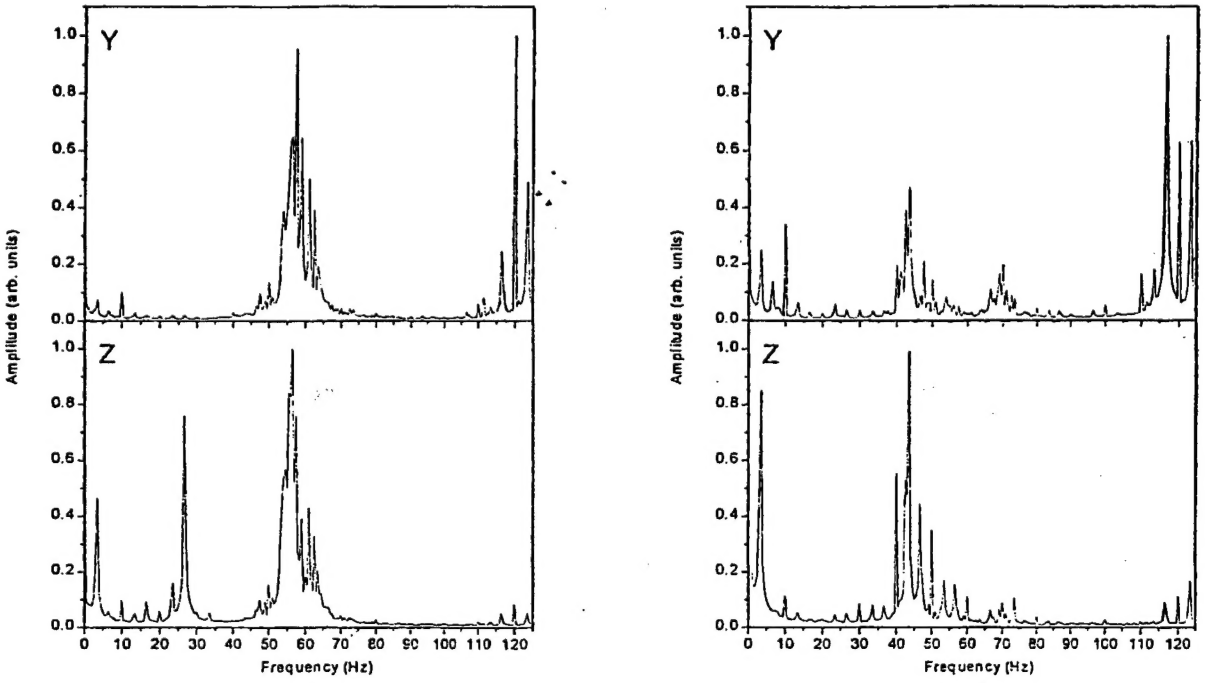

Figure 6. Normalized spectra of the vibration: (a) the cold head is secured in the mechanical holder attached to the optical table; (b) the mechanical holder attached to separated stand. Spectra taken at 8 K and averaged 500 times.

Conducted spectral analysis allows to identify sources of the major vibration components. The component at 3 Hz can be attributed to the motion of the displacer (piston) inside the cold head, which occurs with characteristic frequency 3 Hz. Two stronger components at 60 Hz and 120 Hz are caused by the drive motor inside the drive unit of the cold head. The compressor has been eliminated from the possible sources of vibration: no vibration of the cold finger was detected with running compressor while cold head drive unit has been stopped.

6. CONCLUSION

A simple optical method to evaluate mechanical vibration with sensitivity down to 0.1 μm has been proposed. The developed technique has been applied to investigate the vibration of a closed cycle refrigeration (CCR) system. In all experiments performed, the total amplitude of vibration decreases with warming of the equipment and reaches a stationary

level in a hour and a half. The characteristics of vibration do not show any dependence on orientation of the cold head. Using spectral analysis, two major components of vibration at 60 Hz and 120 Hz were found and their origin was ascribed to the drive motor of the cold head. The other significant detected component at 3 Hz was attributed to the motion of the displacer (piston) inside the cold head. Solid mechanical holder in combination with rigid stand decoupled from the optical table suppressed vibration at a level of 30 μm and 12 μm for Y and Z directions, respectively.

Conducted experimental study demonstrated that observed high level of vibration requires decoupling of the holder with cold head from the optical table. Further decrease of vibration requires use of more sophisticated CCR systems with vibration isolating interface between cold head and sample holder[5].

7. ACKNOWLEDGMENTS

This work was supported in part by the AFOSR. A.A.V. gratefully acknowledge the Summer Research grant by the Office of the Dean of Science and Technology, The College of Staten Island, CUNY.

8. REFERENCES

1. National Media Lab Report (1996) can be obtained at www.nml.org
2. A. Fuaret, M. Mualler, H. Tugal "Vibration analyses to reduce particles in sputtering systems" (Solid State Technology, March 1993)
3. J. D. Smith "Vibration measurement and analysis" (Butterworths, 1989).
4. G. Burdugan, E. Mihailescu, M. Rades "Vibration measurement" (Martin Nijhoff Publishers, 1986).
5. E. De Grave, L.H. Bowen, S.W. Hedges "Mossbauer spectroscopy with a microprocessor: a versatile software package" (Nuclear Instruments and Methods 200, 1982, p. 303).

HBRS'99

Hourtin, France
September 18-23, 1999

6th
International Meeting on Hole Burning and related Spectroscopies: Science and Applications

Supported by

Université Bordeaux 1

CENTRE NATIONAL DE LA RECHERCHE SCIENTIFIQUE (SPM, SC)

Ministère des Affaires Etrangères

Conseil Régional D'Aquitaine

COHERENT.

CREDIT LYONNAIS

MEDOC HOURTIN

Hole-burning Spectroscopy of Thulium Chelates

A. V. Turukhin, A. V. Carpenter and A. A. Gorokhovsky
The College of Staten Island and Graduate School of CUNY, 2800 Victory Blvd., Staten Island, NY 10314
T. Chu and Y. Okamoto
New York Polytechnic University, Brooklyn, New York 11201

Our interest in thulium based organic materials is motivated by the need to combine unique properties of the rare-earth ion (weak electron-phonon interaction, long coherence time) with the ability of an organic surrounding to change its local structure. The latter may serve as a persistent hole-burning mechanism for multi-frequency optical storage. We report on optical absorption, photoluminescence and persistent spectral hole burning studies of four Tm^{3+} ion - organic ligands complexes, specifically β-diketons tris chelats of thulium, blended in a poly(methyl methacrylate) matrix. The Tm^{3+} ion is especially of interest because the transition between the $^3H_6(1)$ and the $^3H_4(1)$ crystal field levels occurs in the region of GaAlAs diode lasers near 800 nm, which is clearly advantageous for possible technological applications. Goal of our research was to characterize these novel materials, as well as to evaluate their prospective for optical hole-burning frequency and time-domain storage applications.

Inhomogeneous broadening of the transition $^3H_6(1) \leftrightarrow {}^3H_4(1)$ was found of about 100 cm^{-1} for all four samples studied. Persistent spectral holes were detected at temperatures between 1.4 K and 20 K. The hole width was determined to be in the range 180-300 MHz by using zero limits of burning intensity and exposure time. Kinetics of the spectral hole-burning were recorded at time scale of 10^{-2} - 10^4 s. They showed dispersive behavior associated with random structure of the Tm^{3+} ion surrounding. The approach to determine quantum efficiency, a critical parameter of hole burning process, was developed. Quantum efficiencies were found and compared for all samples. Hole burning and refilling mechanisms were analyzed in the frame of ion interaction with two-level low-frequency excitations. Parameters of the energy barrier distribution for ground and excited electronic states were determined from hole area temperature cycling and hole-burning kinetics at different temperatures, respectively.

Prospective for hole-burning efficiency improvement and applications of lanthanide ions polymer complexes for frequency-domain optical storage will be discussed.

Oral presentation